The Thesis Committee for Scott Douglas Almond Certifies that this is the approved version of the following thesis:

Proximity Operations of Nanosatellites in Low Earth Orbit

Committee:

Glenn Lightsey, Supervisor

Wallace Fowler

Proximity Operations of Nanosatellites in Low Earth Orbit

by

Scott Douglas Almond, B.S.

Thesis

Presented to the Faculty of the Graduate School of

The University of Texas at Austin

in Partial Fulfillment

of the Requirements

for the Degree of

Master of Science in Engineering

The University of Texas at Austin

December 2013

Proximity Operations of Nanosatellites in Low Earth Orbit

Scott Douglas Almond, M.S.E.

The University of Texas at Austin, 2013

Supervisor: Glenn Lightsey

A mission architecture consisting of two NASA LONESTAR-2 satellites in Low Earth Orbit is considered. The craft are equipped with cross-communication radios and GPS units. Analyses are conducted for ejection, thruster and attitude maneuvers to achieve objectives of the mission, including sustained communications between the craft.

Simulations are conducted to determine the duration of the communication window following the initial separation of the two craft. Recommendations are made to maximize this window while accounting for attitude constraints and the effects of atmospheric drag.

Orbital mechanics and control theory are employed to form an algorithm for filtering GPS position fixes. The orbit-determination algorithm accounts for the effects of drag and Earth's oblateness. Procedures are formed for verifying the initial separation velocities of two spacecraft and for measuring the velocity imparted by impulsive thruster maneuvers. An algorithm is also created to plan the timing and magnitude of corrective thruster maneuvers to align the orbital planes of the two craft.

When the craft pass out of communication range, a ground station is used to relay data and commands to conduct state rendezvous procedures. A plan for coordinated attitude maneuvers is developed to strategically utilize the cumulative effects of drag and orbit decay to align the craft over long time periods.

The methodologies developed here extend prior research into close proximity operations, forming the foundation for autonomous on-orbit rendezvous under a broader set of initial conditions.

Table of Contents

List of Tables

List of Figures

Chapter 1: Introduction

1.1 Mission Overview

The purpose of this thesis is to detail the procedures for choosing, conducting and verifying proximity operation maneuvers for two satellites operating in LEO (Low Earth Orbit) in the context of the LONESTAR (Low Earth Orbiting Navigation Experiment for Spacecraft Testing Autonomous Rendezvous and Docking) Mission 2.

The LONESTAR program hosted by NASA (National Aeronautics and Space Administration) is comprised of four launches to LEO. Each launch consists of a pair of satellites, one developed by the University of Texas at Austin (UT-Austin) and another by Texas A&M University. The goal for the LONESTAR program is to autonomously rendezvous and dock these two satellites in Low Earth Orbit. A demonstration of proximity operations in LEO, with the goal to establish sustained radio contact between two spacecraft, will form the foundation for more ambitious missions in the future.

Autonomous rendezvous and docking is a critical step for large assemblies in LEO. The short orbital periods and low altitudes make ground passes very brief, often lasting only minutes once or twice a day. Rendezvous of un-crewed satellites in LEO using human control requires a sustained connection via several sequential ground stations or space-based relay satellites and may strain the power and bandwidth capabilities of small spacecraft. Autonomous rendezvous greatly reduces the operational overhead in some cases.

The first mission in the LONESTAR program consisted of two satellites, Bevo-1 and AggieSat2. Both craft were identical in size, being cubes measuring about 4 inches (10 cm) along each edge. The objective of the mission was to downlink two orbits' worth of GPS data collected by a GPS unit aboard each craft. The two satellites were

launched as a single unit from the ISS in July of 2009, but failed to separate after deployment.

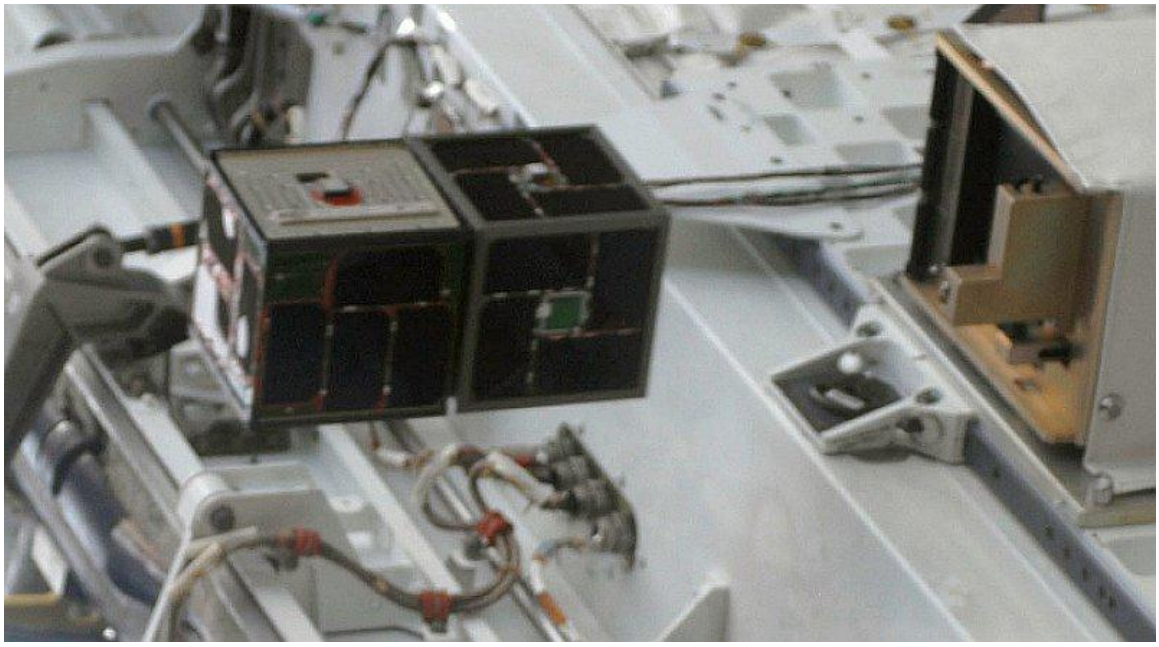

Figure 1.1: Deployment of Bevo-1 and AggieSat2 from the ISS.

For LONESTAR Mission 2, UT-Austin has developed the Bevo-2 spacecraft (named after the UT-Austin mascot, Bevo), and Texas A&M has constructed AGS4 (also referred to as AggieSat4, named for the nickname of Texas A&M students). The chassis for AGS4 is considerably larger than Bevo-2. The primary objective for these two spacecraft on Mission 2 is to demonstrate capabilities that will be required for a future rendezvous mission (Mission 4). Mission 2 goals include demonstrating attitude determination and control, collecting GPS coordinates, imaging another spacecraft, maintaining close proximity with another spacecraft, and conducting communication with another spacecraft and a ground station. GPS coordinates will be transmitted wirelessly between the two spacecraft. By proving the GPS collection and crosslink capabilities in

this mission, future missions will be able to focus on a physical target for rendezvous. The Bevo-2 craft has been equipped with attitude determination hardware, including a star camera that produces arc-minute precision attitude fixes. Reaction wheels provide control to quickly reach and maintain the desired orientation. A thruster has also been equipped on the craft which enables translational actuation. AGS4 also contains equipment designed to deliver similar attitude pointing performance.

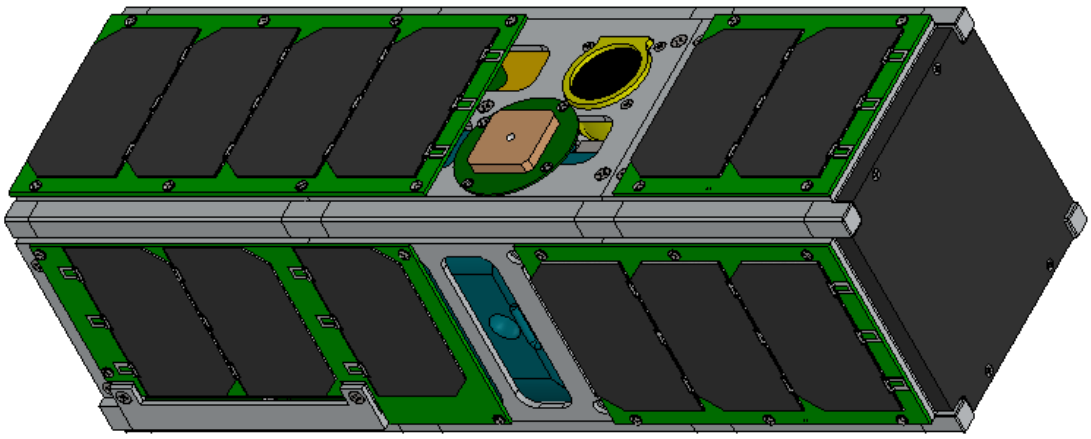

Figure 1.2: Picture of Bevo-2.

1.2 DESCRIPTION

The construction of the Bevo-2 spacecraft is based on the 3 rack unit (3U) Cubesat standard, a satellite mass and volume criterion developed by the California Polytechnic State University (Lee 2009), with a mass of 4 kg and overall dimensions of 34 cm x 10 cm x 10 cm, about the size of a loaf of bread. The Bevo-2 craft fits inside a 2-kg launcher installed in the AGS4 craft. The larger AGS4 has a mass of 50 kg and dimensions 50.8 cm x 50.8 cm x 25.4 cm (20 in x 20 in x 10 in). In 2014, when Mission 2 is anticipated to occur, the AGS4 craft with Bevo-2 loaded inside will be delivered to

the International Space Station (ISS) via a resupply mission, such as CRS-4 or CRS-5 provided by SpaceX, and the combined unit will be deployed into Low Earth Orbit (LEO). According to the Concept of Operations (Johl 2013), approximately one week after launch from the ISS, AGS4 will eject Bevo-2.

1.2.1 Mission Parameters

During the launch window, the ISS will maintain an approximately 410 km circular orbit with an inclination of 51 degrees, and LONESTAR Mission 2 will start with these initial orbit elements. The exact orbit and mission parameters will depend on the actual launch date and mission conditions, and may vary slightly from the assumed conditions.

Due to the presence of sparse molecules in the thermosphere, drag will slowly decay the orbits of each craft over time until they eventually fall out of orbit and burn up in the atmosphere. Each spacecraft is planned to be operated for as long as possible, from deployment until each burns up during re-entry. The anticipated mission duration is 6 to 12 months from deployment from the ISS until orbital decay.

1.2.2 Mission Timeline

Approximately one week after deployment of AGS4 from the ISS, AGS4 will eject Bevo-2 at a speed of approximately 0.8 m/s using a mechanical deployment system. Several events will occur in rapid succession aboard Bevo-2 after it is deployed:

1. The Command and Data Handling Operating System will be initialized.
2. The star camera will capture images of AGS4 during ejection in accordance with objectives mandated by NASA.

3. The Global Position System (GPS) unit, codenamed DRAGON (Dual RF Astrodynamic GPS Orbital Navigator), will be powered on and begin position fixing.
4. The ground communication antennas will be deployed.

The position fixes collected by the Bevo-2 GPS unit will be transmitted to AGS4 using a cross-link antenna. Similarly, AGS4 will collect position fixes and transmit them to Bevo-2. During a future ground pass, the data from each satellite is downlinked to a ground station to confirm successful cross-link operation and to perform orbital analyses.

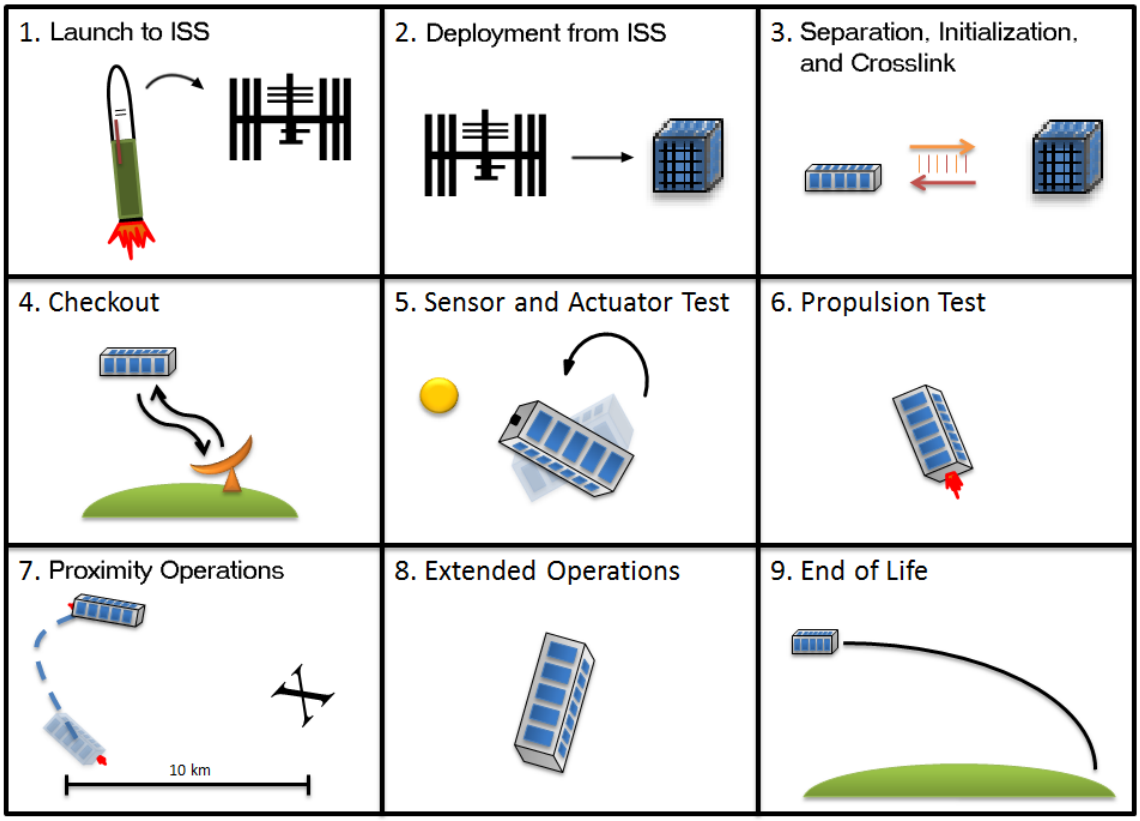

Figure 1.3: Overview of the mission objectives for the Bevo-2 craft (H. Kjellberg 2011).

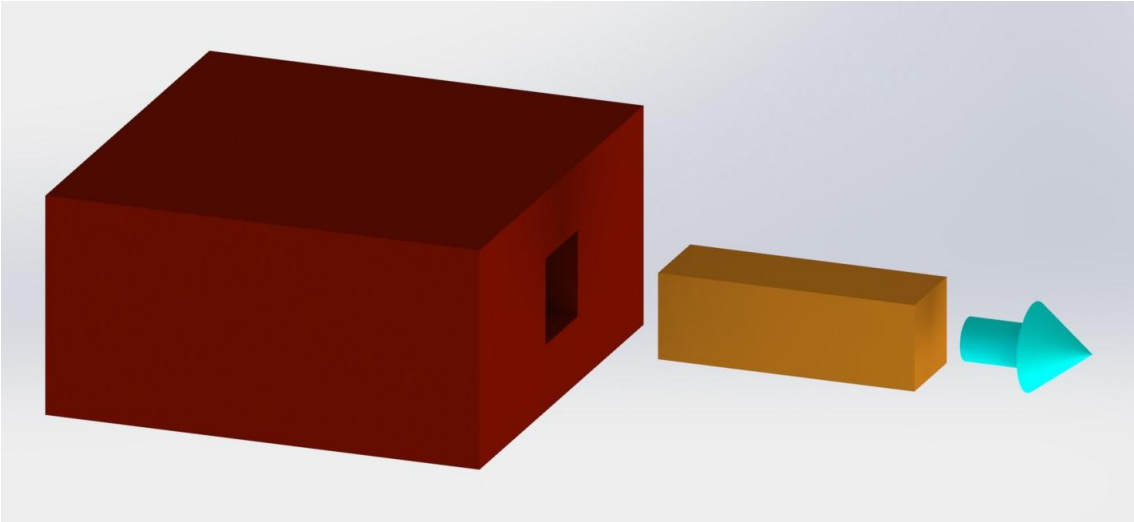

Figure 1.4: Illustration of Bevo-2 (right) separating from AGS4 (left).

Shown above are diagrams illustrating the primary mission objectives for the second LONESTAR mission.

1.2.3 Orbital Proximity Operations

To facilitate the communication of GPS coordinates between the two craft for as long as possible, it is desirable for the two craft to separate in such a way that they remain within transmitting distance for as long as possible. Chapter 2 of this document discusses the effect of ejection direction and velocity on the relative motion of the two vehicles and the optimum ejection direction given the expected environment and goals of this mission.

After separation, it will be desirable to bring the craft back within communication distance. Part of this goal can be accomplished by reducing the side-to-side motion of one craft relative to another by aligning their orbital planes. This can be done by firing the thruster aboard Bevo-2 using a method developed in Chapter 3. A portion of this procedure can be reused to form an algorithm to estimate the separation speed and direction when the two craft initially separate.

1.2.4 Mission Optimization

The Bevo-2 craft contains a low-g accelerometer which will be used to measure the change in velocity imparted by the expulsion of propellant. This device will provide the primary method to verify maneuvers, but due to the noise present in measurements the device will be somewhat imprecise. The acceleration provided by the thruster is anticipated to be on the order of thousandths of Earth's gravity (milli-g's) (Arestie, Lightsey and Hudson 2012), which will approach the resolution capabilities of the device. Since Bevo-2 will not be initialized until after deployment, this component will not be able to make measurements during the deployment from AGS4. To verify the magnitude and direction of the ejection maneuver, the GPS coordinates from both craft will be filtered to form orbital state estimates which can be differenced to produce an estimate of the ejection velocity. Chapter 3 introduces an orbital determination algorithm that can be used to identify the ejection velocity as well as supplement accelerometer measurements to verify thruster maneuvers.

Out-of-plane motion and perturbations to each orbit's eccentricity predominantly result in the oscillatory motion of one craft relative to another. Weeks to months into the mission, the thruster on Bevo-2 will be fired to space-qualify the design and to align the orbital planes of the two craft. This maneuver or set of maneuvers will reduce the relative motion in the out-of-plane direction of one satellite relative to the other. The latter portion of Chapter 3 details the procedure for choosing the time, direction and magnitude of such a maneuver, as well as an algorithm that can be used to verify the maneuver.

The primary driver of separation between each craft, and the cause for the loss of radio contact, is a discrepancy between their semi-major axes. The minimal quantity of

atmosphere present in LEO interacts with each spacecraft, slowing them down at different rates, into lower and lower orbits over time. The attitude of a spacecraft can be actuated to control the orbital decay over long time periods. The position of Bevo-2 is tracked in relation to AGS4. A trajectory is computed, and coordinated attitude maneuvers are conducted to align the craft within communication distance. The procedure explained in Chapter 4 details a process for creating a trajectory to align the craft within an assumed communication distance (150 km).

Following the plane-alignment procedures outlined in Chapter 3, a series of attitude maneuvers will be conducted to reduce the separation between the two craft. The attitude maneuvers will pull the craft together to enable wireless cross-communication. These maneuvers are detailed in Chapter 4. Whereas the procedures described in Chapter 3 are concerned with aligning the orbital planes of the two craft, Chapter 4 aims to simultaneously align their orbits and their positions within the orbit to enable sustained cross-link radio communications.

1.2.5 Previous Research

The work developed in this document serves as an extension of the work presented in "Examining Differential Drag Control in a Full System Simulation" (Lum 2011). This analysis developed an extended Kalman filter that utilized cross-communication of GPS data between craft in LEO to conduct coordinated attitude maneuvers. The algorithm demonstrated the ability to align craft separated by 50 km to within a few meters.

The work in this document extends the previous analysis by focusing on spacecraft deployment behavior, alignment of the orbital planes using a thruster, and

attitude maneuvers conducted beyond the range of cross-communication radios to align spacecraft in LEO.

1.2.6 Summary

Collectively, the contributions that are made in this thesis enable a series of maneuvers to be performed by Bevo-2 to accomplish the LONESTAR-2 mission objectives.

The goal of Mission 2 is to demonstrate fundamental capabilities that will be used in Mission 4 for full autonomous on-orbit rendezvous. If the maneuvers detailed in this document can be conducted successfully, this will be a large step towards the goal of reducing the risk inherent in Mission 3 and Mission 4.

The procedures and algorithms in this document are inspected within the context of LONESTAR Mission 2, but are generalizable to other missions conducted in the LEO environment. The thruster operations are conducted independently of attitude maneuvers and can be implemented independently in follow-on missions. The procedures developed in this document are applicable to missions that include satellite swarms. The primary application of this research is towards complete rendezvous of two spacecraft in LEO.

Chapter 2: Separation Analysis

2.1 Introduction

The goal for this analysis is to maximize the amount of time the two LONESTAR-2 satellites, the AggieSat4 nanosatellite (AGS4) and the Bevo-2 3U cubesat, remain within transmitting distance after Bevo-2 is deployed from AGS4. This will be accomplished by choosing a launch direction for the Bevo-2 ejection.

2.2 Scenario Summary

Due to the geometry of Low Earth Orbits, the maximum line-of-sight range for communication between the two satellites is 4,600 km. Additionally, the distance for a 10 dB drop is 147 km. However, to allow a robust contingency margin, maximum range thresholds of 14.7 km and 60 km were also inspected.

The AGS4 satellite will be launched off the International Space Station (ISS), most likely in late 2014. The ISS has historically varied between an altitude of 330 km to 410 km with a nearly circular orbit. However, due to the solar maximum, the atmosphere is abnormally excited, maximizing the drag on spacecraft. For this reason the ISS has been moved to a higher altitude and is anticipated to be maintained in the 390-430 km range. Approximately a week later, Bevo-2 will be launched from AGS4 at a velocity of 0.8 m/s, with a tolerance to be determined. The precision of the launch direction of AGS4 is unknown.

The AGS4 satellite weighs 52 kg with the ISIPOD installed and without Bevo-2. Bevo-2 weighs 4 kg not including the ISIPOD. Before deployment, the configuration with AGS4 loaded with Bevo-2 weighs 56 kg. Bevo-2 is designed to be a rectangular prism with the dimensions 10 x 10 x 34 cm, whereas AGS4 is 34.5 x 61 x 61 cm (12 x 24 x 24 in).

2.3 ORBITAL DYNAMICS - FUNDAMENTAL

Bevo-2 weighs significantly less than AGS4. To a first approximation, the ejection maneuver can be treated as an impulse that only affects Bevo-2. However, all simulations of the Bevo-2 and AGS4 separation were conducted with the impulse affecting the trajectory of both crafts.

An orbit reference frame is set up with three vectors: A velocity vector (forward), an orbit-normal vector (left) and a co-normal vector (completing the orthogonal triad) with an origin set at the center of mass of the satellite being inspected.

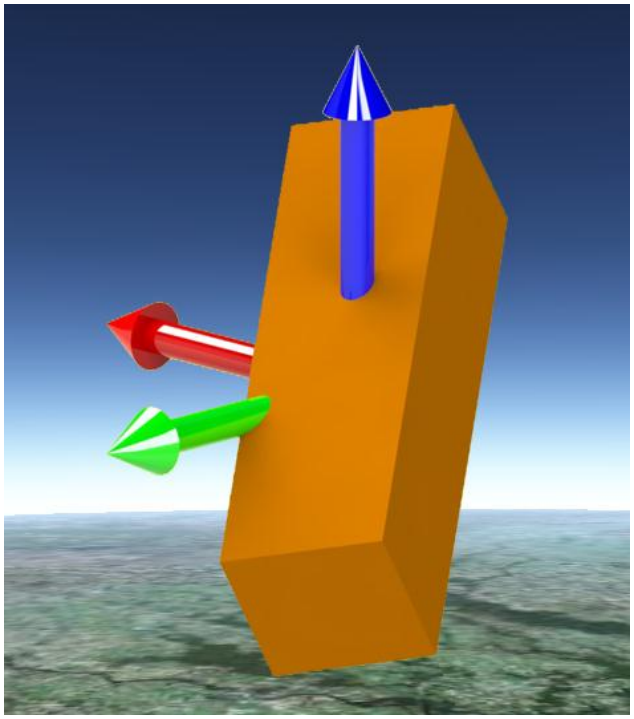

Figure 2.1: An illustration of Bevo-2 with coordinate axes along the X velocity vector (red), Y orbit normal (green) and Z co-normal (blue).

When an impulse is applied to the satellite in either of the orbit-normal directions, then the inclination and/or right-ascension orbital elements are changed. When an

impulse is applied in the co-normal directions, the eccentricity of the orbit is changed. In the previous two cases, the angular momentum of the orbit is not significantly changed and thus the orbital period is unchanged. When an impulse is applied toward or against the direction of motion, the semi-major axis is increased or decreased, altering the orbital period. Below are illustrations of each type of maneuver.

The following illustrations refer to the trajectory of a spacecraft before and after a maneuver in the defined coordinate system. The concepts developed below will then be used to describe the separation of the AGS4 and Bevo-2 satellites.

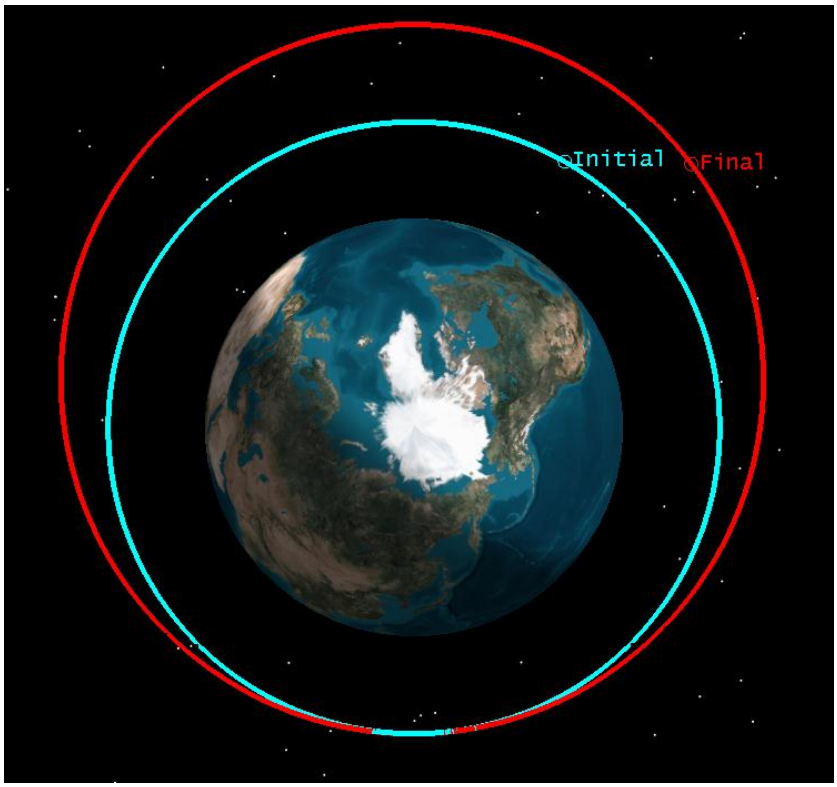

Figure 2.2: An exaggerated example of a burn in the direction of motion changing the semi-major axis and the period of the orbit. The initial orbit is circular (blue) while the final orbit is elliptical (red).

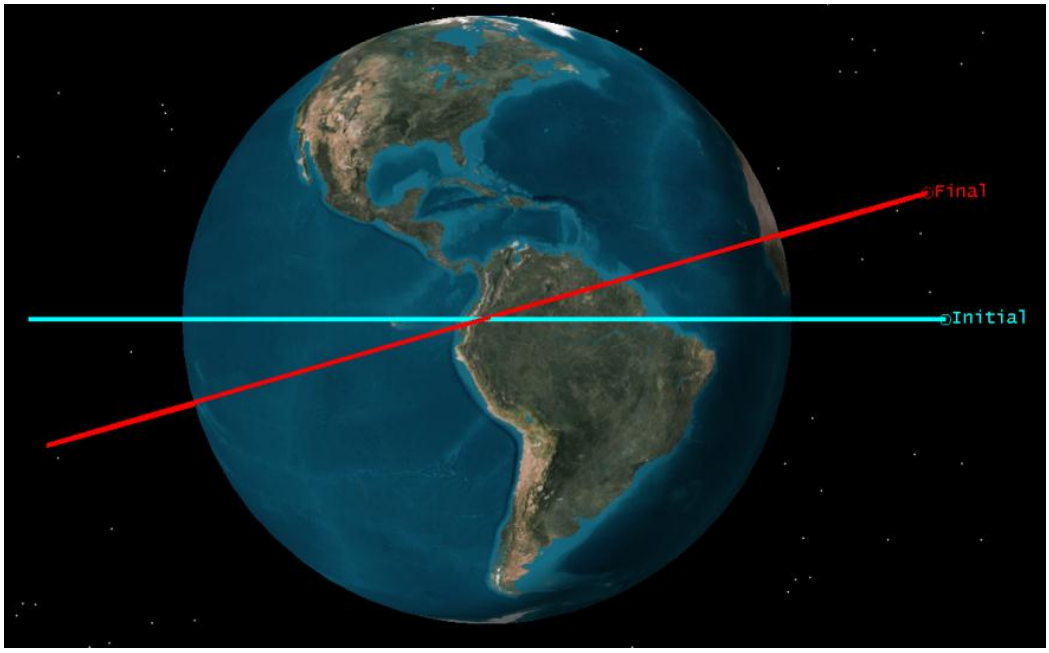

Figure 2.3: An exaggerated example of an orbit-normal burn conducted when crossing the equator which changes the inclination from the equatorial orbit (blue) to the inclined orbit (red).

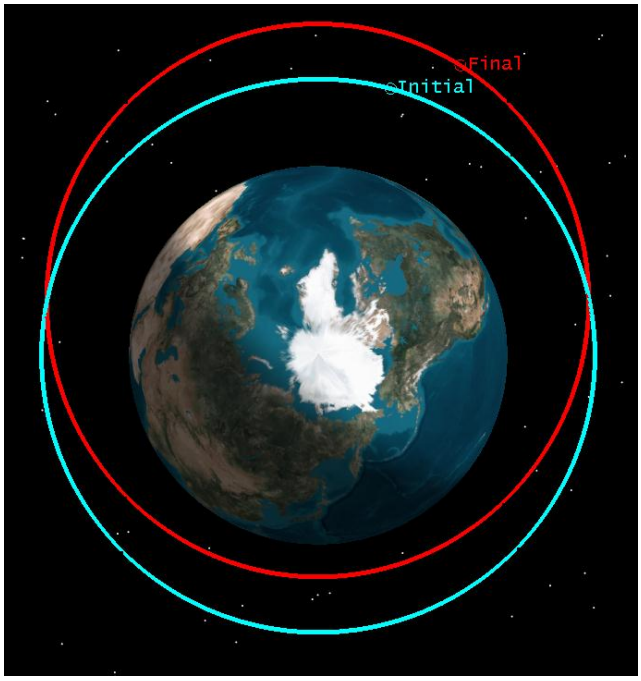

Figure 2.4: An exaggerated example of a co-normal impulse which changes the eccentricity of the orbit from the initial circular orbit (blue) to the elliptical final orbit (red).

While the above figures depict exaggerated maneuvers to demonstrate the separation concept, the calculations below refer to maneuvers conducted at a 400 km altitude circular orbit with a 0.8 m/s impulse directed in the specified direction.

Orbit Maneuver Direction	Semi-major Axis Change (m)	Inclination Change (degrees)	Eccentricity
In/Against Direction of Motion	1.4	0	2.0 E-4
Out of Plane	7.3 E-5	6.8 E-3	1.0 E-8
Co-normal	7.3 E-5	0	1.0 E-3

Table 2.1: The change in the orbital elements after a 0.8 m/s maneuver from a circular orbit, at an altitude of 400 km.

The period of the orbit is related to the three-half power of the semi-major axis. Any significant change in orbital period will impact the separation rate of the two spacecraft and will have a detrimental effect on the communication channel. The semi-major axis will change in all three ideal scenarios because the velocity is being increased in each case as depicted in Table 2.1. This change in velocity has the effect of growing the separation distance over each orbit.

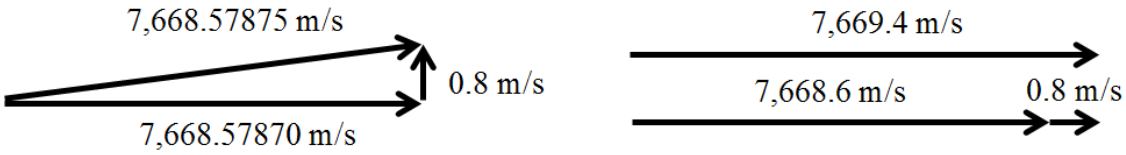

Figure 2.5: Change in velocity for an ideal Co-normal maneuver or an Out of Plane maneuver (left). Change in velocity for an ideal maneuver in the Velocity Direction (right).

The effect each of these maneuvers over a 24 hour period is illustrated in the following plots. The relative position of the spacecraft after the maneuver is plotted against the initial satellite trajectory. The initial trajectory is used as the origin. Only a simplistic two-body model is used; perturbations due to drag and J2 effects are neglected in Figure 2.6, Figure 2.7 and Figure 2.8.

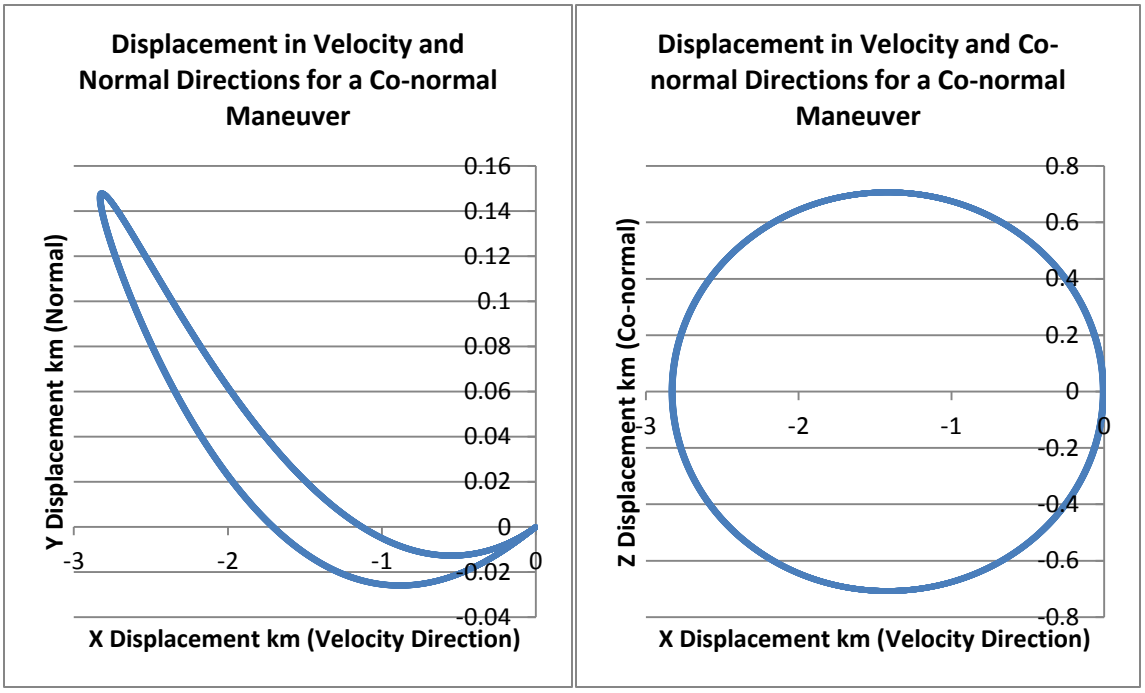

Figure 2.6: Relative displacement in over one day after a Co-normal maneuver.

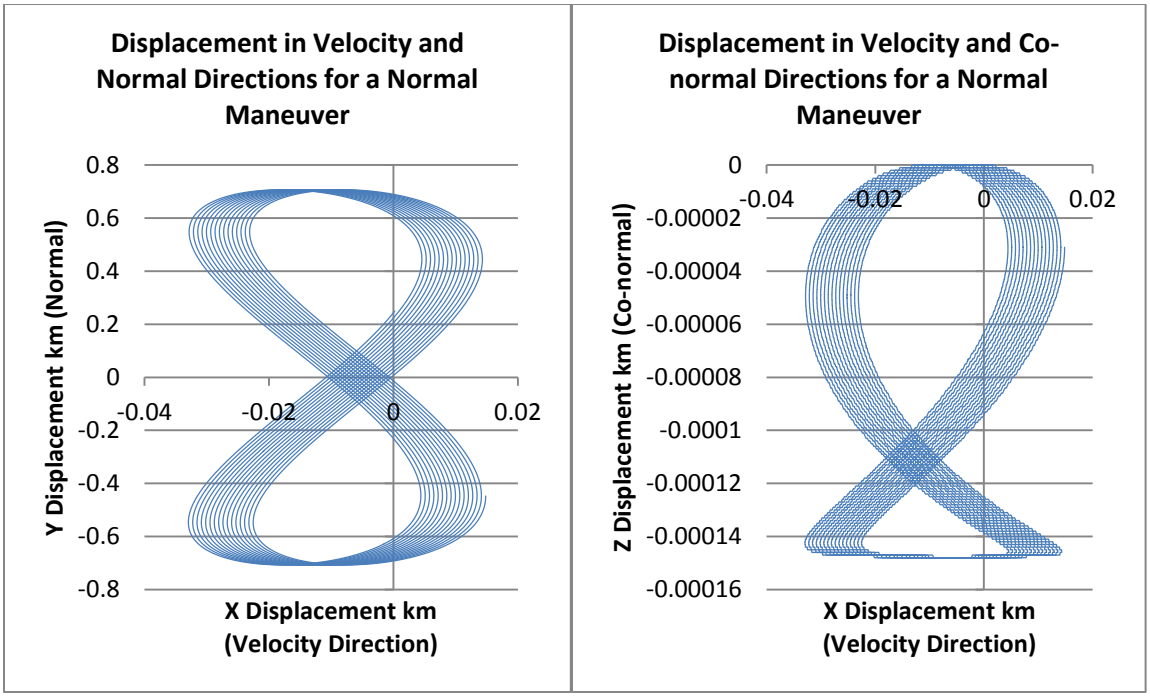

Figure 2.7: Relative displacement over one day after a Normal Maneuver.

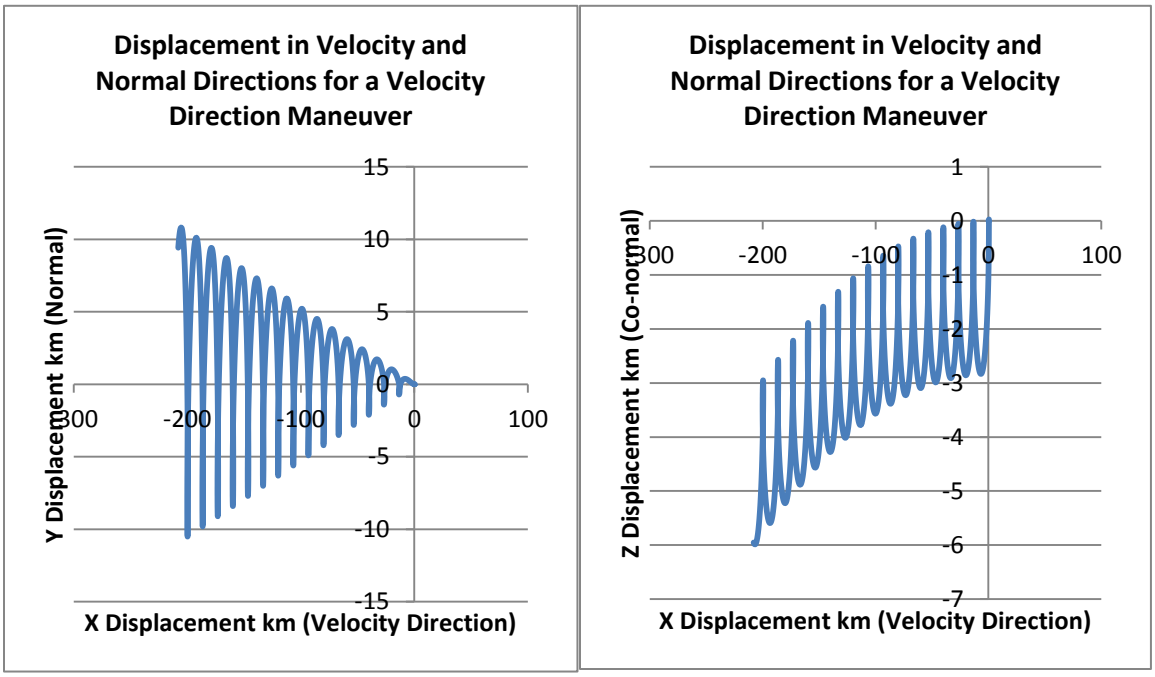

Figure 2.8: Relative displacement over one day after a Velocity Direction Maneuver.

When the impulsive maneuver is fired away from the velocity vector, the simulation software briefly alters the coordinate axes, thus the raw output normal and co-normal maneuvers show spikes briefly after deployment in the two-axis breakdown, but the magnitude of the separation appears smooth as expected. Thus the trajectory immediately following deployment is omitted from the normal and co-normal plots and they do not show the initial separation that passes through the origin.

From the figures above, the normal and co-normal maneuvers alter the orbital period so that the separation accumulates ever so slightly in the velocity direction over the span of a day, gaining as much as three dozen meters over the simulation run. This separation is due to the slight modification to the semi-major axis listed in Table 2.2.

Orbit Maneuver Direction	Semi-major Axis Change (m)	Inclination Change (degrees)	Eccentricity
In/Against Direction of Motion	1.4	0	2.0 E-4
Out of Plane	7.3 E-5	6.8 E-3	1.0 E-8
Co-normal	7.3 E-5	0	1.0 E-3

Table 2.2: Orbital element change as a function of maneuver.

As seen in Table 2.2, the co-normal maneuver introduces a large oscillation in the Velocity direction and thus the accumulation of the separation in the velocity direction is

harder to discern than in the Orbit-Normal plot. A sub-plot for the co-normal maneuver zoomed-in around the origin is shown in Figure 2.9.

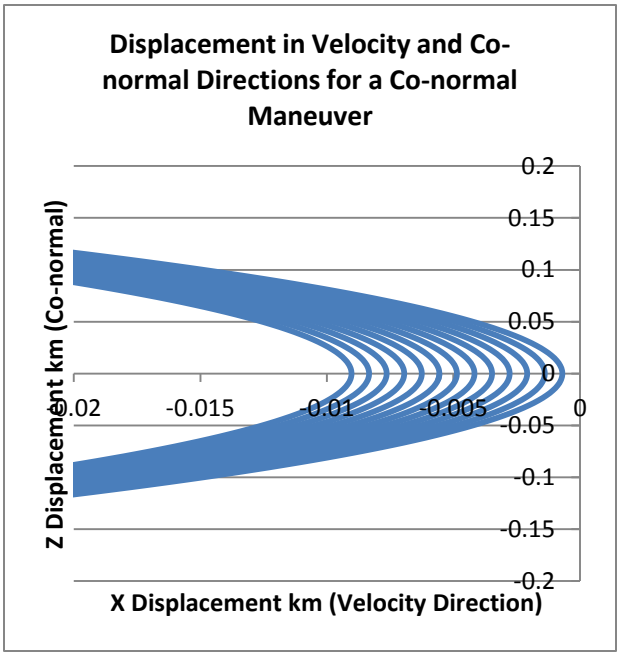

Figure 2.9: Detail of the origin for a Co-normal maneuver.

The accumulation of the separation in the velocity direction is significant in the Velocity Direction plot. In this scenario, the period of the orbit has been altered much more than in the other cases. When speaking about identical spacecraft starting from identical orbits that must stay in close proximity, it is desirable to avoid ejection maneuvers that fire in or against the direction of motion.

However, for the LONESTAR-2 mission, the AGS4 satellite is much more massive and has a larger cross-sectional area than the Bevo-2 spacecraft, necessitating further analysis due to the effects of drag.

2.4 Orbital Dynamics - In Depth

Three major orbit perturbations considered in classical orbital simulators are the J2 effect, three-body effects and atmospheric drag. The J2 perturbation, due to the oblateness of the Earth, and the three-body effect, due to the orbit of the moon, have the effect of applying a torque to the orbit and rotating the orbit's right ascension of the ascending node (RAAN). At a 400-km altitude circular orbit with an inclination of 51.6 degrees (when launched from the ISS, the inclination is maintained in the new orbit), the RAAN precesses around the Earth approximately 5 degrees a day (which is due almost entirely to the J2 perturbation). However, because the two satellites are orbiting at nominally the same altitude and inclination, the J2 effects precess the RAAN of both orbits at the same rate, and are neglected when looking at the relative positions of one satellite in regard to another.

Drag is a major factor in LEO orbits. The force due to drag is traditionally calculated thusly:

$$F = m * a = \frac{1}{2} * \rho * v^2 * C_d * A \tag{2.1}$$

To compare the effects of drag on each spacecraft, the equations of drag must be compared. Rearranging yields the following:

$$a = \frac{1}{2} * \rho * v^2 * C_d * A/m \tag{2.2}$$

The goal is to equate the acceleration due to drag between the two satellites:

$$\left(\frac{1}{2} * \rho * v^2 * C_d * A/m\right)_{AGS4} = \left(\frac{1}{2} * \rho * v^2 * C_d * A/m\right)_{Bevo2} \quad (2.3)$$

The two satellites will be in approximately the same orbit, meaning their velocities will be nominally equal. The density of the air will be equal at equal altitudes:

$$\left(\frac{1}{2} * C_d * A/m\right)_{AGS4} = \left(\frac{1}{2} * C_d * A/m\right)_{Bevo2} \quad (2.4)$$

The drag coefficient (C_d) is traditionally approximated at 2.2 for spacecraft in LEO, although it may vary between 1.9 and 2.6 (Tribble, p. 86). Assuming the C_d values are equal between the two spacecraft yields the following:

$$(A/m)_{AGS4} = (A/m)_{Bevo2} \quad (2.5)$$

Thus, for the effects of drag to be equated, the two craft must match their area-to-mass ratios.

	Bevo-2			AGS4		
	Minimum	Tumble	Maximum	Minimum	Tumble	Maximum
Mass (kg)	4	4	4	52	52	52
Average Area (cm^2)	100	339	491	1858	3858	4551
Area-to-mass ratio (cm^2/kg)	25	85	123	36	74	88

Table 2.3: Mass and area properties of Bevo-2 and AGS4.

The two craft have overlapping area-to-mass ratios. By changing the attitude (how much area is facing into the wind), Bevo-2 can change its area to mass ratio between 25 cm^2/kg and 123 cm^2/kg. Similarly AGS4 can alter the area to mass ratio between 36 cm^2/kg and 88 cm^2/kg. It can be seen that Bevo-2 is more maneuverable than AGS4 in this regard. This fact can be used to keep the two craft in close proximity after separation by controlling Bevo-2's attitude alone.

By matching the area-to-mass ratios, the two craft can potentially be kept within a 14.7 km distance for multiple weeks or longer. However, the attitude control system on Bevo-2 is not anticipated to be initialized for a minimum of two days after Bevo-2 deployment, and even then various attitude tests will be conducted for a period of seven weeks. Thus a deployment procedure that employs a pre-determined routine to maximize in-range time without active control of Bevo-2 will be developed below.

An additional constraint has been imposed on deployment. When AGS4 deploys Bevo-2, AGS4 will keep the deployment face pointed at Bevo-2 in order to capture

images of the separation. Thus once a launch direction has been chosen, AGS4 will be constrained in the amount of cross-sectional area that can face into the ram direction immediately following deployment.

The design specifications for the Bevo-2 craft dictate less than a 5-degree pointing precision maintained over the span of one 90-minute orbit when the attitude control system is active. If the same specification is applied to the AGS4 craft, the deployment may still impose a rotation rate which could change the craft's attitude by 90 degrees over the span of a day. Additionally, the force of drag may not act along the center of mass (which may be offset from the craft's center of pressure by as much as 2 cm according to the Cubesat standard), creating a torque on the craft on the order of 0.5 mNm (Kjellberg, 2012). However, additional mass will be added to the craft prior to delivery to attempt to place the center of mass at the geometrical center of the craft.

An additional consideration to be taken into account is the rotation of AGS4 that is then transferred to Bevo-2 during deployment. There are three axes (and combinations thereof) that AGS4 may be rotating about during ejection. In the ideal case, AGS4 is rotating with the Earth. When Bevo-2 is deployed, any initial rotation of AGS4 will be conserved. Additionally, launching in any manner other than through the center of mass of the two vehicles will impose a torque on the system, however briefly, resulting in residual rotation.

A major contributor to attitude drift over time is antenna deployment. The UHF/VHF antenna on the top small face of the satellite has four tendrils that are released sequentially. The wires are not released through the center of mass, they are different lengths and masses, and they are not released in any symmetric manner (each is extended

sequentially). Once the antenna deploys, the craft will change its attitude and attitude drift rate substantially.

Antenna	UHF	VHF
Length (cm)	18	55
Approximate Mass (g)	2	5

Table 2.4: Antenna masses and lengths.

Considering cross-sectional changes as a function of time and launch direction, a first approximation simulation was conducted as if Bevo-2 were "tumbling". Here, "tumbling" is treated as any case where the craft rotates by 90 degrees or more over the span of 24 hours, enough that the attitude at any given point in time is unpredictable after separation. The simulation software Systems Tool Kit (STK) was supplied an initial cross-sectional area that remained constant and equaled the average cross-sectional area of the craft over all possible attitudes.

This average cross-sectional value was calculated via numerical integration. Since only three faces can be visible to the ram direction at any point in time, and the craft is symmetric in three axes, only three faces that shared a corner were modeled. The corners of each face were represented as points in three-space. The points were then rotated in the azimuth and elevation directions in order to represent each possible attitude. The points were projected onto a plane (the plane that faces into the wind) by removing

the x-component of the points, creating a 2D representation of the corners. The area of each face was found by taking the 2D cross product of the diagonal vectors on each face. The areas of these three faces were then added up to find a cross-sectional area for that particular attitude. An average was found across all possible attitudes. The average tumbling values for both craft are presented in Table 2.3

Using this method, the average cross-sectional area of Bevo-2 is found to be 339 cm^2 (area-to-mass ratio: 85 cm^2/kg). If Bevo-2 is truly tumbling, AGS4 will be just able to match the area-to-mass ratio by maximizing the cross-section facing into the wind. Thus for deployment, it is recommended that AGS4 maximize its cross-sectional area as much as possible to attempt to match Bevo-2's area-to-mass ratio, and thus orbital decay rate. AGS4 can maximize the cross-sectional area by pitching the corner of the craft 54 degrees away from the direction of motion as shown in Figure 2.10. This results in a cross-sectional area of 4,551 cm^2 (area-to-mass ratio: 88 cm^2/kg).

Note that the AGS4 does not need to pitch down to maximize its area prior to separation. That is, there are not attitude constraints on AGS4 before Bevo-2 is deployed. Rather, it is only once the craft have separated that AGS4 should attempt to maximize cross-sectional area facing into the direction of motion.

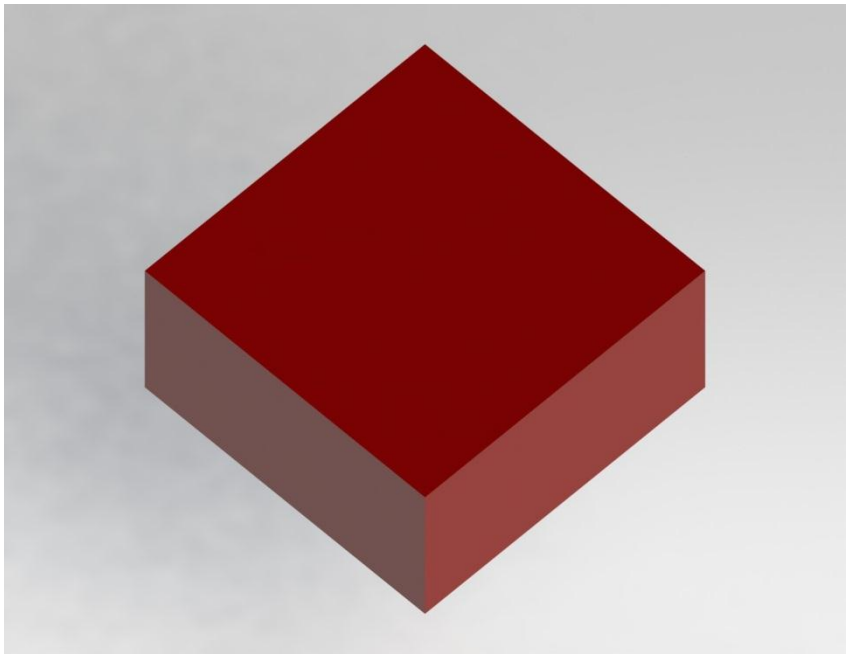

Figure 2.10: Visualization of the AGS4 craft with a corner pitched down 54 degrees to maximize cross-sectional area. The direction of motion is towards the viewer.

When these assumptions are taken into account, a heat map of time-in-range can be created as a function of launch direction as shown in following figures.

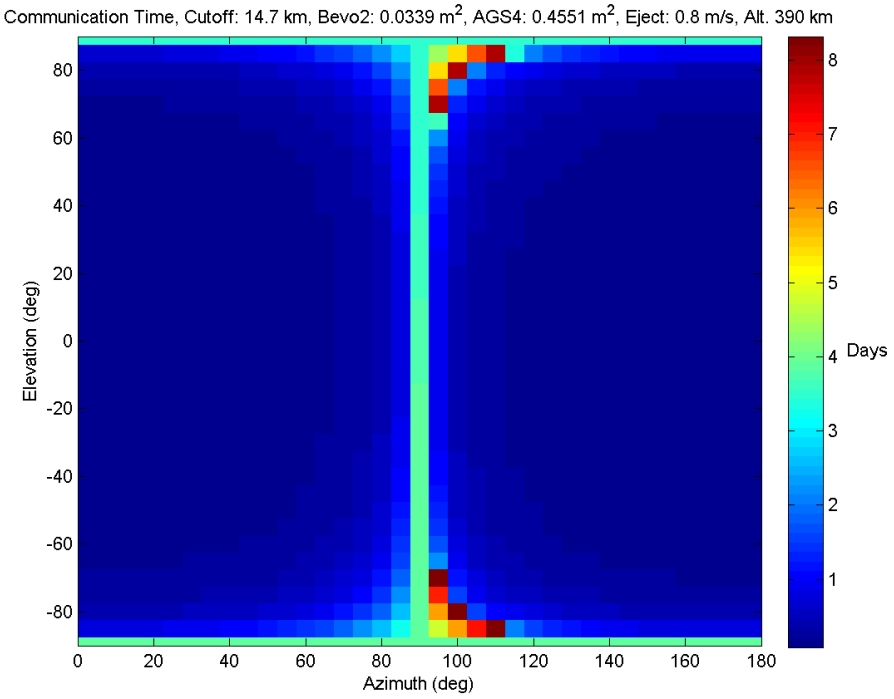

Figure 2.11: Heat map representing the cross-link time with a cut off of 14.7 km when launched from a circular orbit at 390 km.

The right of the heat map, 180 degrees azimuth, represents ejection opposite the velocity vector. The left side represents ejection in the forward direction. The vertical axis represents the elevation of the ejection maneuver (the bottom of the plot represents ejection of Bevo-2 towards the Earth). This is a projection of a single hemisphere onto a 2D plot.

The map was vertically symmetric about the 180 degrees azimuth (the full plot is not shown in this report), indicating that ejection out of plane in either direction is equivalent, thus only the ejections into the left hemisphere were simulated. Additionally, the plot is mostly symmetric about the horizontal as well, indicating a launch in the zenith direction has relatively the same characteristics as a launch in the nadir direction.

A region of light green is seen proceeding down the center of the plot, indicating that launching in any direction perpendicular to the velocity vector will ensure a relatively-long communication time span. There are patches of deep red, indicating a long time in-range, at roughly ±80 elevation and 110 degrees azimuth. Because these simulations were conducted with a 339 cm^2 Bevo-2 cross-sectional area, the craft has slightly less relative drag than AGS4, meaning it is beneficial to launch slightly away from the velocity vector.

The 14.7-km range limit is a rough worst-case scenario approximation. According to theory, the 10 dB drop off limit occurs at 147 km. When considering this alternative range limit, the Bevo-2 craft spends considerably more time in-range.

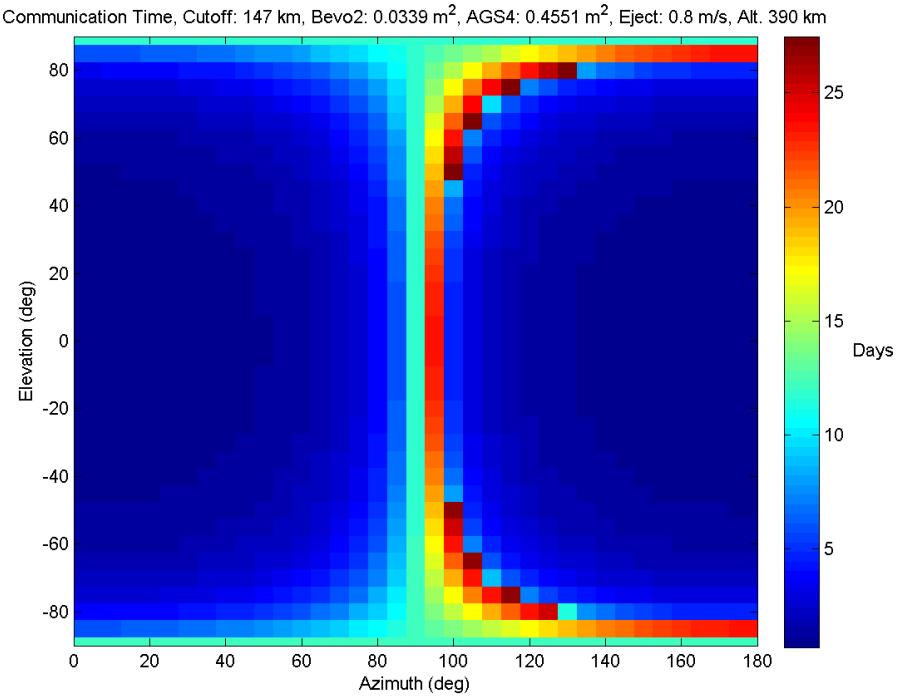

Figure 2.12: Heat map representing the cross-link time with a cut off of 147 km when launched from a circular orbit at 390 km.

The AGS4 craft will attempt to maintain one face pointed toward the location of Bevo-2 in order to capture images. Thus the cross-sectional area cannot be guaranteed at any particular value. In order to gain a perspective on the potential outcomes after ejection, simulations were run comparing the separation time when AGS4 minimized the cross-sectional area rather than maximized it.

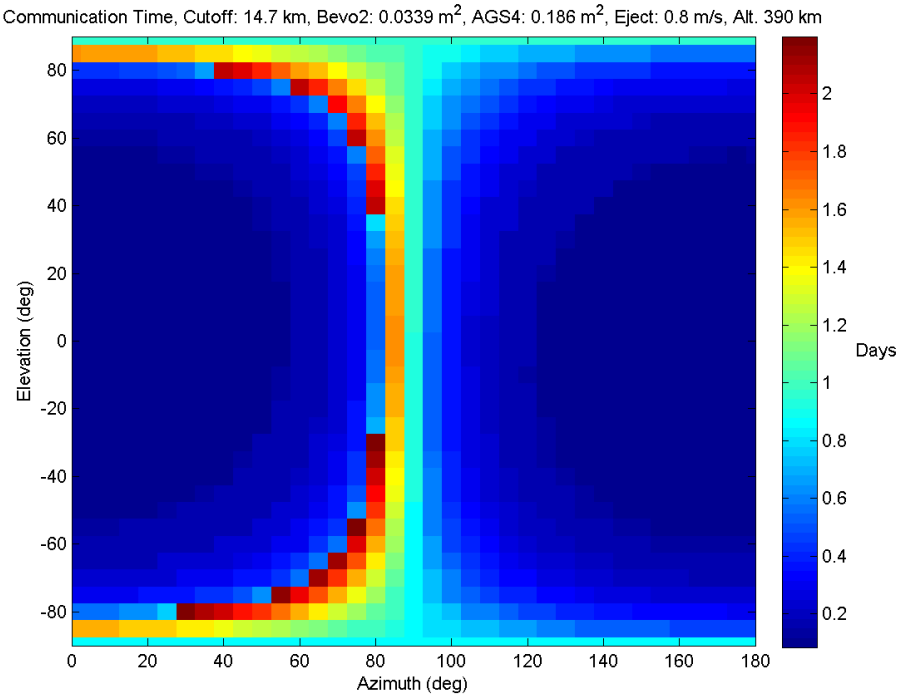

Figure 2.13: Heat map representing the cross-link time with a cut off of 14.7 km when launched from a circular orbit at 390 km. The cross-sectional area of the AGS4 craft is simulated at 1,860 cm^2.

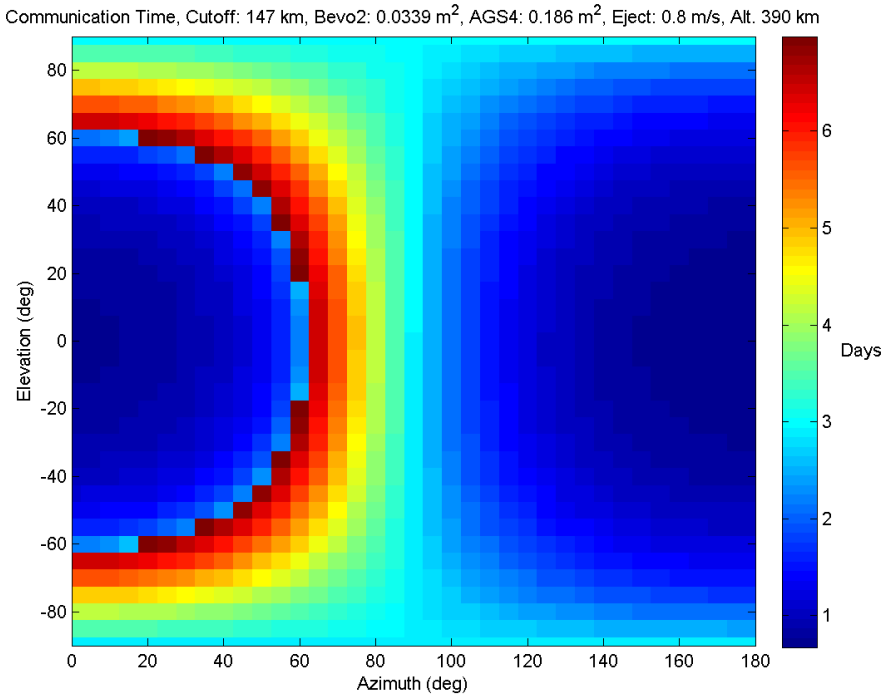

Figure 2.14: Heat map representing the cross-link time with a cut off of 147 km when launched from a circular orbit at 390 km. The cross-sectional area of the AGS4 craft is simulated at 1,860 cm^2.

Given that the optimum launch angle and time-in-range is a function of the communication cut-off distance, a tradeoff was made between a conservative number that would ensure communication and a larger value that would enable a longer communication time. A middle-ground case is considered with a cut-off distance of 60 km and AGS4's area is maximized, the results are presented below:

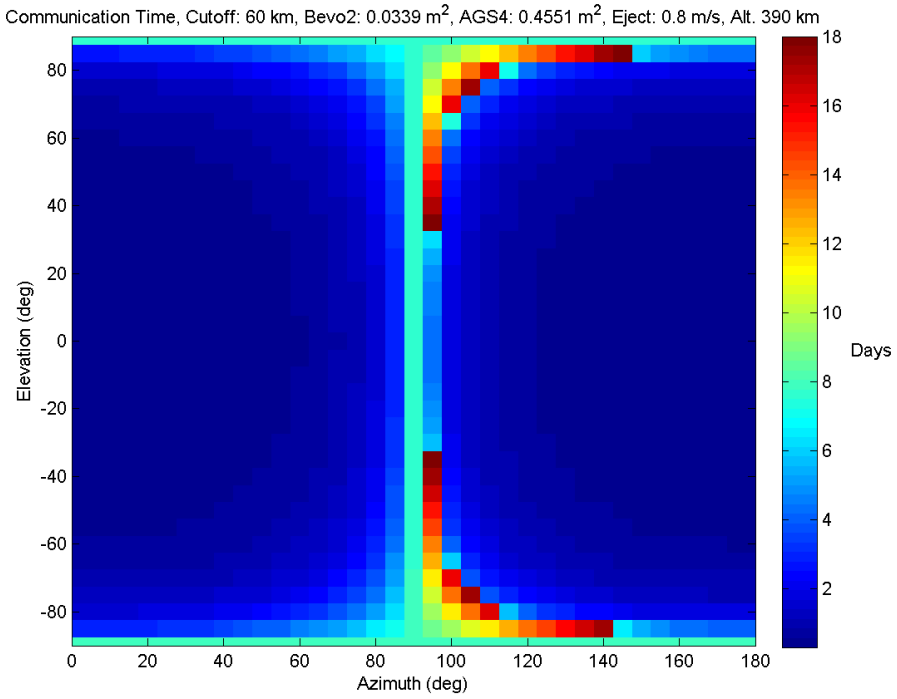

Figure 2.15: Heat map with a 60 km cut-off distance.

The AGS4 craft will be ejected from the ISS, which has historically varied in altitude from 330 km to 410 km in a nearly circular orbit. However, because the sun is passing through a solar maximum, and will continue to do so for the next few years, the ISS has been raised to a higher altitude orbit (400 km at the end of 2012). This orbit will be maintained for some time to reduce drag, and thus orbital decay, during the solar maximum. The previous simulations were conducted at a 390-km altitude. If the ejection instead occurs at 430 km, drag is reduced on both spacecraft, increasing the distance Bevo-2 travels away when launched in the velocity direction.

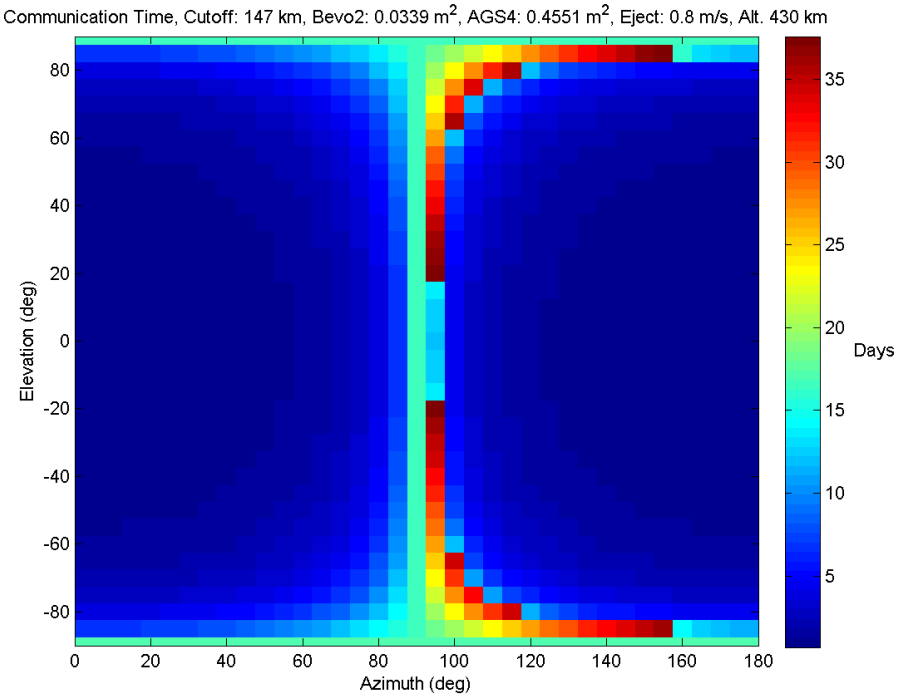

Figure 2.16: Communication time at 410 km altitude with a cut-off distance of 147 km.

However, since a 60-km cut-off distance is the favored constraint distance, the communication time is shown in Figure 2.17 at 430 km altitude:

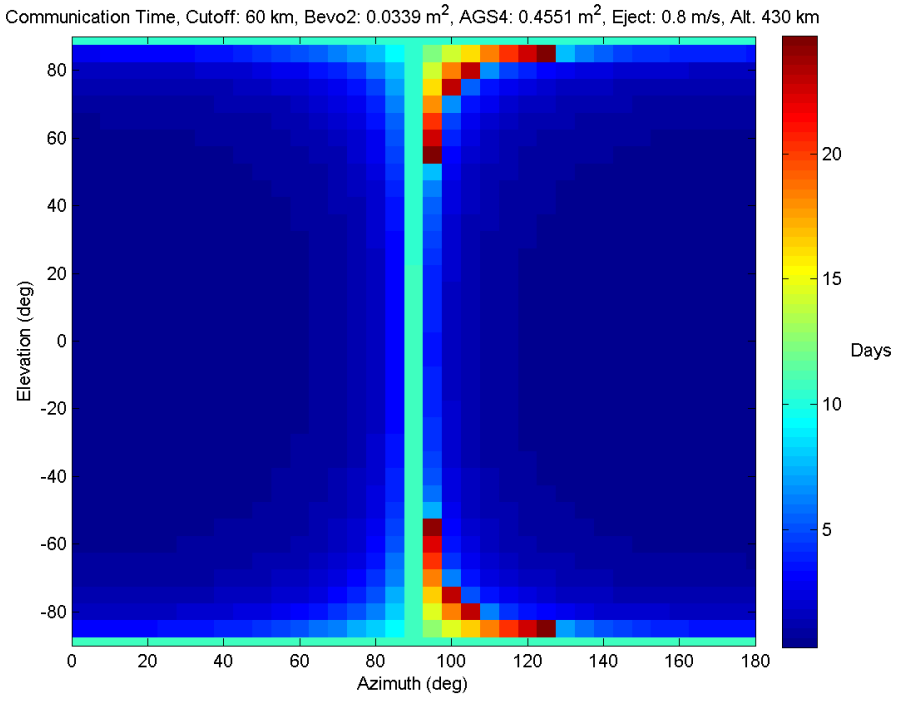

Figure 2.17: Communication time at 410 km altitude with a cut-off distance of 60 km and AGS4 has maximized its area at 411 cm^2.

The previous cases have looked at the scenario where AGS4 maximizes its area. If the craft instead minimizes its area, the optimum launch angle is approximately unchanged as seen in Figure 2.18:

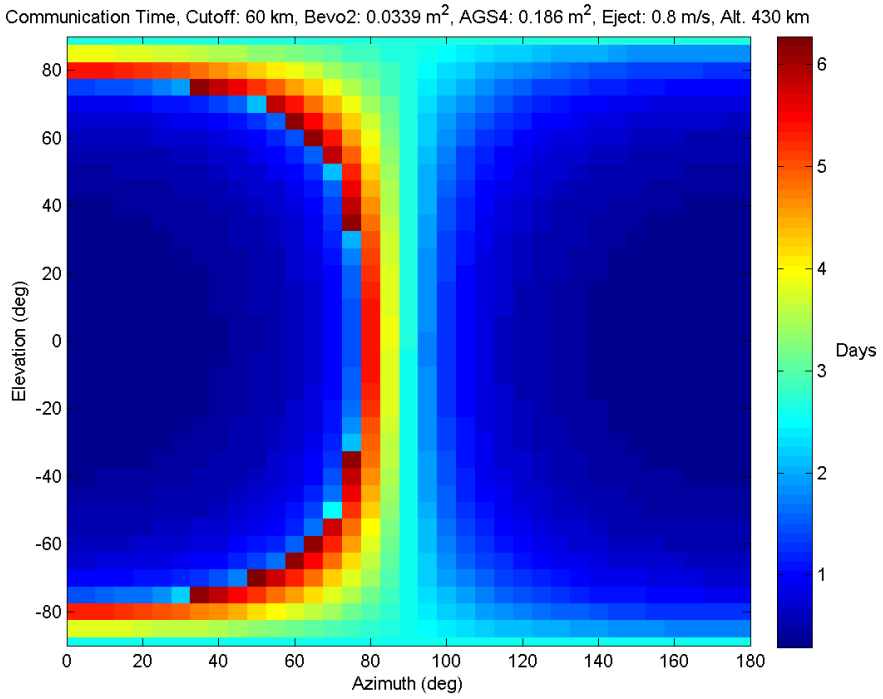

Figure 2.18: Communication time at 410 km altitude with a cut-off distance of 60 km and AGS4 has minimized its area at 411 cm^2.

The optimum azimuth launch angles are summarized in the following table. Because the optimum launch direction roughly lies in a ring around the velocity vector, a single metric is used below: the offset from the ram vector. This value represents the angle between the velocity vector and the launch vector. The data shows trends across launch altitude and across communication cut-off distance. These trends are not represented perfectly due to the resolution of the simulations conducted.

Altitude (km)	COM Cut-off (km)	Separation Time (days)	Offset from Ram Vector (degrees)
390	14.7	2-8	81-92
	60	4-18	72-98
	147	7-27	62-96
410	14.7	2-10	83-92
	60	5-21	75-94
	147	8-31	67-95
430	14.7	2-11	84-91
	60	6-24	77-92
	147	9-37	70-94

Table 2.5: Optimum azimuth and elevation launch angle as a function of altitude, cut-off distance and AGS4 cross-sectional area.

In Table 2.5: Values are presented as a range based on the cross-sectional area of AGS4 facing into the wind which varies between 0.186-0.4551 m^2.

It is recommended that Bevo-2 be launched perpendicular to the ram vector and that AGS4 maximize the cross-sectional area facing into the wind for as long as possible following deployment until AGS4 gains attitude control. This will maximize the time Bevo-2 spends in close proximity to AGS4, allowing the communication channel to be used most effectively and to minimize propellant use and mission time for later rendezvous.

2.5 SENSITIVITY ANALYSIS

Given the chosen ejection angle, a sensitivity analysis will now be conducted. Two cases will be inspected: one ejecting away from Earth in the Zenith direction, the other 20 degrees rotated about the ram vector (thus pointing between the zenith and orbit-normal directions). The former case would ensure the craft remain in the same orbit plane post-ejection (which would minimize thruster actuations later in the mission); the latter case would be closer to maximizing the time-in-range. For these cases, the cut-off distance was chosen to be 50 km, Bevo-2 was assumed to be tumbling while AGS4 maximized the cross-sectional area, the ejection speed was 0.8 m/s and the initial orbit altitude was 410 km.

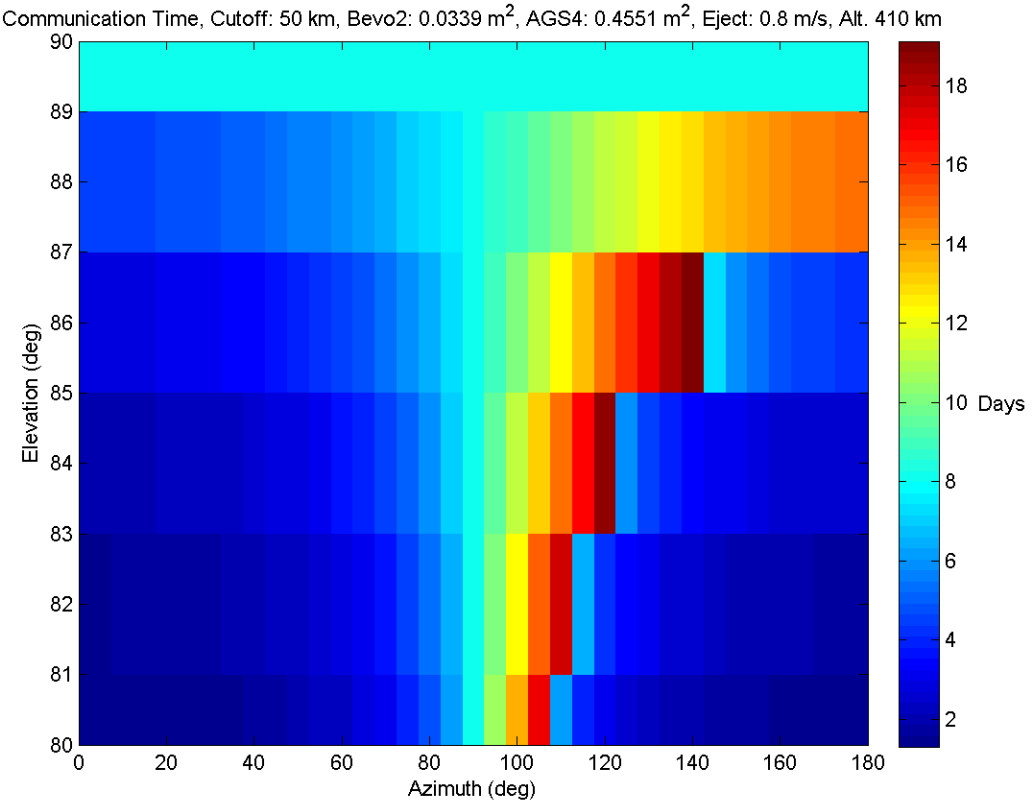

Figure 2.19: Communication time at 410 km altitude with a cut-off distance of 50 km, AGS4 has maximized its area and Bevo-2 is tumbling. This projection focuses on ejection immediately in the vicinity of a Zenith ejection angle.

Similarly, an analysis was conducted about an angle 20 degrees away from Zenith, towards the out-of-plane direction:

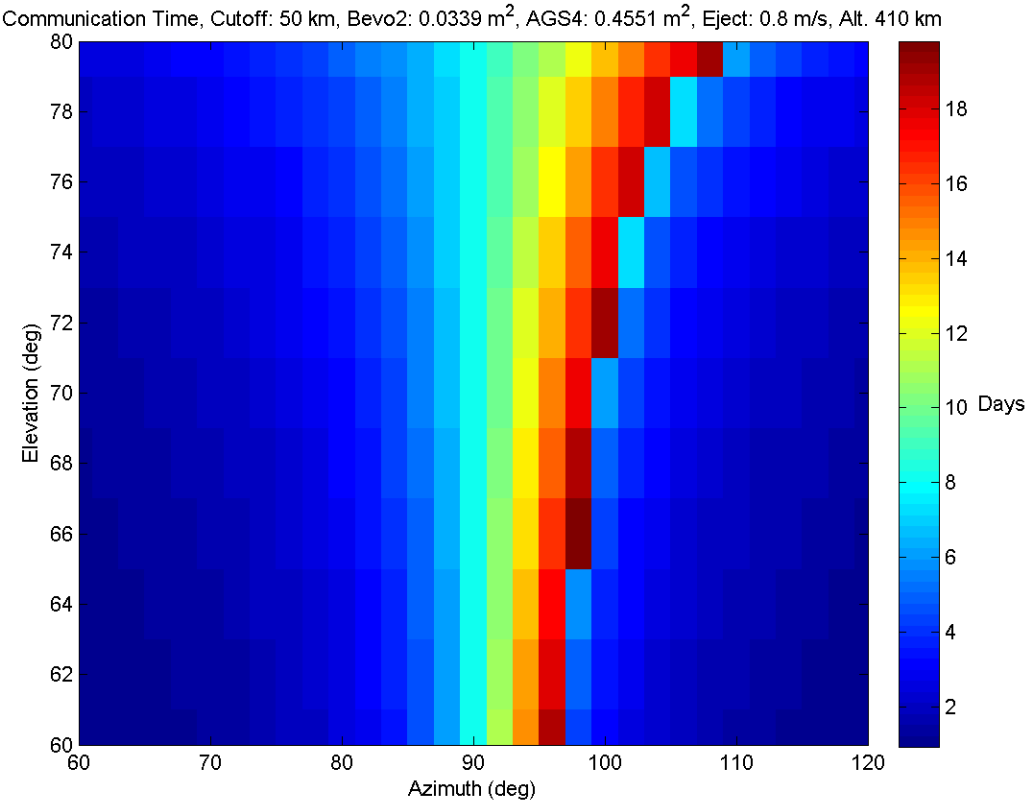

Figure 2.20: Communication time at 410 km altitude with a cut-off distance of 50 km, AGS4 has maximized its area and Bevo-2 is tumbling. This projection focuses on ejection 20 degrees away from the Zenith in the Orbit-Normal direction.

Using this second case as a baseline, several parameters can be changed. By altering the altitude from 410 km to 390 km, the maximum time-in-range is dropped from 19 to 16 days.

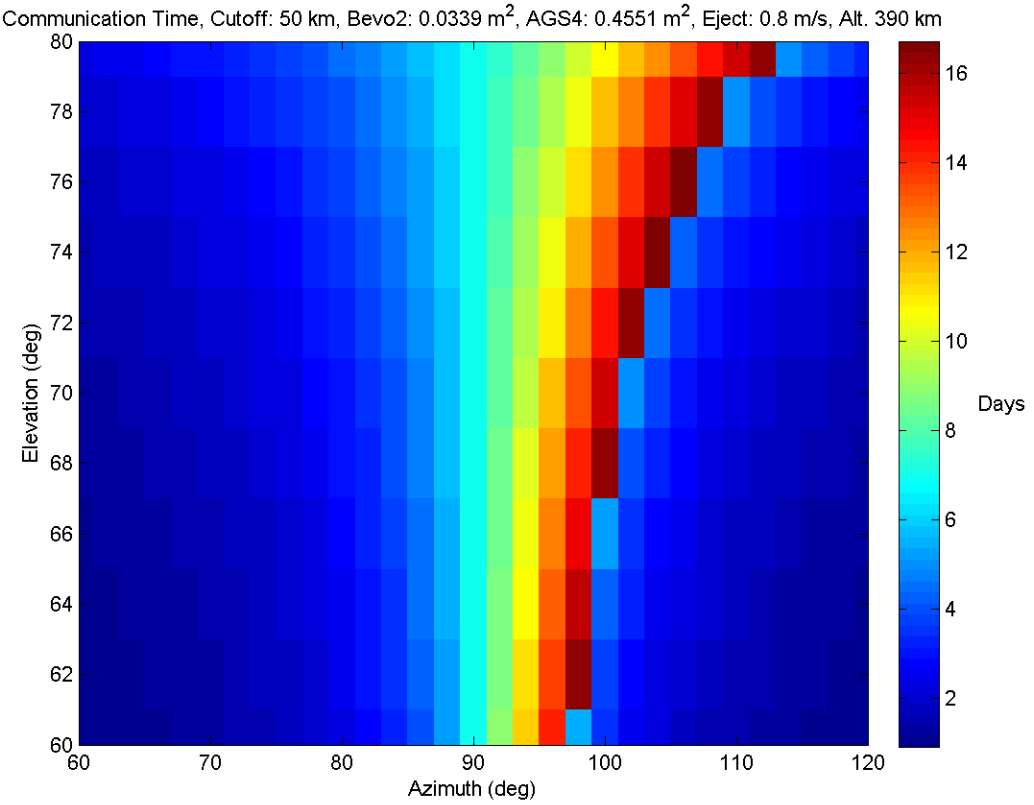

Figure 2.21: Communication time at 390 km altitude with a cut-off distance of 50 km, AGS4 has maximized its area and Bevo-2 is tumbling.

Returning to the baseline and increasing the ejection velocity from 0.8 to 1 m/s alters the maximum time in range by a few hours.

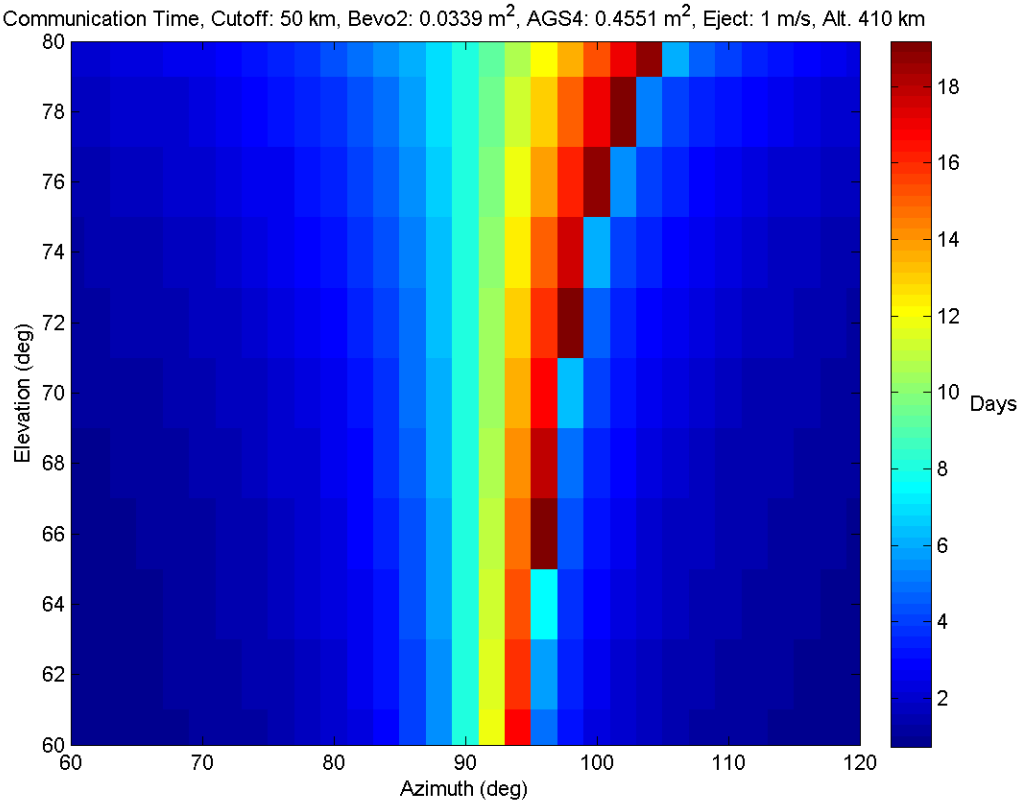

Figure 2.22: Communication time at 410 km altitude with a cut-off distance of 50 km, AGS4 has maximized its area and Bevo-2 is tumbling. Ejection speed has been increased to 1 m/s.

Starting from the baseline and increasing the communication cutoff distance from 50 to 60 km increases the maximum time-in-range from 18 days to nearly 21 days.

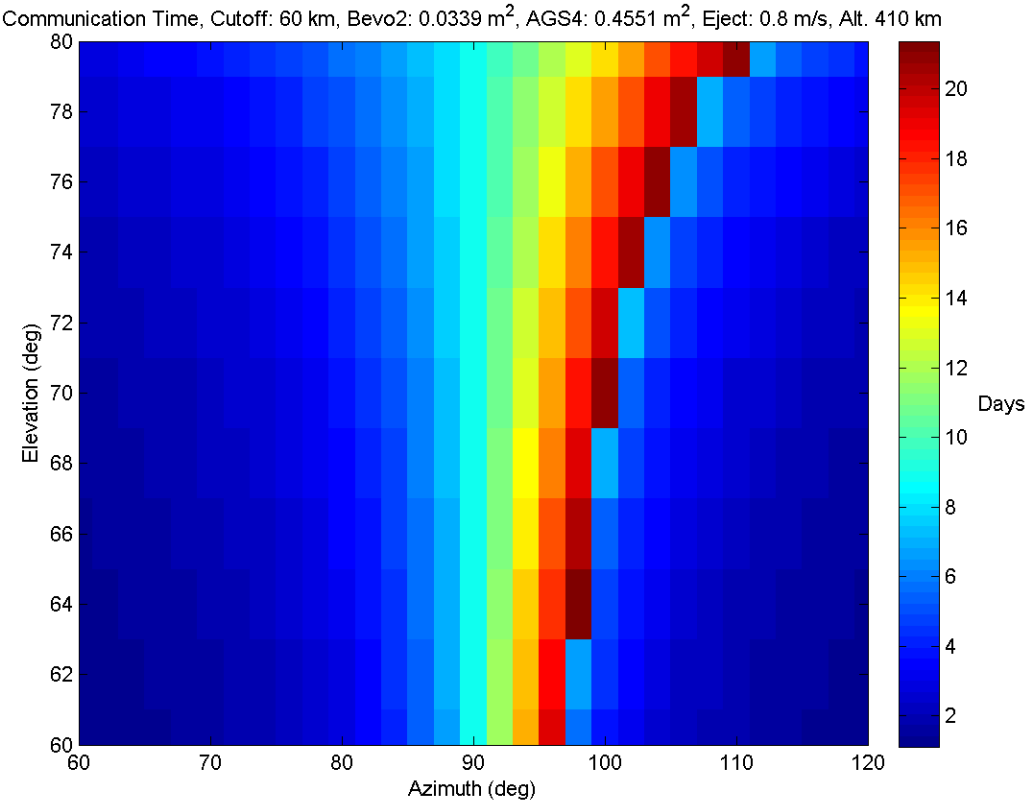

Figure 2.23: Communication time at 410 km altitude with a cut-off distance of 60 km, AGS4 has maximized its area and Bevo-2 is tumbling.

Returning again to the baseline scenario, the AGS4 craft is at a maximum cross-sectional area facing into the wind. Assuming the Bevo-2 craft is tumbling, it has an average area of 0.0339 m^2. Changing this value to 0.3 m^2 the time-in-range drops by a factor of two, from 18 days to 9 days as shown below. A small change in cross-sectional area has the largest effect on the separation time of the spacecraft.

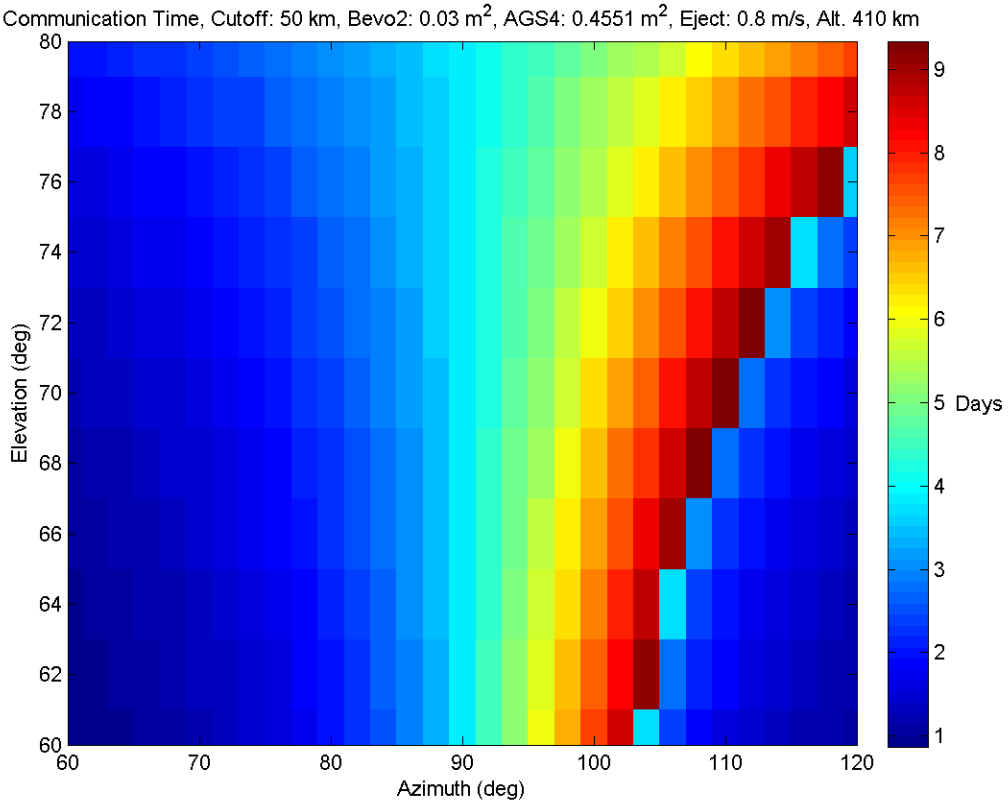

Figure 2.24: Communication time at 410 km altitude with a cut-off distance of 60 km, AGS4 has maximized its area and Bevo-2 places a long face fully toward the ram direction.

The fact that spacecraft attitude has the most significant effect on separation time is intuitive. The motion of Bevo-2 relative to AGS4 is bounded when their area-to-mass ratios are matched. The motion in the nadir-zenith direction and out-of-plane directions are oscillatory. Separation outside of 50 km is ultimately driven by the drift of the crafts away from one another due to drag. Thus when the attitude of one craft is altered, the separation time should be strongly affected, as is seen in the simulation.

Chapter 3: Orbit Determination and Thruster Operations

3.1 Introduction

This chapter explains the procedure to align the orbital planes of two satellites in LEO with similar orbital parameters, but that may be separated spatially in the direction of motion. This procedure will aim to reduce or eliminate the out-of-plane motion of Bevo-2 relative to AGS4.

In the pursuit of this goal, an orbit determination algorithm is developed to process Global Positioning System (GPS) coordinates supplied by each spacecraft. Using post-processed GPS data, the algorithm will refine the spacecraft's position and velocity at a chosen point in time. By using data before and after a thruster maneuver, the algorithm can compute and verify the magnitude and direction of the maneuver. Similarly, GPS data from two spacecraft collected after a separation maneuver can be fed into the algorithm in order to compute the ejection magnitude and velocity of separation.

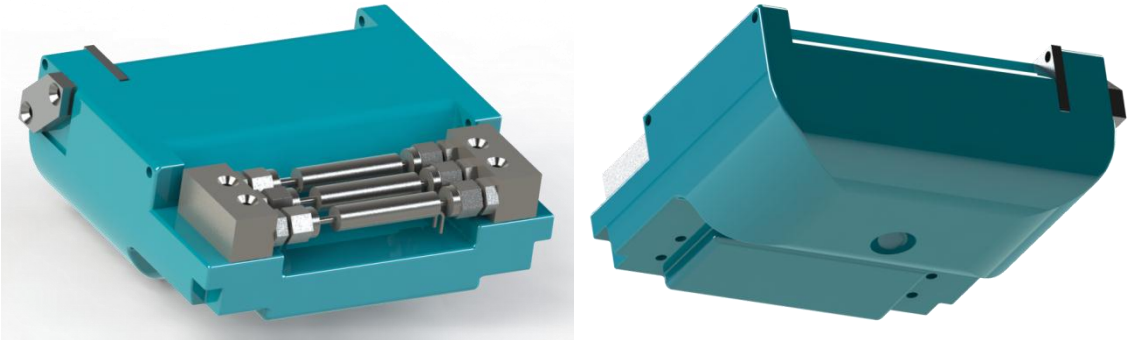

Figure 3.1: Pictured above is a CAD model of the Bevo-2 thruster.

This chapter is comprised of three sections. The first section explains the process by which the GPS data retrieved from the spacecraft are processed to form an orbital state estimate. The second section uses this procedure to estimate the ejection velocity

between the two craft at the start of the mission, as well as the velocity of maneuvers executed by the thruster. Finally, these procedures are expanded to choose the maneuver to align the orbital plane of one spacecraft with that of another.

The objective for Section 3.4 will be to actuate the thruster on one satellite in such a way that the resulting orbit is co-planar with another satellite. To accomplish this goal, an orbit determination algorithm is developed in Section 3.2 and the procedures for verifying maneuvers are expanded in Section 3.3.

3.2 ORBIT DETERMINATION

3.2.1 Background

Before development could begin, a fundamental decision needed to be made: whether to process the GPS coordinates by downlinking them to the ground station, or to conduct calculations on the spacecraft in orbit.

By doing computations in orbit using the satellite's on-board computer, the maneuvers could be executed immediately without the need for two ground passes (one to downlink data and another to upload the final commands).

However, this approach has several drawbacks. Previous approaches to orbital drag maneuvers relied on a state-based approach which is computationally simple. However, to plan high-precision thrust maneuvers that account for orbit perturbations, a reliable orbit propagation model must be employed, necessitating greater computing power. Aboard the spacecraft, computing power, time and memory are limited. Adding greater complexity to the on-board software also carries the increased risk that something may go awry, causing the spacecraft to become inoperable.

Because the LONESTAR-2 mission is fundamentally a technology demonstration and testing mission, it is expected that ground personnel will be involved in all major decisions, including when to fire the thruster and planning long-term attitude maneuvers.

Additionally, the design of the thruster necessitates ground support oversight. The thruster aboard Bevo-2 is comprised of a series of three primary chambers. The first is the main tank which holds the propellant until it is needed. To conduct a maneuver, a valve is opened between the main tank and a small plenum. This second chamber is filled with a small amount of highly-pressurized gas. The first valve is closed and the second valve is opened into a third chamber so that the gas is now far less compressed because the small quantity of gas now fills a larger volume. The second valve is closed and the third is actuated in short busts to expel the propellant into space.

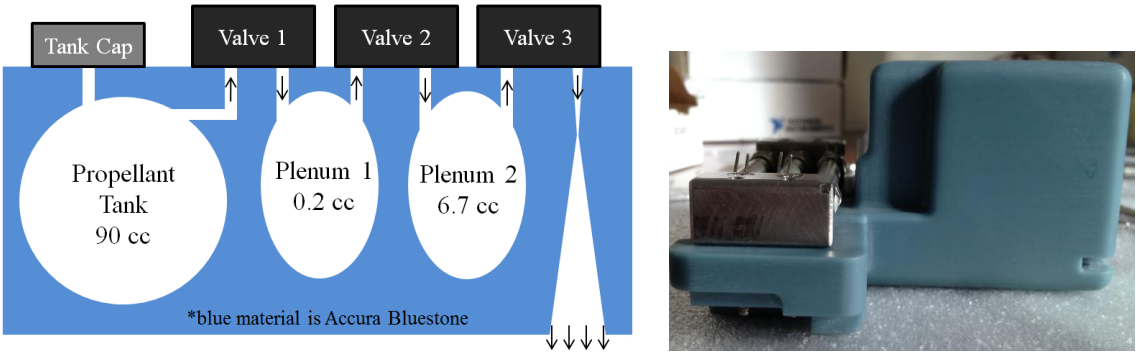

Figure 3.2: Single-axis thruster module design.

As shown in Figure 3.2, the design operates by transferring propellant in a sequential manner through a series of tubes and valves as shown on the left. Valve 1 is opened to extract a portion of propellant from the main tank into Plenum 1. Valve 1 is closed and Valve 2 is opened to expand the gas sample in Plenum 2. Valve 2 is closed

and finally the last valve is actuated in quick bursts to expel a precise quantity of propellant into space.

The tank pressure varies significantly as a function of temperature. The pressure is expected to increase by up to 50% from the lowest pressure simply as a function of the time spent in the sun. As can be seen from the ideal gas law, if the volume V of a vessel, in this case the main thruster tank, remains fixed while the temperature T is increased, the pressure P increases. R is a scaling constant and n is a quantity representing the number of molecules of gas present:

$$P * V = n * R * T \tag{3.1}$$

The choice of the duration and number of valve timings is determined by the details of when and where a maneuver should be executed. The precise variation of pressure is not known, so it will be necessary to conduct maneuvers experimentally in orbit to determine how well the models match the performance in the space environment. Because of the dynamics of orbital mechanics, the mass of propellant expelled at a certain velocity to propel a spacecraft of a certain mass can be generalized using a single parameter, deltaV. However, the thruster takes as input a set of valve actuations rather than the more convenient deltaV term, further complicating the process of conducting a maneuver.

During the weeks and months following deployment, it is probable that the spacecraft will drift out of range of the crosslink antennas. It will be impossible for the two craft to communicate and conduct coordinated maneuvers with each other if they are separated by too great a distance. The ground station team will need to transfer any critical data between the craft using sequential ground passes.

Due to the limitations of the communication and design of the spacecraft, the decision was made to conduct all maneuver planning using the ground station. This imposes a delay on when data is received, processed and commands uplinked. However, running computations using a ground station computer allows for greater computing power to be used in solving for maneuvers. Since humans will be in the loop on all critical decisions, this allows for major decisions to be inspected before being uplinked and executed.

3.2.2 GPS coordinate Simulation

The software package Systems Tool Kit™ (STK) by Analytical Graphics, Inc. (Analytical Graphics, Inc 2003) was used to generate simulated GPS coordinates for testing.

While STK simulates precision orbit measurements, actual measurements collected in flight will have errors. Satellites operating in LEO travel at approximately 7.7 km/s relative to an inertial reference frame compared with observers on the ground moving at roughly 0.5 km/s, where GPS was designed to be most useful. To approximate this effect, a normally-distributed, zero-mean error with a standard deviation of 25 meters was added to each three-dimensional simulated GPS coordinate (Misra and Enge 2010). Additionally, since the error in each measurement is presumed to be in part a function of the orientation of the satellites in the GPS network, errors were generated with 50% correlation between the Bevo-2 and AGS4 position estimates. The following steps were used to generate the error vectors:

1. The AGS4 position error, $\boldsymbol{e_A}$, is sampled from a zero-mean normal distribution with a standard deviation of 25 meters. Three samples are drawn from this distribution to from a vector in three-space.

2. The Bevo-2 position error $\boldsymbol{e}$ sampled independently from zero-mean normal distribution with a standard deviation of 25 meters. Three samples are drawn from this distribution to form a vector.
3. The final correlated Bevo-2 position error, $\boldsymbol{e_B}$, is created using the equation

$$\boldsymbol{e_B} = p * \boldsymbol{e_A} + \boldsymbol{e} * \sqrt{1 - p^2} \tag{3.2}$$

4. A correlation coefficient $p = 0.5$ was used
5. Position errors $\boldsymbol{e_A}$ and $\boldsymbol{e_B}$ are added to the simulated GPS coordinates for each satellite
6. This procedure is applied to generate other satellite position coordinates

Because the satellites have the capability of sampling at up to 1 Hz, it is assumed that GPS data sampling can be aligned to within 1 second between the two satellites. The modeled correlation between each satellite's GPS measurements is shown below:

Finding the expected value of the equation for e_B yields

$$E(e_B) = pE(e_A) + \sqrt{1 - p^2}E(e) = 0 \tag{3.3}$$

The variance of this expression is

$$Var(e_B) = E[(pe_A + \sqrt{1 - p^2}\, e)^2] \tag{3.4}$$

$$= p^2E(e_A^2) + 2p\sqrt{1 - p^2}\, E(e_A e) + (1 - p^2)E(e^2) \tag{3.5}$$

$$= p^2Var(e_A) + (1 - p^2)Var(e) \tag{3.6}$$

Since $E(e_A e) = 0$ by the independence of e_A and e

$$Covar(e_A, e) = E[e_A(pe_A + \sqrt{1 - p^2}\, e)] \tag{3.7}$$

$$= pE(e_A^2) + \sqrt{1 - p^2}\, E(e_A\, e) \tag{3.8}$$

$$= pVar(e_A) \tag{3.9}$$

3.2.3 Assumptions

Simplifying assumptions were required to conduct the analysis in this report.

J2 is the constant term related to the oblateness of the Earth. Primarily due to the centripetal force of the Earth's rotation, the Earth's equator is pulled away from a perfect spherical shape. This bulging mass near the equator perturbs Earth orbits away from the ideal two-body motion, particularly LEO orbits as they pass closest to this mass and are affected most strongly.

A J2 orbit propagator model with atmospheric drag was employed. This model is expected to capture the predominant errors in position and velocity over a multi-day period. From anecdotal observation, the typical maximum position error is approximately 250 meters for LEO orbits.

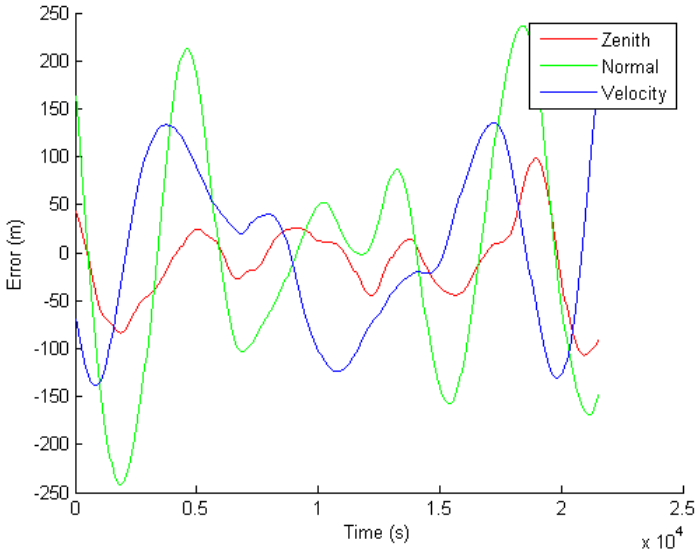

Figure 3.3: Example residual error when using a Matlab J2 propagator to fit STK simulated GPS coordinates.

Because both spacecraft share a similar circular LEO orbit, both craft will exhibit roughly the same perturbations from the J2 model when traveling over similar locations on the Earth. Perturbations caused by higher-order gravitational effects are relatively small and transitory; the primary concern for maneuver planning and execution is the timing and the velocity of the maneuver. As seen in Figure 3.4 and Figure 3.5, the J2 model is a far superior fit to the High Precision Orbit Propagator (HPOP) orbital data than the 2-Body model. While the 2-Body propagation has position and velocity errors of 70 km and 30 m/s, respectively, the J2 propagation has errors of 800 meters and 0.4 m/s, respectively. These values were found by propagating forward from a common state. Using the algorithm developed later in this chapter would reduce these error values even further. The factor to note is that a model that accounts for J2 orbital perturbations greatly reduces the observed error in position and velocity.

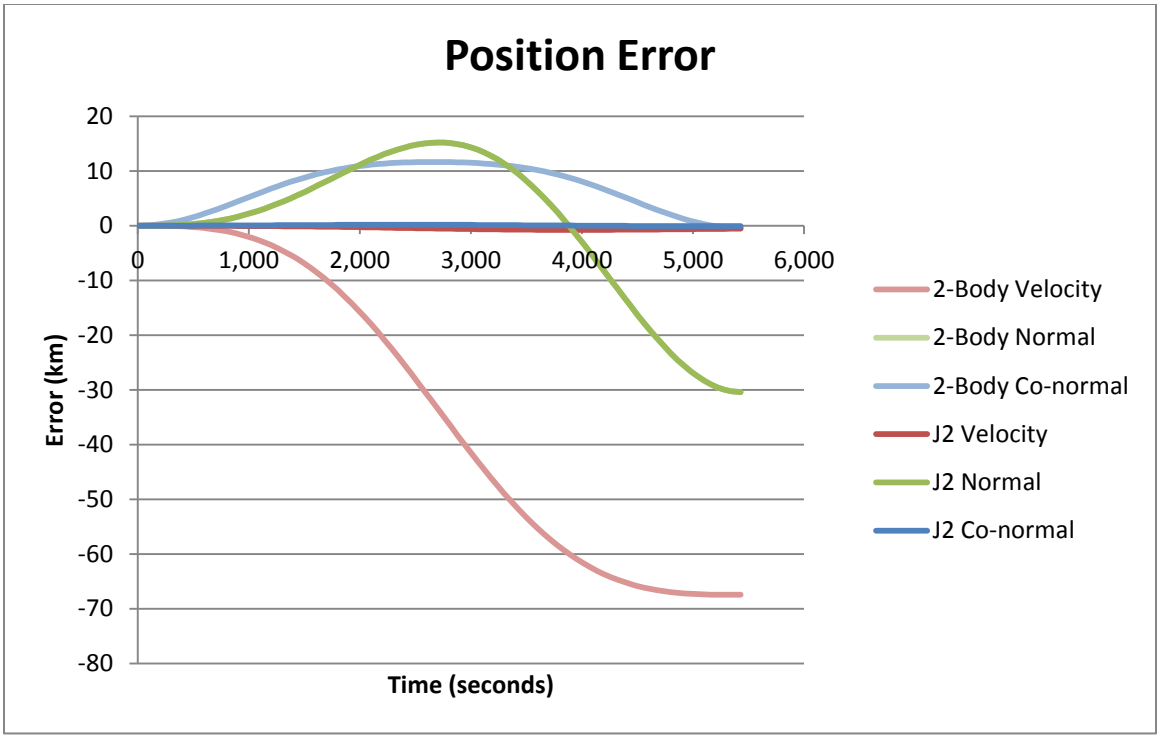

Figure 3.4: Position error of 2-Body and J2 propagated orbits over HPOP base line.

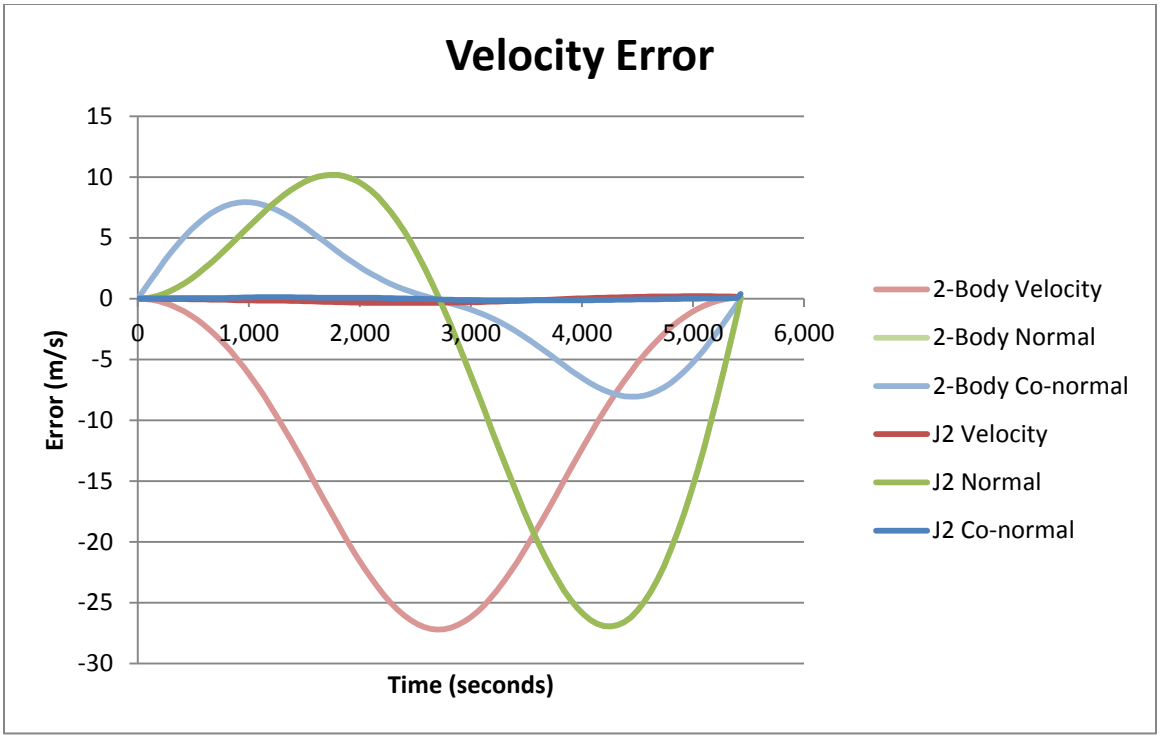

Figure 3.5: Velocity error of 2-Body and J2 propagated orbits over HPOP base line.

Excluding drag, all other orbital perturbations are assumed to be minimal and are neglected. These include the solar radiation pressure caused by the solar wind and the third-body effects of the moon. The Earth is modeled as a mass fixed in an inertial reference frame; effects due to the motion of the Earth about the Sun are not considered.

LONESTAR Mission 2 will begin with the launch of the AGS4-Bevo-2 combined construct from the ISS. Due to increased solar activity in the 2014-2015 time frame (solar maximum), when Mission 2 will begin, the atmosphere will be slightly warmer and extend slightly higher than during previous years. This increased atmosphere increases the drag imposed on vehicles in LEO. The ISS is periodically boosted to a higher orbit to counteract the accumulating effects of drag. In past years, the ISS has been maintained at an altitude of roughly 370 km to minimize the amount of fuel expended by resupply

missions. However, during solar maximum, the ISS is scheduled to be held at roughly 410 km as seen in Figure 3.6. There are no current plans to alter the orbital inclination of the ISS, which is nominally 51 degrees.

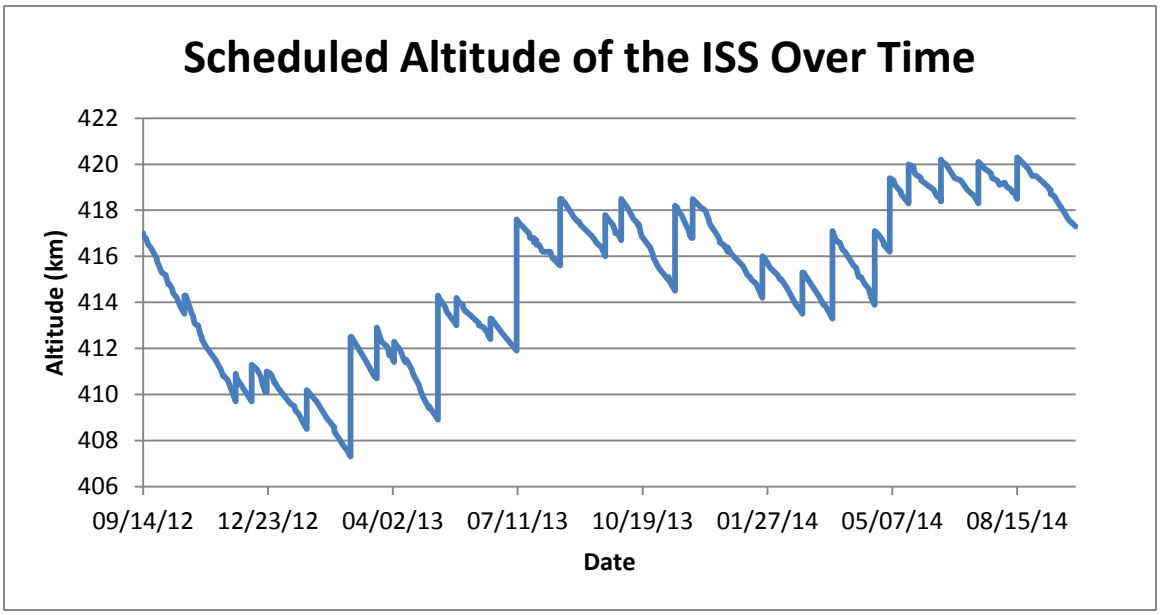

Figure 3.6: Scheduled altitude for the ISS.

NASA and international partners regularly send resupply missions to the ISS. Excess fuel is used to boost the orbit of the ISS, shown in Figure 3.6 as vertical jumps in the scheduled altitude for the ISS. Drag gradually decays the orbit, seen above as a continual downward slope.

The combined AGS4-Bevo-2 unit will be carried to the ISS aboard CRS-5 in Fall 2014 and later deployed from ISS using the JEM robotic arm. This ejection speed is presumed to be negligible. The initial orbit of the craft is assumed to be roughly the same as the ISS. Following the release from the ISS, the AGS4-Bevo-2 couple will remain inactive for one week in compliance with ISS regulations.

The initial separation between the Bevo-2 craft and AGS4, as well as the Bevo-2 thruster operations, is modeled as instantaneous and impulsive. A circular orbit at 410 km has a period of 93 minutes whereas the maneuver is predicted to be quite short, lasting only a few seconds. Maneuvers executed by the craft are also quite small, up to a meter per second, compared with a speed of 7.7 km/s of the craft in LEO.

Due to the high speed of each craft in LEO, the GPS position fixes are expected to have greater position error than typical ground-based receivers. Simulated measurements are provided by a software package and then corrupted with noise to simulate errors in GPS measurements. A three dimensional vector with a magnitude that is normally-distributed with zero mean and standard deviation of 25 meters along each axis is used to represent the position error collected by each GPS unit. It is assumed the error is uncorrelated with position and is present equally in all directions; discrepancies that are a function of altitude, longitude or latitude are neglected by using this model.

This document is written under the supervision of the UT-Austin Texas Spacecraft Laboratory and for that reason focuses on maneuvers conducted by the Bevo-2 craft. This craft contains a star camera as well as several redundant systems for determining attitude. The craft contains reaction wheels as well as magnetorquers to control attitude. It is presumed that the craft will be able to maintain the required attitude for extended periods of time with a minimal pointing error.

J2 and Earth's gravitational constant μ are known with a high level of accuracy and are not estimated in the propagation model. The values for these parameters are instead provided as known constants. The 1984 World Geodetic System model for these constants is used in this document.

Parameter	Value
J2	0.00108262668355315130
μ	398600441800000 m^3/s^2

Table 3.1: Values of constants used in propagation

The constants used in the propagations in this document are included above. Slight perturbations from these values in the propagator have the effect of introducing position and velocity errors when integrated over long time periods.

The density of air at LEO altitudes is assumed to be constant over a period of days. According to the US Naval Research Laboratory Mass Spectrometer and Incoherent Scatter Radar through the Exosphere 2000 (NRLMSISE-00) model used in STK, the density can fluctuate by ±30% over the period of one orbit, primarily due to altitude changes as seen in Figure 3.7. However, the cumulative effect of drag is minimal over the span of one orbit and is nearly unobservable. Instead of modeling the full atmospheric model, a simpler model that decreases exponentially with altitude is used in the propagator. As will be discussed in section 3.2, the atmospheric density estimate is updated when the propagator is run.

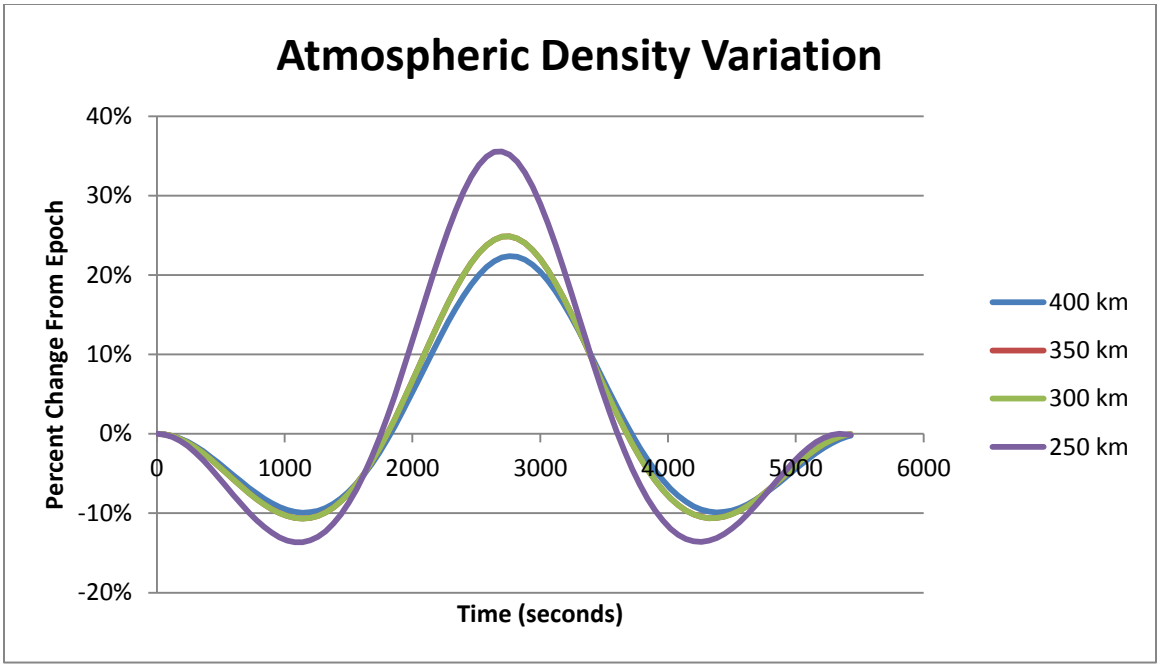

Figure 3.7: Atmospheric destiny fluctuation over one orbit as a function of orbit altitude.

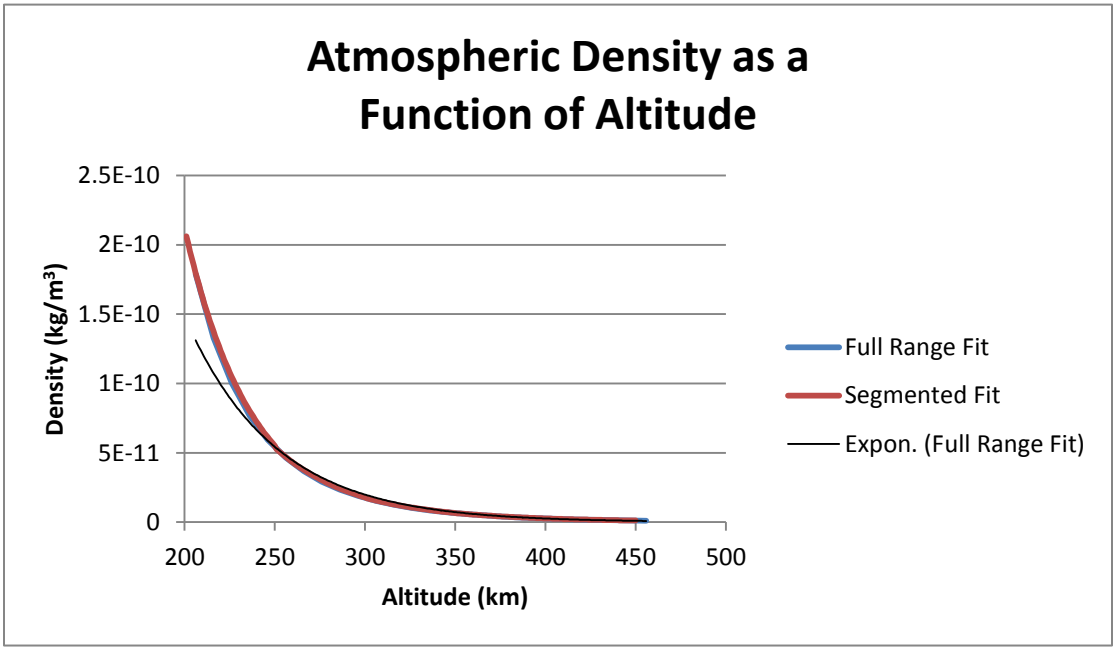

Figure 3.8: Two models for the density of the atmosphere.

The blue line in Figure 3.8 represents raw data collected during solar maximum from STK. The black line represents an exponential best-fit of the entire STK data set. The red line represents a segmented fit to the STK data. While the atmospheric density decays exponentially over altitude, an exponential fit is not ideal for capturing the edge cases.

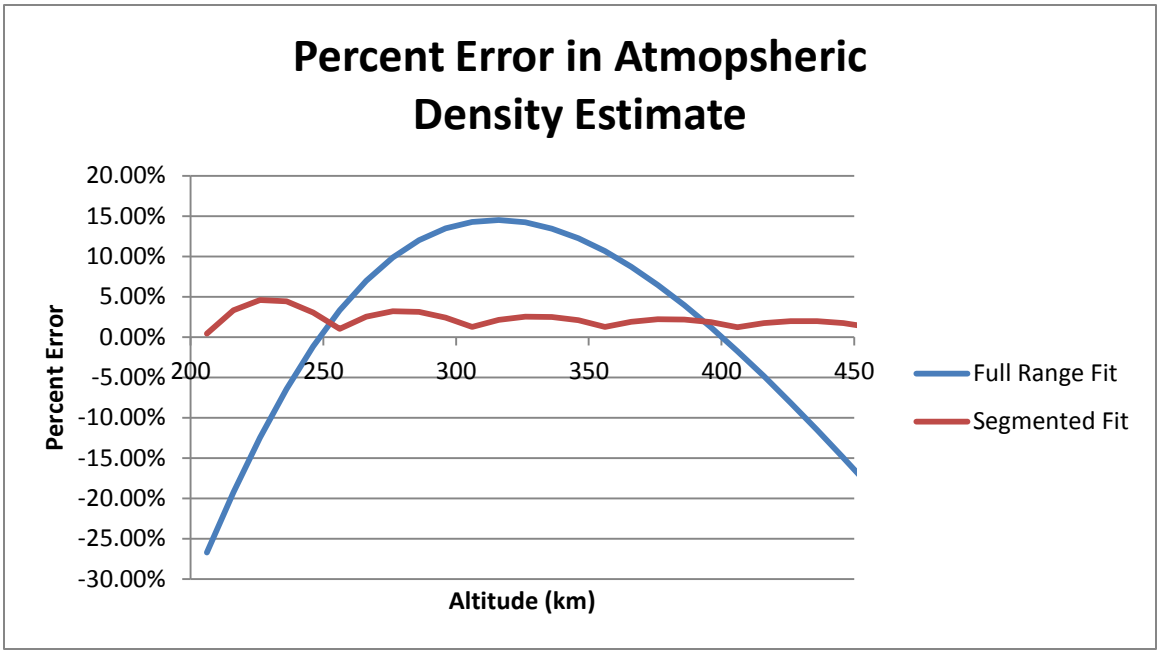

Figure 3.9: Error comparison between two atmospheric density models.

Above, Figure 3.9 shows a plot of the atmospheric density error using two models. The full range exponential fit has large errors in the middle and at the tail ends. An exponential fit broken into five sections produces a much smaller error and a better fit to simulated atmospheric density measurements.

A ballistic drag coefficient C_d with a constant value of 2.2 is used in the drag model. A drag parameter ρ is formed by multiplying the drag coefficient by the cross-sectional area facing into the direction of motion, A, divided by the mass, m. This

parameter is multiplied by a function of the altitude and other variables to estimate the deceleration due to atmospheric drag.

$$\rho = C_d \, A \, / \, m \tag{3.10}$$

$$a = -\rho \, c_1 * e^{c_2 \, h} * F(X) \tag{3.11}$$

The batch process described in Section 3.2 is used to holistically estimate the effect of drag. Any small error in any related parameter, such as C_d, area, mass or the atmospheric coefficients, will be minimized through the batch process.

As discussed in Chapter 2, the cross-sectional area of each craft is estimated based on a rectangular prism model. Each craft has minor irregularities along the surface such as solar panels or ground support interfacing, but the predominant shape of the craft can be explained with rectangular prisms.

Additional mission constraints may impose attitude limitations. The Bevo-2 craft can theoretically capture over 8 Watts from solar power but is anticipated to operate on 5 Watts. This power is provided either directly from the solar panels on the surface of the craft or through its batteries. Each orbit consists of roughly a 60-minute charge cycle as Bevo-2 traverses in sunlight, and a 30-minute discharge cycle when the craft passes into the Earth's shadow and must rely on the energy stored in its batteries. When trying to accomplish most tasks, Bevo-2 will be in an energy deficit mode. If maneuvers, communication or other tasks are run for too long, the batteries will be exhausted, even with energy provided by the solar panels. For this reason, energy collected by the solar panels is vital to continued operation of Bevo-2. It is likely that the craft will need to maintain as much area pointed at the sun as possible for an extended portion of each orbit. This requirement restricts the possible attitudes the craft can maintain. Maneuvers for attitude-controlled drag impose their own attitude requirements which may come into

conflict with solar panel pointing requirements. Potential conflicts and their resolution are not inspected in this document.

During each orbit, it is desirable to point a pair of body surface mounted solar panels towards the sun. Initially, the craft can freely rotate about this attitude constraint. However, it may not always be possible to simultaneously satisfy the requirement to minimize or maximize the cross-sectional area of the craft pointed into the direction of motion.

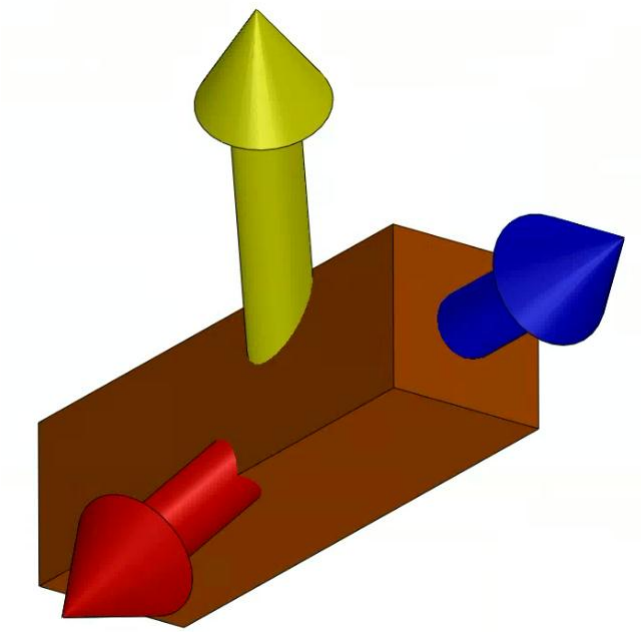

Figure 3.10: Visualization of a pointing scenario that cannot be fully satisfied.

As shown in Figure 3.10, imagine a scenario where the Bevo-2 craft is orbiting the Earth and the sun appears directly in front of the craft, where the direction of motion and the sun vector align in the direction of the yellow arrow. In this scenario it is desired to minimize the cross-sectional area (blue arrow) and also maximize the sunlight captured

by the solar panels (red arrow). Simply stated, the goal is to align the blue and yellow arrow while also aligning the red and yellow arrow. This is not physically possible and by extension it is not always possible to conduct an ideal attitude maneuver over long time periods.

Additionally, the star camera located on one small face of the Bevo-2 craft should not be pointed at the sun for extended periods to avoid overheating. Up to twice per day, the Bevo-2 craft passes over the Austin ground station for up to 15 minutes, during which time the antennas should not be pointed directly in line with the ground station vector, otherwise the signal will not reach the ground station. The electromagnetic waves propagate in a toroidal shape, and aligning the hole of this shape in the direction of the ground station results in a dead communication zone.

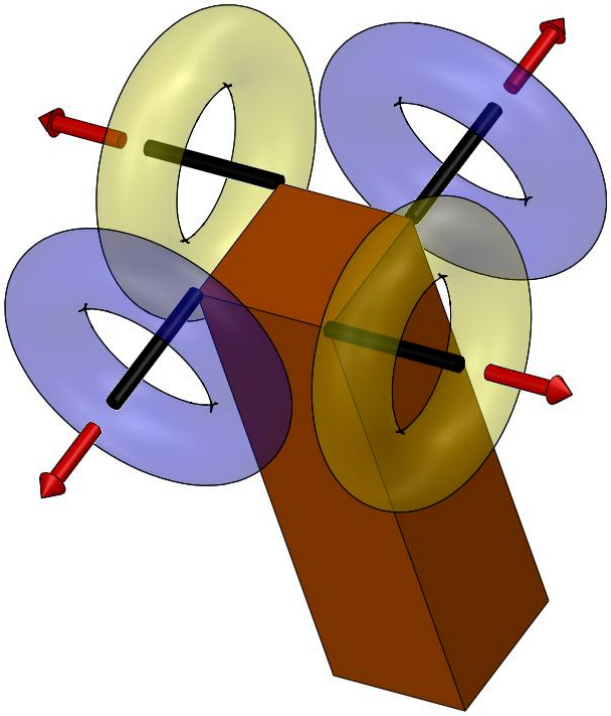

Figure 3.11: Visualization of toroid emanation of radio waves from the Bevo-2 antennas.

The radio waves for downlink from Bevo-2 (blue toroids in Figure 3.11) and the region of greatest reception for uploads (yellow toroids) impose pointing requirements on the Bevo-2 craft during a ground pass. Red arrows indicate directions of signal loss. The craft must be oriented with no red arrows pointing toward the ground station to allow for bi-directional communication with the ground.

The effects of these attitude constraints are outside the scope of this analysis and are not considered here. It is assumed that these constraints can be generally satisfied while meeting the maneuver and pointing requirements that are needed for proximity operations.

The Bevo-2 craft contains a thruster that will expel a quantity of mass during controlled burns. It assumed that the mass expelled is negligible compared with the mass of the craft. However, the mass of the craft is modeled as a constant. The thruster is loaded with 90 g of Dupont Suva 236-fa before launch while the craft weighs 4 kg. The mass of the propellant is significantly less than the mass of the vehicle, supporting the assumption that the vehicle will not significantly change mass over the duration of the mission.

It is assumed that the execution of maneuvers, such as separation of the two craft near the start of the mission as well as thruster maneuvers conducted by Bevo-2, are impulsive. It is assumed these operations are conducted within a precision of 0.1 seconds of the target execution time. Small errors in timing produce a negligible impact on maneuver verification calculations, and are thus neglected compared with other error sources such as GPS position error. This assertion was confirmed through simulation.

3.2.4 Procedure

Because GPS data will be post-processed, a batch algorithm was chosen to form the desired state estimate. This procedure gives superior error reduction (as measured by final root mean square error) to typical Kalman filters (as used in previous reports) because state estimates are iterated upon multiple times. The first iteration of a batch process produces identical results to a sequential Kalman algorithm, but a batch process refines this output in sequential iterations.

There are two primary methods for orbital analysis and maneuver execution. One method focuses on relative maneuvers where data is shared between each craft. The other option entails downlinking data to a ground station and then uploading commands during a later pass. Since the satellites inspected here would likely be out of

communication range for many initial maneuvers and some maneuvers only require one vehicle, a choice was made early in this analysis to focus on the latter option for orbital analysis. Some maneuvers in this chapter may be conducted blindly relative to another spacecraft (for example maneuvers that test the thruster aboard Bevo-2 or align the orbit plane with an arbitrary target). Also, the two satellites may not be close enough to crosslink data, requiring information to be shared through the ground stations, regardless of the orbital analysis approach chosen.

3.2.5 Algorithm Development

A model incorporating J2 and atmospheric drag was employed to account for the predominant sources of error as compared to a two-body model. Due to its programming flexibility and support, Matlab was used as the primary analysis tool in this document. An ODE45 finite element propagator was used to compute the state estimates. The ODE45 toolkit supplied with Matlab provided the required settings and an acceptable run time without introducing significant propagation errors.

The objective of the batch algorithm developed below is to accept GPS coordinates collected from a satellite and update an initial state vector such that the propagated state is as close as possible to the observed GPS samples.

The first step is to form a state vector containing position, velocity and a parameter related to drag. At a given instant, this vector represents the position and velocity of a craft while also estimating the atmospheric drag. An *a priori* estimate of the initial state is provided. Here, the x, y and z coordinates refer to a location in an inertial reference frame and B is the cross-sectional area which is later used to compute the effective drag.

$$\boldsymbol{X_0^*} = \begin{bmatrix} position \\ velocity \\ attitude \end{bmatrix} = \begin{bmatrix} x \\ y \\ z \\ \dot{x} \\ \dot{y} \\ \dot{z} \\ B \end{bmatrix} \tag{3.12}$$

Next, parameters used in the propagator are defined. Λ is the inverse of the covariance matrix for the *a priori* estimate. $\bar{x}_0$ is the unbiased estimator of $\hat{x}_0$, which in turn is the best estimate for x, the difference between the true state X and the reference solution X^*.

$$\Lambda = {\bar{P}_0}^{-1} \tag{3.13}$$

$$N = {\bar{P}_0}^{-1}\bar{x}_0 \tag{3.14}$$

The batch algorithm consists of two loops. The inner loop iterates over each data sample and produces an update to the initial state estimate. The outer loop executes the inner loop multiple times. The number of time the outer loop is run is referred to as the number of "batch iterations" the algorithm executed.

The following procedure is the inner loop and is iterated upon for each GPS sample:

A state equation is derived that relates the derivative of the state, $\dot{X}$, to the current state, X.

$$\dot{\boldsymbol{X}} = F(\boldsymbol{X}(t), t) \tag{3.15}$$

The A matrix is formed by taking the gradient of the above with respect to the state vector. The A matrix is used in the computation that is needed to quickly propagate small errors back to the initial state, allowing the *a priori* estimate to be updated accordingly.

$$A(t) = \partial F(\boldsymbol{X}, t)/\partial \boldsymbol{X} \tag{3.16}$$

The Φ matrix is used to propagate errors back to the initial state. The derivative of this matrix is formed by multiplying A by Φ

$$\dot{\Phi}(t, t_0) = A(t)\Phi(t, t_0) \tag{3.17}$$

The X and Φ values are then integrated from the previous time step to the current time step using an ordinary differential equation propagator such as ODE45.

The separation in time between each sample is a time step. The following parameters are defined and updated after each time step with the goal of computing corrections to the *a priori* estimate.

G is defined as the state observation matrix. It relates observation of the state to the state itself. In this case, GPS coordinates are used, so the position is being directly observed. Other models might use range and range rate measurements to determine the orbit of a craft which would require a different G matrix. An expression for the observation of the state can be written as:

$$\boldsymbol{Y}(t) = \boldsymbol{G}(\boldsymbol{X}(t), t) + \boldsymbol{\epsilon}(t) \tag{3.18}$$

y_i is formed as the error between the observed GPS coordinate and the propagated model.

R is the inverse of the weighting matrix

$$R = E[\boldsymbol{\epsilon}\boldsymbol{\epsilon}^T] \tag{3.19}$$

The standard deviation of the *a priori* estimate is used to fill this matrix.

$$\widetilde{H}_i = [\partial G(\boldsymbol{X}, t_i)/\partial \boldsymbol{X}] \tag{3.20}$$

$$\boldsymbol{y_i} = \boldsymbol{Y_i} - G(\boldsymbol{X_i^*}, t_i) \tag{3.21}$$

$$H_i = \widetilde{H}_i \Phi(t_i, t_0) \tag{3.22}$$

$$\Lambda = \Lambda + H_i^T R_i^{-1} H_i \tag{3.23}$$

$$\mathrm{N} = \mathrm{N} + H_i^T R_i^{-1} y_i \tag{3.24}$$

The above process is iterated upon for each GPS coordinate.

At the end of the data set, the normal equations below are solved

$$\Lambda\hat{x}_0 = N \tag{3.25}$$

The *a priori* estimate is updated

$$\boldsymbol{X}_0^* = \boldsymbol{X}_0^* + \hat{x}_0 \tag{3.26}$$

$$\bar{x}_0 = \bar{x}_0 - \hat{x}_0 \tag{3.27}$$

The above batch procedure is iterated upon for the entire data set multiple times to reduce the root mean square error. The root mean square error is the sum of the squares of the errors between the observed GPS coordinated and the reconstructed trajectory. The iteration over the entire data set terminates when the process has converged. The process can stop after a fixed number of batch iterations is reached or by defining a cutoff value for the root mean square error and observing when the root mean square of the cumulative error ceases to decrease between sequential batch iterations. If the initial state estimate is relatively close to the true value, then the process will converge. However, if the initial guess is poor, the assumption in the batch algorithm that the initial guess produces minimal errors will be violated and the process will diverge. The length of the data sets fed into the algorithm was chosen to be such a length that the linearity assumption of the sensitivity matrix was not violated to prevent the process from diverging.

This procedure was implemented using Matlab and an ODE45 propagator. From this procedure, a refined *a priori* estimate is produced. This algorithm is used to produce a refined initial state estimate in the following sections.

3.2.6 Simulation Validation

Simulated GPS coordinates were generated using STK scenarios. Multiple models were available in the software package, including two-body, J2 and complete High Precision Orbit Propagators (HPOP). These models represent varying level of gravity field complexity (the HPOP incorporated drag effects as well). The Matlab model developed in section 3.2.5 closely matched the STK initial conditions in the two-body and J2 propagator case. From this set of simulations, the Matlab models were validated against industry software.

STK Propagator	Matlab Propagator	Initial State Position Error (m)	Initial State Velocity Error (m/s)
2-Body	2-body	7 E-6	5 E-9
J2	J2	10	9 E-2
HPOP	J2	170	0.4

Table 3.2: State errors between STK and Matlab after propagating for one orbit.

Table 3.2 shows that the position and velocity are in agreement when the same models are used for both Matlab and STK. When a J2 model is propagated against an HPOP, errors are present, but these are small in practice over the span of a small number of orbits

The Matlab model could not perfectly match the STK model when the HPOP was employed. STK is capable of generating data that is more accurate than the Matlab

model. The Matlab propagator uses a simpler model to enable the orbit data to be fitted to the model and refined. The data from the HPOP in STK cannot be perfectly fit using the Matlab model since the latter model does not incorporate higher order gravity field perturbations.

It should be noted that the J2000 reference frame used in STK produces results that are inconsistent with text book models (Tapley, Schutz and Born 2010). While no long-period oscillation should be present in the inclination (Kaula 2000) when only J2 perturbations are present, STK clearly produces such an oscillation. Over the span of a few days, this oscillation manifests as a linear drift in inclination over time.

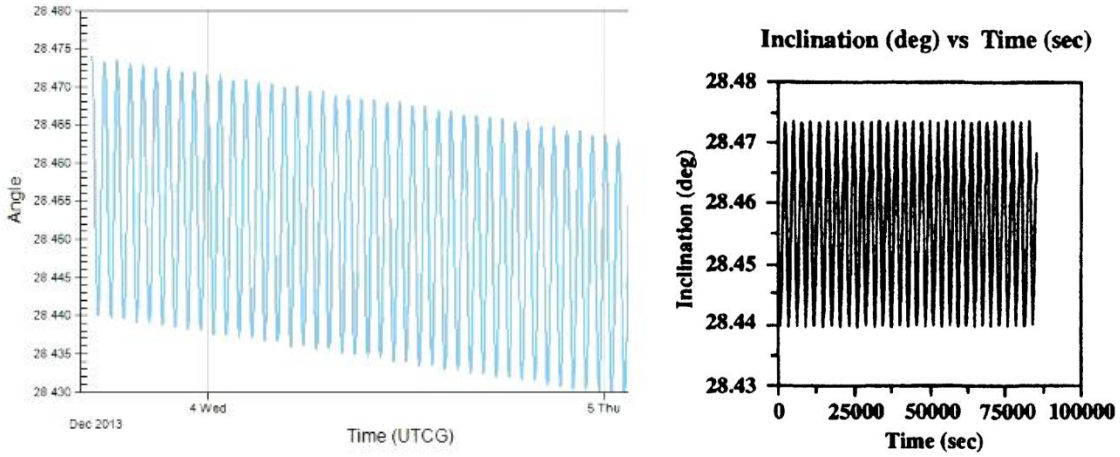

Figure 3.12: Inclination over time from STK (left) and Statistical Orbit Determination (right) using the same initial conditions.

It is presumed that the error in inclination arose from the use of true-of-date coordinates within STK, which introduce a small oscillation in the coordinate system. The RAAN of simulated orbits were chosen to be 270 degrees so that this error was minimized.

It was observed that the error in inclination varied the simulated GPS coordinates by as much as 400 meters from the correct position during any given orbit. Since the Earth continues to rotate below the satellite during the simulation period, the choice of a RAAN of 270 degrees is not expected to impact any results derived in this document.

When a RAAN of 270 degrees was used in STK, the output simulated GPS coordinates showed no significant divergence from theory. If the RAAN is changed from this value, the orbit appears to oscillate beyond what it should. This oscillation is assumed to be due to the modeling method employed within STK. This oscillation was negated through the choice of a convenient RAAN.

3.3 VELOCITY DETERMINATION

The batch algorithm developed in the previous section is used to determine the velocity of various maneuvers. Two sets of GPS coordinates (one for each vehicle, Bevo-2 and AGS4) are provided to the algorithm and propagated to a common epoch. The position at the epoch is matched between the propagations, but the velocity is allowed to vary individually. By differencing the initial velocities generated for each satellite, the velocity change imparted by of the maneuver can be determined.

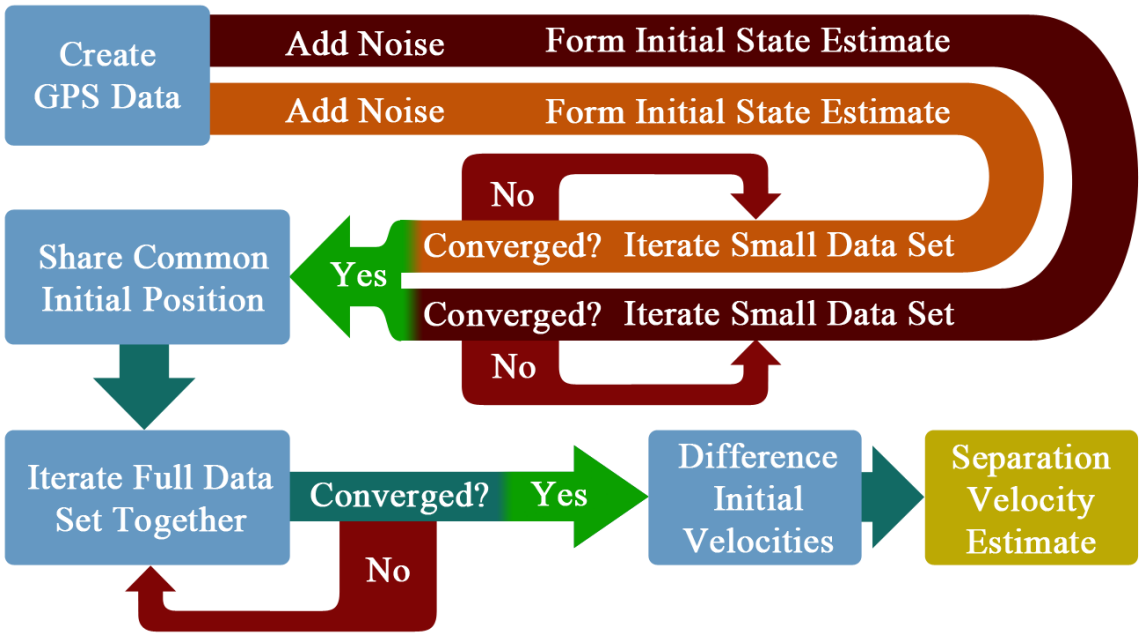

Figure 3.13: Block diagram of separation velocity determination algorithm.

For each set of GPS data, one quarter of an orbit's worth of data, sampled every 60 seconds, is fed into the batch algorithm. The *a priori* state is estimated by using the first GPS coordinate as the initial position. The velocity is determined based on differencing the positions of sequential GPS coordinates and dividing by the time step, in this case one minute. The seventh element of the state vector, the atmospheric quantity, is initially estimated based on the best-guess vehicle attitude and mass parameters. Experimentally, it has been seen that this batch process typically requires 7 to 10 iterations to converge during STK simulations including measurement noise.

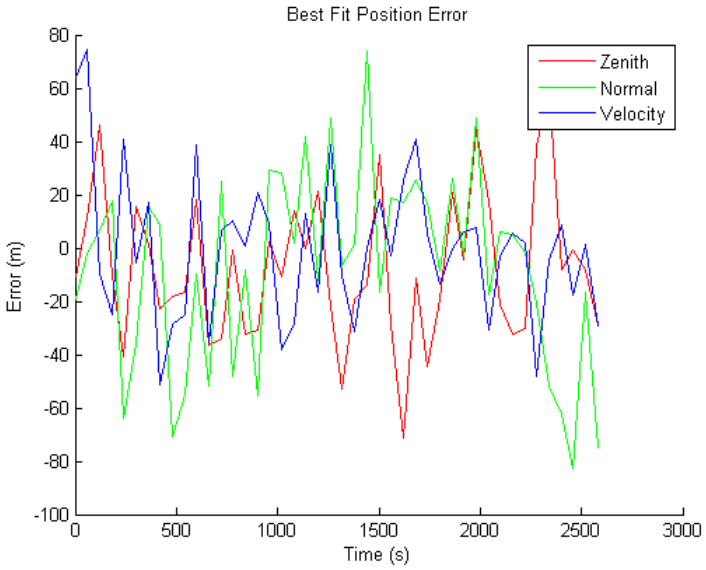

Figure 3.14: Error in the velocity, normal and co-normal directions after the batch process has been executed.

The first refinement of the initial state estimate with a quarter of an orbit's data is required due to the coarse initial estimate. The batch algorithm is based on an assumption that the *a priori* estimate is close to the true value. The longer an incorrect *a priori* estimate is propagated, the further the modeled state diverges from the observed GPS coordinates. If the divergence is too great, the batch process can no longer refine the *a priori* estimate to correct the discrepancy between the modeled GPS coordinates and the sampled GPS coordinates, and as a result the batch process does not converge.

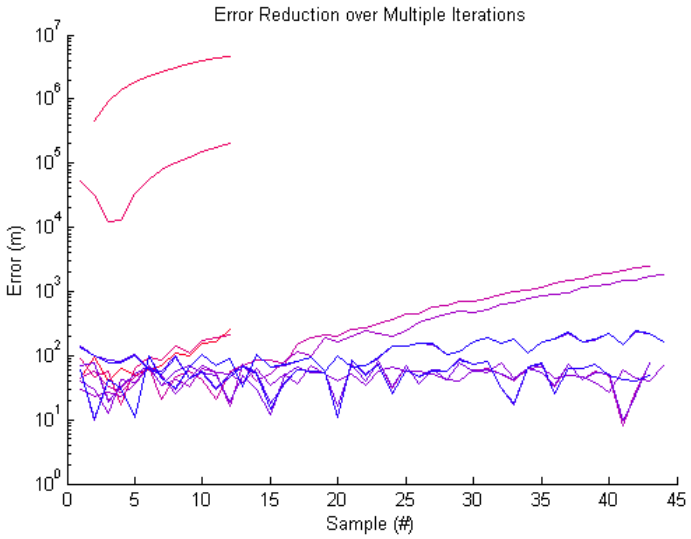

Figure 3.15: Error as a function of iteration number.

In Figure 3.15, the error between the physical measurements generated by STK and the Batch process is reduced with successive iterations. The first iterations are shown in red and only rely on a subset of the available data. Later iterations, shown in deeper blues, rely on more data to refine orbital state estimates.

Once the *a priori* estimate is fit to a small amount of data, the data set used is expanded to utilize more GPS samples in the next iterations of the batch algorithm in order to further refine the initial state estimate.

3.3.1 Ejection Maneuver Verification

The onboard thruster will be used to align the orbital planes of the two spacecraft as discussed in Section 3.3.2 or to conduct a similar demonstration capability. This will be the first time this thruster will be used in space, and thus is highly experimental. GPS samples will be used to verify the maneuvers that were conducted. This process will

provide a redundant method to confirm the spacecraft attitude when the maneuver was conducted and to supplement accelerometer data to gauge the magnitude of the burn.

To estimate the initial separation velocity of the two spacecraft, two data sets are used. One set comes from AGS4 immediately following deployment and the other set comes from Bevo-2 after deployment. An epoch time is chosen at the moment of deployment. The GPS coordinates for one quarter of an orbit's data from each craft are provided to separate batch processes to form an initial state estimate for each craft.

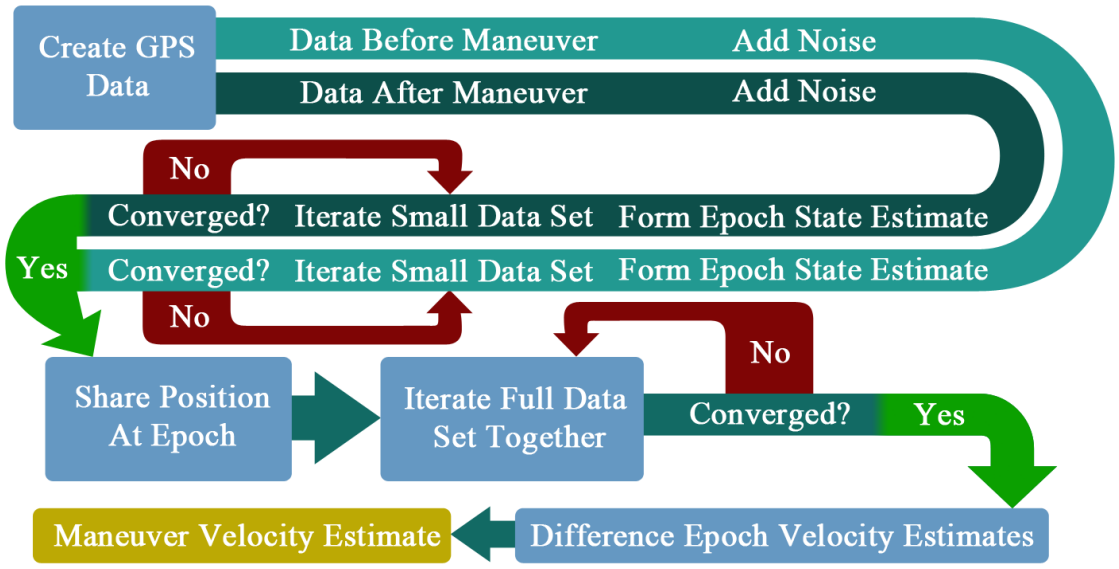

Figure 3.16: Block diagram of maneuver velocity determination algorithm.

The initial state estimate for each satellite contains a velocity component. The difference in these velocities is the estimate for the ejection maneuver.

3.3.2 Thruster Maneuver Verification

While Section 3.3.1 uses the GPS samples from two craft to estimate the velocity of an ejection maneuver, this section utilizes GPS samples from one satellite collected before and after a thruster burn to estimate the velocity of the maneuver.

The process for measuring the ejection maneuver entails propagating GPS samples from two satellites to a common ejection time. Conversely, a thruster maneuver operates on data from one satellite before and after a maneuver. The epoch for a thruster maneuver lies between two data sets. To account for this one data set is propagated forward while the latter set is propagated backward. This scenario ultimately means that the data sets no longer share common error factors.

In Section 3.3.1, the two data sets came from identical time periods, and since the satellites traversed similar sections of the globe during that period, perturbations are expected to affect each orbit in roughly the same way, meaning the relative velocity measurement of the velocity maneuver is largely unaffected. However a thruster maneuver entails working with data sets from different time periods, potentially introducing more error in the velocity measurement than in the previous case because the two data sets share fewer error sources.

While GPS position errors and gravity effects may be correlated in the data sets used in section 3.3.1, no such correlations are assumed in this section. Thus, the divergence of GPS samples from the model potentially has a greater impact here. To minimize the impact of this divergence, less data is used in the last stage of the batch algorithm in order to focus on the time period immediately surrounding the maneuver. This means that the higher-order gravitational effects have a smaller effect, but the state estimate is further corrupted by GPS measurement noise than in the previous section.

The data set collected from Bevo-2 is separated into two sections, the GPS samples before and after the thruster maneuver. The initial data fed into the algorithm is a small fraction of one entire orbital period. Starting at the maneuver time, a quarter-orbit's data is used from both spacecraft data sets to calculate independent epoch initial states.

Following this initial batch estimate, the data fed into both propagators is increased to about half-an-orbit's worth. Additionally, the same process is used as in section 3.3.1, and the two propagators are run sequentially to refine the initial state estimate. The objective to determine a separation velocity between the craft is satisfied by linking the data sets to a common shared position (the location of deployment) at the epoch and allowing the velocity to be determined freely. That is, the Bevo-2 batch process is run once and the output initial position is fed into the AGS4 initial position estimate. The AGS4 batch process is run once and the output initial position is fed back into the Bevo-2 epoch state estimate. Finally, the process is repeated until the estimate converges.

The difference between the two initial state velocities is used to estimate of the thruster maneuver.

The data set is increased to use one orbit’s worth of data. The batch process is then run on both data sets at the same time to form an initial state estimates for each craft. That is, the algorithm is used to refine the initial state of Bevo-2, and then the resulting initial position (but not velocity) is fed into the *a priori* estimate for the AGS4 batch process. The AGS4 batch process is run once and the resulting initial position estimate is fed back into the initial state estimate for Bevo-2. This back-and-forth process is

repeated, and in this manner the batch process is used to jointly refine both the Bevo-2 and AGS4 state estimates, assuming they started from a shared position at the epoch.

3.4 Thruster Maneuver Planning

While the previous sections pertained to validation of commanded maneuvers, this section pertains to the planning of maneuvers.

3.4.1 Introduction and 2-body Orbit Example

Before explaining the full procedure to align the orbital planes of two spacecraft about the Earth, it is helpful to begin with a simpler two-body model, neglecting the effects of J2 and drag. In a two-body model, the Earth is modeled as a point mass fixed in an inertial reference frame while a satellite, also modeled as a point mass, orbits about it. The satellite exerts a negligible force on the Earth, so its orbit is modeled as a circle.

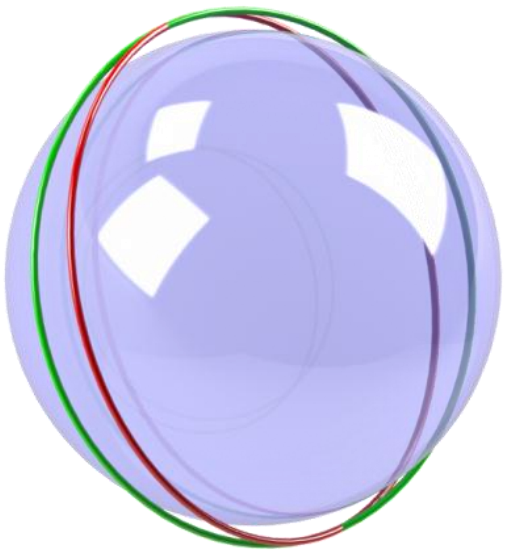

Figure 3.17: The Earth (transparent blue) and two LEO orbits (red and green).

Imagine another satellite also in a circular orbit about the Earth at the same altitude, but with other characteristic parameters chosen randomly. The requirement for equal semi-major axes is assumed here for simplicity but will be relaxed in the detailed analysis. The position of each craft within its orbit can be described by an angle in relation to an arbitrary reference point, such as the right ascension of the ascending node. Additionally, there exists an angle between the two orbits, defined at the intersection of the two orbital planes. This angle represents a combination of a change in inclination and the right ascension of the ascending node.

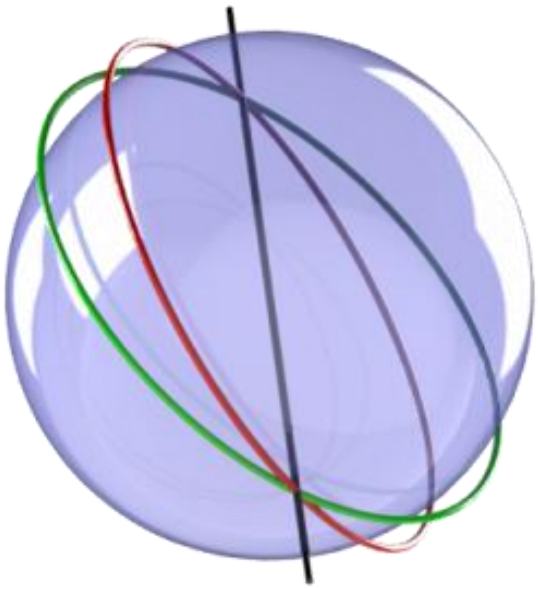

Figure 3.18: The two orbit planes intersect in a line (black).

Aligning the position and velocities of the two craft in space requires a series of maneuvers. A direct route involves a Lambert targeting approach, where the Bevo-2

chaser spacecraft initiates a burn to move from the initial orbit into a transfer orbit, and then upon arrival at the AGS4 target craft, conducts another burn to match the target's velocity to enter the final orbit.

In this document, the processes of aligning the orbital plane and lining up the chaser with the target are pursued independently. The plane change maneuver is a relatively rapid procedure utilizing the thruster aboard Bevo-2. Conversely, the attitude maneuvers can take days or weeks to perform and could require more fuel to complete than is physically present in the thruster. The first step consists of aligning the orbits of the chaser and target, and the second step involves reducing the separation between spacecraft in a co-planar orbit. In the 2-body scenario, co-planar orbits remain co-planar, but high order effects perturb this balance, as will be seen in the detailed analysis.

This approach was chosen because a Lambert targeting approach would likely use more fuel than physically available in the Bevo-2 craft. Instead, the thruster is used purely for the plane-change maneuver, and the differential drag attitude maneuvers described in Chapter 4 are used to conduct the long-term phasing maneuvers once the orbital planes are aligned.

In this simplistic model, the two orbital planes of the chaser and target meet in a line since they share a common center in the Earth. The chaser spacecraft crosses this line twice per orbit. The thruster maneuver is conducted on one of these crossovers, which allows the chaser craft to move immediately from its initial orbit to a transfer orbit that is co-planar with the target orbit.

The magnitude and direction of this maneuver are determined by computing the velocity vector of the target craft as it crosses the orbit-intersection line and subtracting that vector from the velocity vector of the chaser spacecraft as it crosses the line. The

difference of these two vectors defines the maneuver that must be conducted to shift the chaser from its initial orbit into the transfer orbit.

If the state vector containing the position and velocity of both craft is known at some time, each state can be propagated forward in time until the positions intersect the orbit-intersection line. The burn that needs to be conducted, $\Delta \boldsymbol{V}$, is computed by subtracting the initial velocity, $\boldsymbol{V}_i$, from the desired velocity, $\boldsymbol{V}_f$.

$$\Delta \boldsymbol{V} = \boldsymbol{V}_f - \boldsymbol{V}_i \tag{3.28}$$

3.4.2 Full J2 Procedure

Section 3.4.1 explained the procedure for aligning the orbital planes of two craft in a two-body model. However, higher-order effects complicate the procedure, necessitating a more precise approach. The effects of J2 oblateness and the required modification in the alignment procedure are discussed below. The effects of drag are also discussed in this section; however, drag acts predominantly in-plane to alter the orbit's eccentricity and semi-major axis, and produces a significantly smaller effect over short time periods.

The most significant effect to note is that J2 precesses the right ascension of the ascending node (RAAN) by a secular rate of roughly 5 degrees per day. Within one period of a single orbit, the RAAN and inclination oscillate.

Altitude (km)	RAAN Rate (degrees/day)
400	-5.35
350	-5.45
300	-5.55
250	-5.70
200	-5.77

Table 3.3: Secular rate of change of RAAN as a function of altitude for circular orbits.

The secular rate of change of the RAAN is computed using the following formula. Ω is the RAAN, n is the mean motion, a_e is the equatorial radius of the Earth (6378.1 km), e is the orbital eccentricity, a is the semi-major axis, i is the orbital inclination, and μ_e is the standard gravitational parameter for Earth (398,600.44 km^3s^{-2}) (Kaula 2000).

$$\frac{d\Omega}{dt} = \frac{-3nJ_2{a_e}^2}{2(1-e^2)^2a^2}\cos i \tag{3.29}$$

$$n = \sqrt{\frac{\mu_e}{a^3}} \tag{3.30}$$

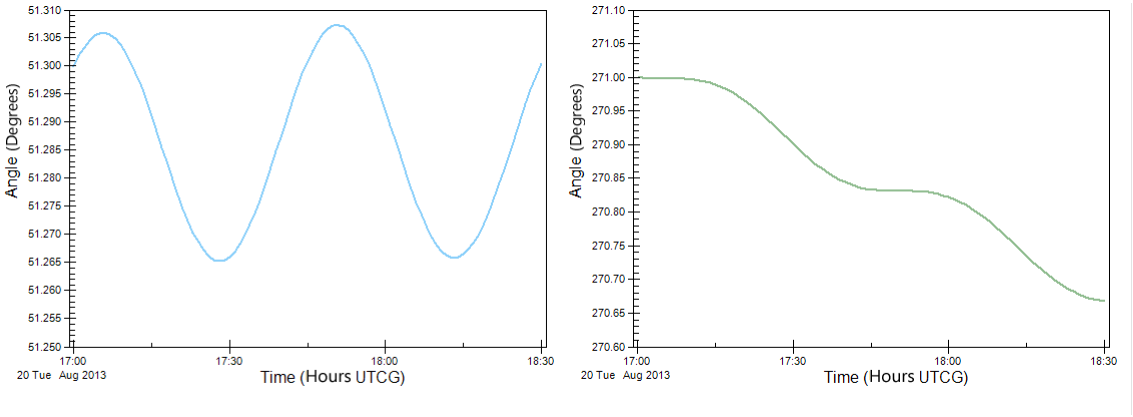

Figure 3.19: Changes in Inclination (left) and RAAN (right) over the span of one orbit using the HPOP.

Under these conditions, it is no longer trivial to locate the orbit-intersection line. Instead, the angular momentum vector, $\boldsymbol{L}$, of each orbit is utilized as discussed below. The position of the craft is represented with the vector $\boldsymbol{r}$, the speed is represented with $\boldsymbol{v}$ and the mass with m. Since only the direction of the angular momentum vector is utilized, the scalar value of the mass is neglected in later steps.

$$\boldsymbol{L} = \boldsymbol{r} \times m\boldsymbol{v} \tag{3.31}$$

In the two-body case, it can be seen that if two orbits are co-planar with the same orbital altitude at the same points in the orbit, they pass through the same positions with the same velocity, separated only in time. It follows that co-planar orbits in the two-body scenario can be achieved by conducting a burn along the orbit-intersection line, or by aligning the orbital angular momentum vectors by performing a similar burn along the line formed by the cross product of the angular momentum vectors. In the two-body scenario, these two approaches generate the same line.

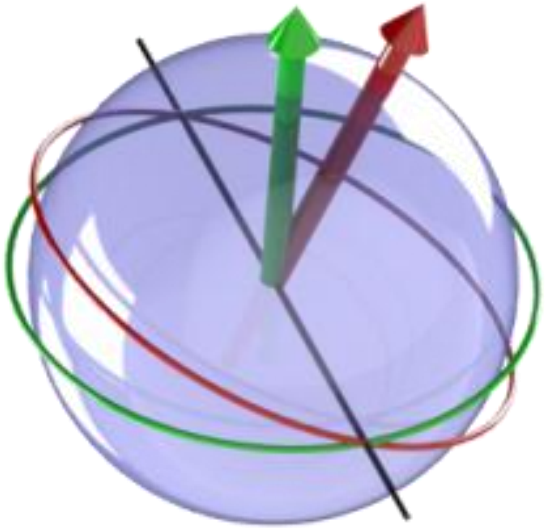

Figure 3.20: The orbit angular momentum vectors are shown with red and green arrows.

The general procedure for executing an orbital plane-change maneuver that includes J2 effects consists of the following steps:

1. Determine the orbital period of one satellite. The two satellites are assumed to be orbiting the Earth in orbits with similar semi-major axes. The larger the difference in altitude between the orbit of each craft, the larger the difference in the precession of the RAAN. A larger vertical separation requires greater maintenance to keep the orbit planes aligned.
2. Propagate both orbits for one orbital period, starting from epochs with the same time stamp and using the same time step (e.g., every 30 seconds). Orbital period computations are discussed in Section 3.4.3.

3. Sample the angular momentum vectors from the propagator at even intervals by taking the output from Step 2 and computing $\boldsymbol{r} \times \boldsymbol{v}$ in for each time step.
4. Combine the angular momentum samples from each orbit to determine an average angular momentum vector for each orbit.
5. Perform a cross product on the average angular momentum vectors to find the orbit-intersection line. This line represents how the chaser's angular momentum vector needs to be rotated to align with the target's angular momentum vector. The maneuver to align the planes will be conducted on this line.
6. Using the propagator samples from Step 2, find the two closest samples to the orbit-intersection line by maximizing the dot product between the position vector and the orbit-intersection vector.
7. Interpolate/propagate more finely between these two points (i.e., every 0.01 seconds). Refining the simulated state in this step allows the propagator to only be run in small time steps in the vicinity of cross the orbit-intersection line. If this step was skipped, Step 2 would need to propagate the entire orbit at a very high resolution which would take a substantial amount of computing time.
8. Find the position (and time stamp) for the chaser craft's orbit that is closest to the orbit-intersection vector. This will be the position that maximizes the dot product with the orbit-intersection vector.
9. Find the velocity of the chaser and target craft as they cross over the orbit-intersection line. The difference in these two velocities is the ΔV maneuver that needs to be conducted to align the orbital plane of the chaser with the orbital plane of the target.

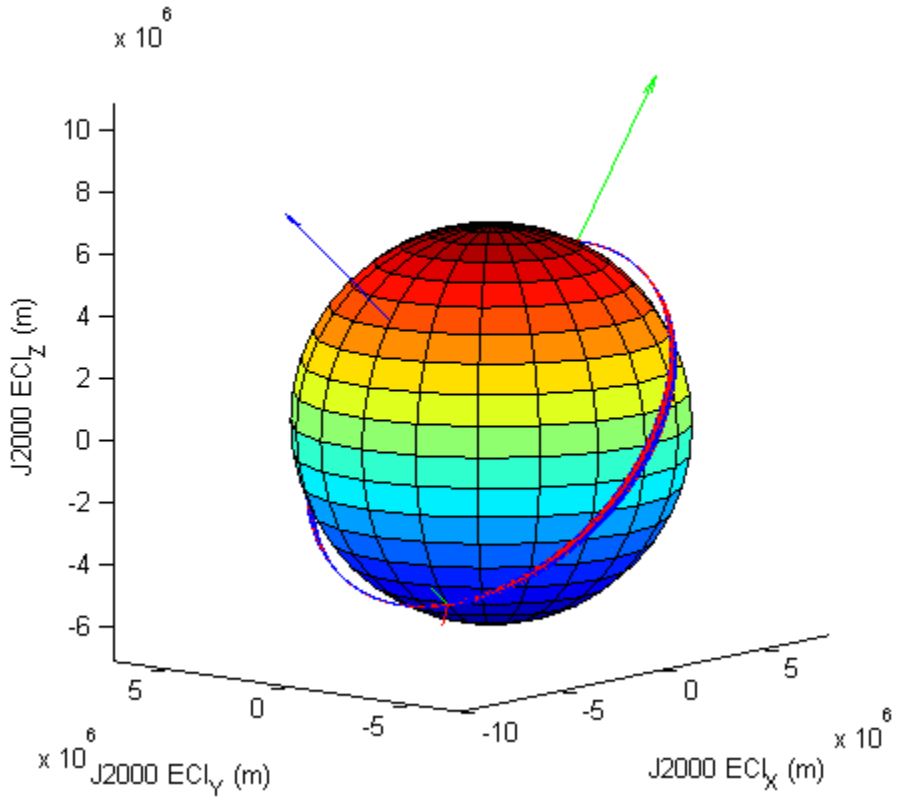

Figure 3.21: Matlab visualization of two orbits with angular momentum vectors shown at the top left (red and blue arrows) along with the orbital plane intersection line (green).

A plot from the algorithm is shown in Figure 3.21. STK was commanded to generate two orbits separated by a 10 m/s burn. The algorithm discussed above derives a location near the original burn location, but on a successive fly over, and recommends a 10 m/s burn in the opposite direction as the original command (to counter induced the out-of-plane motion). The angular momentum vectors (red and blue arrows) are so close they are indistinguishable in the above figure (only the blue is visible). The green arrow represents where in the orbit the corrective burn would be conducted. Figure 3.22 shows

the change in the angular momentum vectors before and after the recommended maneuver.

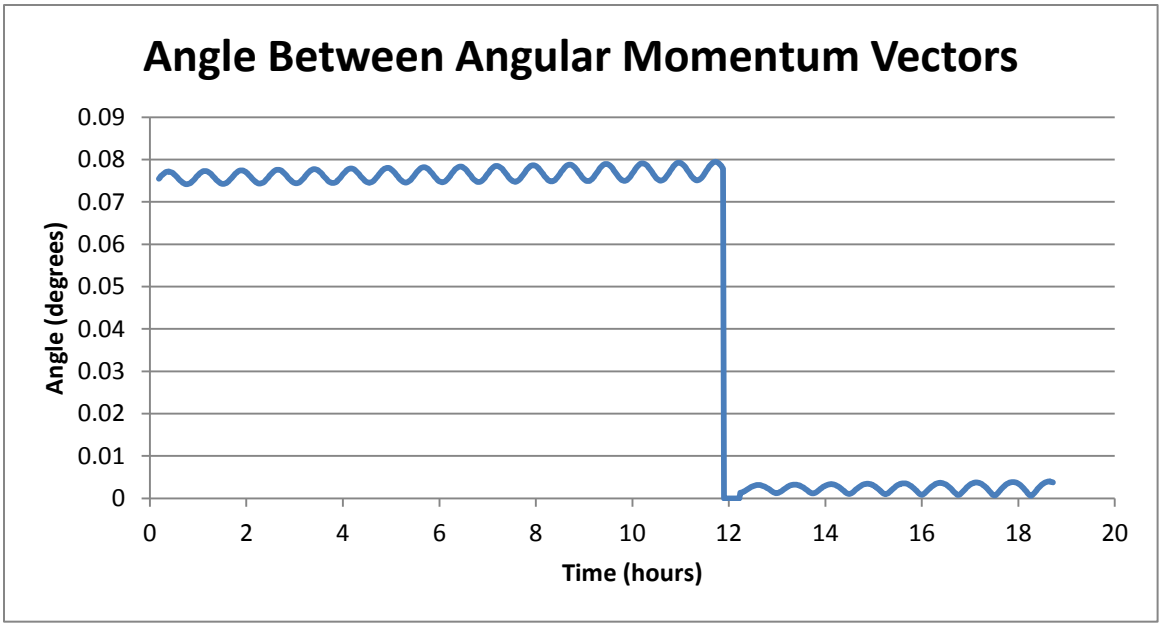

Figure 3.22: Angle between the angular momentum vectors of Bevo-2 and AGS4 before and after executing the recommended maneuver.

3.4.3 Orbital Period Determination

Here, one orbital period is defined as the length of time between successive crossings of the RAAN. However, due to the oscillations caused by the oblateness J2, it is difficult to determine the orbital period since the path traversed is no longer planar. Rather, an alternate procedure is employed by measuring the time between crossings of the right ascension of the ascending node. While the RAAN changes with time, the ascending node remains attached to the X-Y plane in the J2000 reference frame. Thus the orbital period can be found by differencing sequential crossing times of the X-Y plane. Specifically, the following procedure was employed in this analysis:

1. Form the initial state for a given epoch and refine the estimate using the techniques in Section 3.2.5.
2. Propagate the orbit using a reasonable time step, for example 30 seconds, for a minimum of three cycles. Using three cycles ensures that one full orbit is contained in the data set, even if the first point lies right after the first RAAN. LEO orbits are roughly 90 minutes, so a propagation time of 300 minutes is used
3. Find the points bordering the RAAN. These points can be found as the positions where the Z-values in the J2000 frame transition from negative to positive
4. Propagate the orbit between the points found in Step 3 using a small time step such as 0.01 seconds.
5. Find the points in both data sets from Step 4 with the minimum Z-value.
6. Difference the time stamps of the points found in Step 5 to determine the orbit period.

3.5 SIMULATION

A panel of simulations was conducted to test the thruster measurement algorithm under a variety of conditions. A circular orbit with an altitude between 200 and 400 km was assumed. Thruster maneuvers were simulated at even intervals along the orbit. The thruster was actuated with impulsive burns between 0.01 m/s and 1 m/s in three directions (in the velocity, normal and co-normal directions). Across 650 simulations, the average error was 0.11 m/s.

Additional tests were run, allowing the timing of the maneuver to be corrupted by noise within ±0.1 seconds. This timing noise did not significantly impact the precision of the maneuver determination algorithm.

More simulations were generated to observe the effect of removing measurement error. By removing the simulated error in the GPS coordinates the average error was reduced to 0.10 m/s.

Another set of trials were conducted. This set commanded STK to use a J2 propagator rather than a HPOP and did not add any measurement noise to the simulated GPS data. Simply stated, this aimed to allow the batch process to converge much more closely to the simulated GPS coordinates since the HPOP includes perturbations that are not modeled in the batch algorithm. With this trial, the error dropped to 0.03 m/s. This suggests that the predominant source for error arises from higher-order gravity effects not modeled in the batch algorithm. To reduce this error, a higher-precision orbit propagator would be required in the batch algorithm. However, to calculate the exact nature of the gravity field, a higher order gravity model relies on knowledge of time in addition to the existing state of the craft. While a similar approach could be used to linearize the equations of motion and compute a refined trajectory, this would be much more computationally intensive than using the current gravity field and drag model.

3.6 CONCLUSION

The batch algorithm detailed in this chapter may be used as part of a procedure to verify maneuvers conducted by two spacecraft separating, or by one conducting a thruster maneuver. The latter procedure can be used to verify any short impulsive maneuvers that may be conducted in the process of qualifying the thruster hardware on orbit. This procedure also provides redundancy to the measurements collected by the accelerometer on-board.

Finally, a section is devoted to detailing the process of planning the thruster maneuvers required to bring the orbital planes into alignment. When the craft are in close

proximity, this co-planar state reduces out-of-plane motion of one craft relative to the other.

Chapter 4: Attitude Maneuvers

4.1 Introduction

LEO offers a unique environment in which to conduct maneuvers. In contrast with higher orbits such as geosynchronous orbits or orbits about the moon, LEO is permeated with a faint atmosphere. Over time, the plasma in the troposphere impacts spacecraft, decelerating them. As the craft lose orbital energy, they descend into lower orbits about the Earth. Spacecraft in lower orbits travel faster than those above them. Atmospheric drag has the counter-intuitive property of speeding up craft over the span of several orbits. The gradual decay of LEO orbits ultimately limits the maximum lifespan of cubesat missions. Long-term missions in LEO, such as the ISS, rely on regular booster missions to raise their orbits to counteract the effects of drag.

The drag effect can be modeled and strategically utilized to conduct useful maneuvers between spacecraft. For example, if two spacecraft start in co-planar orbits at the same altitude, then the effects of drag can be used to lower the orbit of one craft faster than another by altering the cross-sectional area of each craft. One craft experiences more drag than the other and descends more quickly towards the Earth. In a lower orbit, its period is shorter and it begins to advance relative to the target craft. This process can bring two craft in LEO closer together, and when several maneuvers are combined, can keep them in close proximity.

4.1.1 Basics

The acceleration due to drag is a function of the density ρ of the medium, the ballistic drag coefficient C_d, the speed $\boldsymbol{V}$ of the craft relative to the medium, the area A of the surface facing into the wind, and the mass m of the craft.

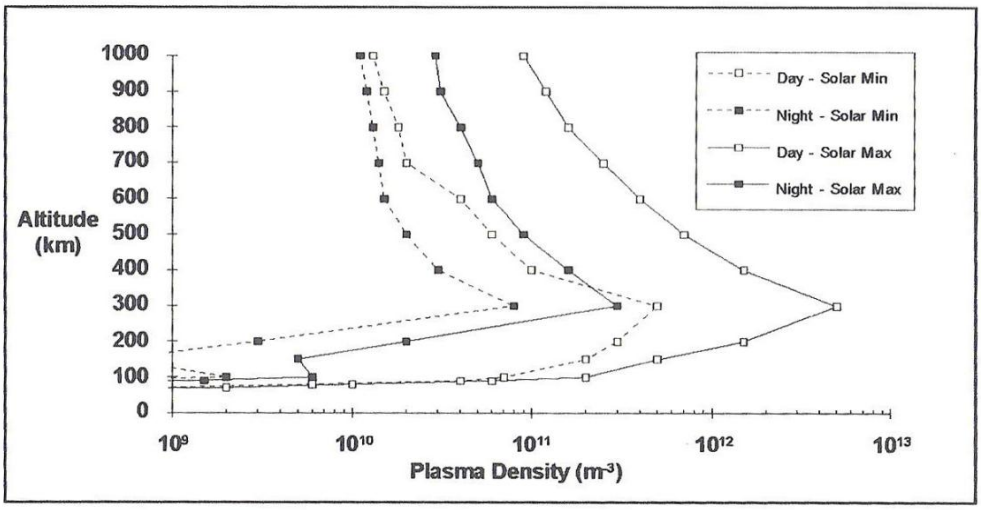

Figure 4.1: The LEO Plasma (Tribble 2003).

Atmospheric particles are attracted to the Earth through the force of gravity. However, just as hot air rises in a closed room, so too do high-energy particles rise up through the atmosphere. The troposphere, where LEO satellites pass through, is permeated with plasma particles including atomic oxygen, helium, hydrogen, nitrogen and molecular oxygen.

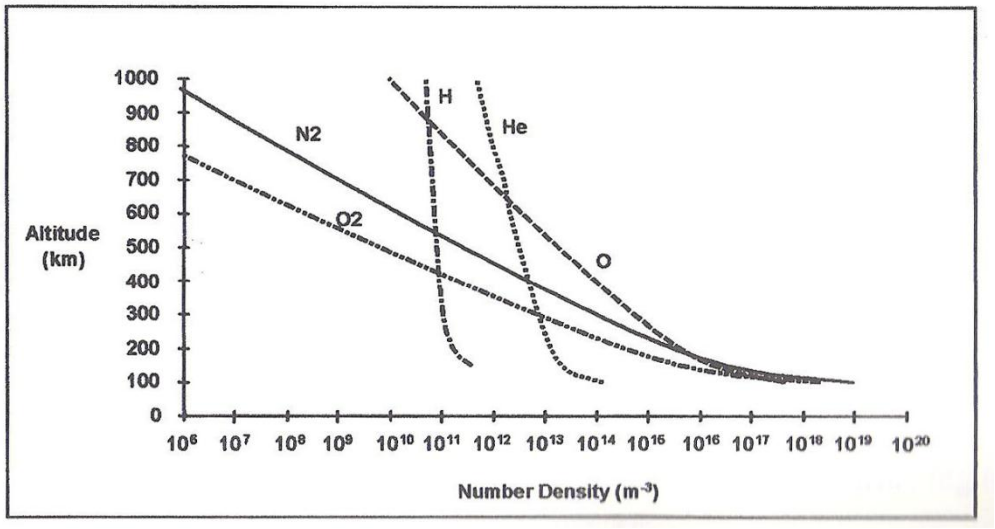

Figure 4.2: LEO neutral species abundance (Tribble 2003).

Atmosphere	Density (kg/km^3)	Pressure (atm)
Sea Level	$1.2 * 10^{9}$	1
250 km orbit	$7.7 * 10^{-2}$	$3.0 * 10^{-10}$
300 km orbit	$2.1 * 10^{-2}$	$1.0 * 10^{-10}$
400 km orbit	$3.0 * 10^{-3}$	$2.0 * 10^{-11}$

Table 4.1: Example atmosphere density and pressure values at varying altitudes

To a first approximation, the decay in atmospheric density can be modeled as an exponential function of rising altitude.

$$\rho = \rho_0 * e^{h*\rho_1} \quad (4.1)$$

Due to the different atmospheric consistencies at different altitudes, the model can be broken up into zones. For example, the calculation of the atmospheric density at an altitude of 330 km may rely on constants that are only valid between 300 and 350 km, whereas a density calculation at 240 km may rely on constants that are valid between 200 and 250 km. This process of chopping up the model allows for a more precise match with simulated data as seen in Figure 3.9.

4.1.2 Assumptions

It is assumed that the satellites referred to in this section would initially be separated by more than 150 km, which is an approximation for the theoretical upper bound of the maximum communication distance between two satellites. If the satellites are closer than 150 km, it is assumed that they will be capable of communicating with one another and conducting coordinated maneuvers without human intervention. Since autonomous maneuvers executed via cross-communication between the satellites is the subject of future missions, this chapter focuses predominantly on the methods to bring two distantly-separated satellites into communication range with the intent to allow them to remain in range for an extended period.

The condition for communication is modeled as a sphere of a constant radius about the target craft, AGS4. If the Bevo-2 chaser craft is in an orbit sufficiently lower than AGS4, it will eventually slip ahead of AGS4 to the point where it circumnavigates the globe an extra time and comes up behind AGS4 later in the mission, but soon slips out of communication range again. While this 'fly-by' of Bevo-2 past AGS4 will give the opportunity for testing cross-communication hardware, it will not enable the sustained

communication that will be required for rendezvous in Mission 4. This chapter focuses on matching the semi-major axes of the two craft while also bringing them close together.

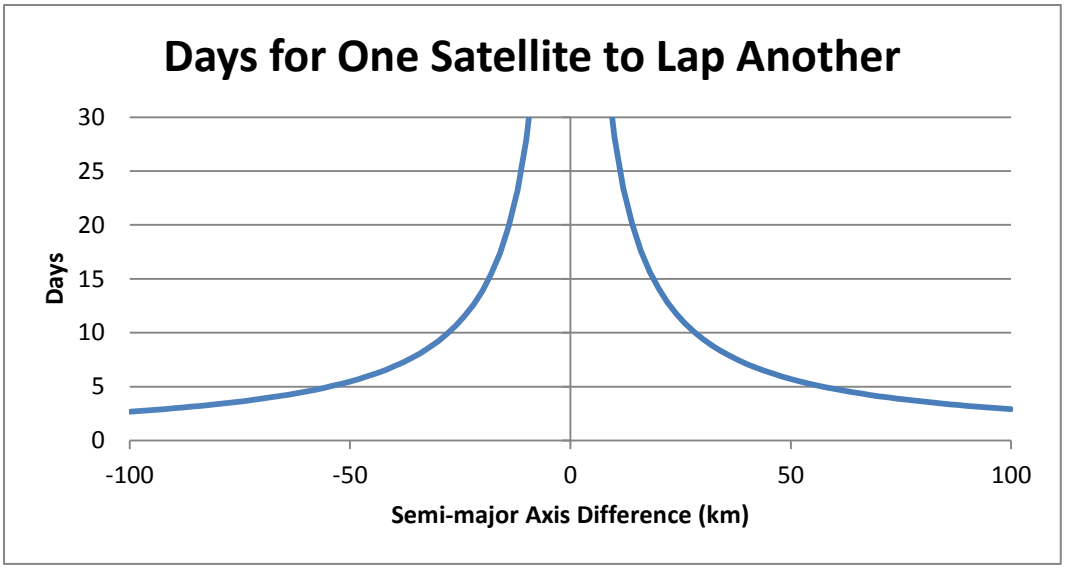

Figure 4.3: Synodic period of two craft in LEO.

Figure 4.3 shows the time required for one craft to lap another in a circular orbit. With a reference craft in a 300 km orbit, scenarios are computed to determine how long a craft in a higher or lower orbit will require to cover one extra or fewer orbit than the reference. When the craft are in identical orbits, with no vertical separation, an asymptote is formed in the plot where the craft will never reach one another. Conversely, the greater their vertical separation, the more quickly they will approach each other. A separation of 10 km allows one craft to reach another within the span of 30 days.

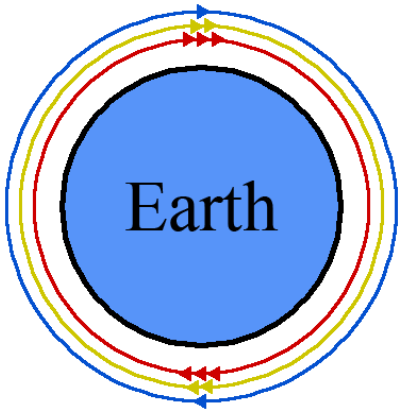

Figure 4.4: Simplified illustration of circular orbits with different altitudes.

To illustrate the desired outcome for proximity operations, imagine the following scenario depicted in Figure 4.4. Assume that the target craft is initially in the orbit depicted in gold. If the chaser is initially above the target in a circular orbit (shown in blue), it will have a longer period than the target and slip behind the target. If the chaser is in a lower orbit (shown in red), it will have a shorter period and will drift ahead of the target. After circling the Earth, the chaser may have a brief window to communicate with the target, but will continue drifting out of range. To maintain radio contact between the chaser and target, it is desirable to have the two craft in orbits with identical semi-major axes to prevent drifting due to orbit period discrepancies.

Due to the fact that the satellites are initially separated by a great distance and unable to communicate with one another, it is assumed that sequential ground passes will be used to download data and upload commands. This process imposes a delay between when GPS data is collected and when the commands are executed.

To simplify the computations conducted in the models, circular orbits are assumed when predicting the long-term effects of drag. This has the effect of slightly

underestimating the effect of drag over long periods. When considering purely gravitational effects, craft follow trajectories of equal potential. When a point mass is considered with a satellite of negligible mass orbiting about it, this path is circular. When the oblateness of the Earth is included in the model, it introduces mass about the equator, pushing out the equal potential region further away from the Earth around the equator and closer around the poles. In LEO, craft drift away when passing closest to the poles and dip down when passing over the equator, speeding up and temporarily increasing their drag due to the denser air. Compared with a circular orbit, the dip has a greater effect on total drag experienced since density increases exponentially with decreasing altitude. By choosing a circular orbit approximation, the model slightly underestimates the true drag experienced by a craft subjected to perturbations caused by the Earth's oblateness.

It is assumed that each craft can reach and maintain its minimum and maximum theoretical cross-sectional areas. Due to mission requirements such as pointing solar panels at the sun and pointing antennas toward the Earth during ground passes, it is unlikely this will hold true during the entirety of the mission, however the effect can be approximated using time-averaged control of each spacecraft's attitude.

4.2 MODELS AND ON-ORBIT TESTS

Akin to terrestrial weather, the upper atmosphere is volatile. Seasonal and daily variations can alter the density of the atmosphere by more than an order of magnitude, as seen in Figure 4.1. However, to make decisions rapidly over a span of days, it is necessary to estimate the atmospheric density on orbit. Additionally, measurements taken in orbit will validate the models used in trajectory planning; perturbations in the values of C_d or cross-sectional area will be included in the atmospheric model and incorporated in future calculations.

Two methods can be used to estimate atmospheric density. The algorithm developed in Chapter 3 estimates an atmospheric quantity, if atmospheric constants are known and supplied to the program. This method is limited to processing about one day's worth of data because the algorithm becomes increasingly sensitive to measurements taken at the end of the data set, making it unable to converge. For shorter data sets, this method can be used to approximate density at a specific altitude.

Alternatively, the semi-major axis can be calculated from GPS data at two points in time separated by days. The decay in the semi-major axis is directly related to the cumulative drag experienced by the craft. The GPS coordinates are used to estimate the semi-major axis at the start of a maneuver and at the end.

The maneuvers inspected in this section span days and weeks; it is more useful to use an atmospheric estimate derived from several days' worth of data that minimizes daily fluctuations than an estimate derived from a shorter time span.

Since the maneuvers developed later in this chapter span long distances and multiple days or weeks, it is more useful to take a holistic approach to modeling. Rather than focus on minutia such as orbit perturbations, it is simpler to model average effects over long time periods and use these as initial seed estimates when conducting a maneuver. While the maneuver is being conducted, these rough estimates can be updated and refined to allow the chaser to more precisely reach the target.

4.2.1 Example on-orbit testing

To estimate the average atmospheric density, two sets of GPS data are needed. When the maneuver begins, two orbits' worth of data must be collected. Several days later, at the end of the maneuver, another two orbits' worth of data should be collected. The mission environment dictates the duration of the maneuver (the separation between

the data sets are collected). If the craft is lower in the atmosphere, its semi-major axis will drop quicker due to increased drag and the maneuver will not need to be as long.

The craft should maintain a constant attitude relative to the direction of motion during GPS data collection. This allows the orbital decay rate to be directly related to the area exposed to the atmosphere.

This procedure should be executed twice. One iteration should orient the craft with the minimum area facing forward. The second iteration should orient the craft with the maximum area forward. By observing the orbital decay in these two scenarios at similar altitudes, this will give mission planners a realistic benchmark for orbital decay when planning future missions.

4.2.2 Rules of thumb

As a rule of thumb, it may be useful to inspect a mission lifetime plot before determining what proximity operation maneuvers should be attempted. Craft that are separated too far vertically may not be able to match their orbital altitudes before impacting the Earth, let alone align with each other in a proximity operation.

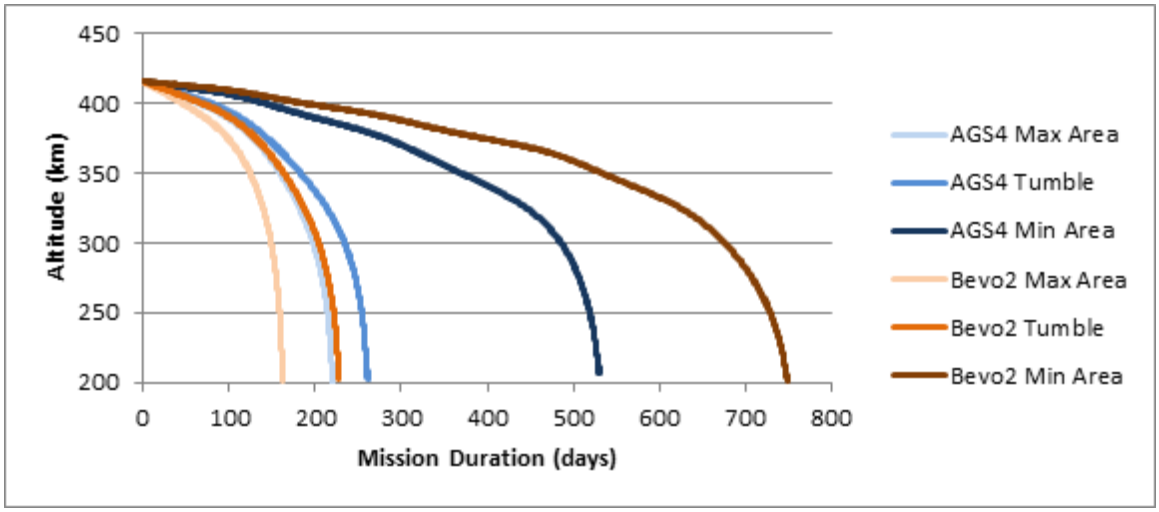

Figure 4.5: Simulated mission lifetime plot.

Figure 4.5 is a simulated mission lifetime plot generated in STK using the HPOP. Varying attitudes were simulated for the craft in LONESTAR Mission 2, with the mission beginning in the late 2013 time frame. One factor to note is that with AGS4 maximizing its area facing into the wind and with Bevo-2 tumbling, the craft are predicted to fall to Earth at nearly the same rate. This is indicative of drag affecting both craft approximately equally, and recalls the results from Chapter 2 which aim to keep the craft in close proximity.

4.3. LONG-RANGE PROCEDURES

The objective for this section is to align two spacecraft in co-planar LEO orbits. The two craft are initially separated by more than 150 km.

Since the maneuvers to align the two craft will take multiple days as will be seen in the following section, it is desirable to simplify the model and use a circular-Earth approximation. Under this condition, the craft can be characterized as being separated by

an orbital phase and a discrepancy between their semi-major axes. The target is placed at the origin; the objective is then to move the chaser to the origin.

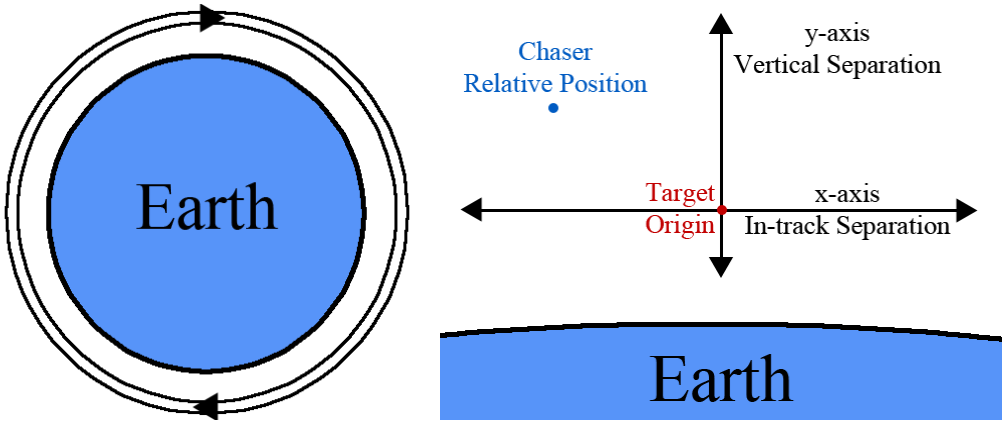

Figure 4.6: Two circular orbits about the Earth.

On the left in Figure 4.6, a simplified illustration of two circular orbits about the Earth is shown. The region the satellites sweep out during the period of one orbit forms an annulus. The annulus is cut and displayed on a Cartesian reference frame (right). The target is placed at the origin, the x-axis encompasses the in-track separation between the chaser and the target, and the vertical axis represents the vertical separation between the craft (a difference in orbital altitudes). Here the chaser is shown as being behind and above the target.

A few points should be noted. Both the target's and chaser's orbits continually decay. While the origin is fixed to the target, both the target and chaser are moving downwards over the long term. This is important to note because the quickest way to align the craft is to have both craft conduct attitude maneuvers. Such a maneuver may

entail the target minimizing its area and the chaser maximizing its area. As will be shown, this results in the chaser moving down *relative* to the target when in fact it is moving closer to the Earth at a faster *rate* than the target. Similarly, in the relative frame, it may appear that the chaser 'rises', but in fact it simply falls at a slower rate than the target.

These min/max and max/min maneuvers accelerate orbital decay as compared to operations that match the area-to-mass ratios between the craft. The trade-off between total mission duration and the benefit of conducting state rendezvous should be weighed by the mission planners. A series of minimum duration plots specific to LONESTAR Mission 2 are presented in Section 4.3.5.

Additionally, the x-axis repeats every orbital circumference. That is, if the chaser is below the target, the chaser can either 'brake' and go into an orbit higher than the target then later descend, or it can wait until the target moves around the Earth and then rise later. The following analysis focuses on whichever operation takes the shortest amount of time.

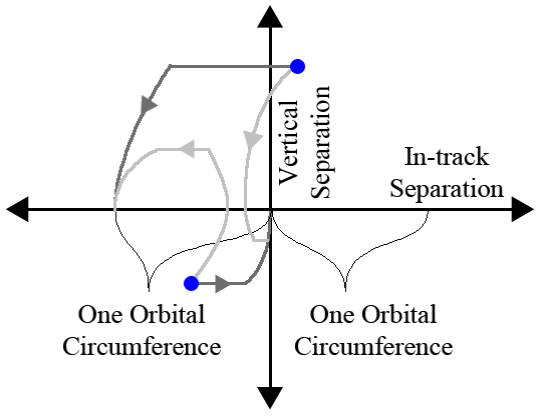

Figure 4.7: Target/chaser relative reference frame.

In Figure 4.7, the x-axis of the reference frame repeats for every orbital circumference of the target. Two examples are shown where the chaser is initially located at different locations (blue) relative to the target. It is possible for the chaser to follow a trajectory (different shades of gray) that reaches any one of the repeating origins.

The dynamics of this relative frame of reference are as follows. When the chaser is in a higher orbit than the target, it has a longer orbital period. To the target, this looks as through the chaser is falling behind and moving in the negative x-direction. Conversely, if the chaser is in a lower orbit below the x-axis, it appears to move in the positive x-direction. The further the craft are away from the x-axis, the faster is this motion along the x-axis.

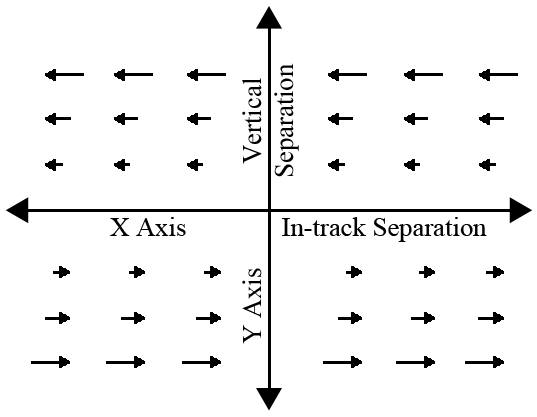

Figure 4.8: Motion of the chaser relative to the target as a function of position.

In Figure 4.8, the target is moving to the right about the Earth, but the target is set as the origin of this reference frame. When the chaser is in a higher orbit than the target (above the x-axis) it has a longer orbital period and thus appears to slip further and further behind the target. The further from the x-axis the chaser is, the faster this effect

occurs. The reverse is true below the x-axis where the chaser moves forward relative to the chaser due to a shorter orbital period.

Motion along the y-axis is conducted via attitude maneuvers executed by both craft. If the target maximizes its cross-sectional area and the chaser minimizes, the target will fall toward the Earth faster than the chaser. In the relative frames, this appears as though the chaser is moving upwards. This motion is combined with the sideways motion described above to produce an arc over time. Below the x-axis, this arc moves up and slows the motion in the positive x-direction until the chaser stops moving horizontally upon reaching the x-axis. If the coordinated attitude maneuver continues, then the craft will continue moving up and will start moving along the negative x-direction.

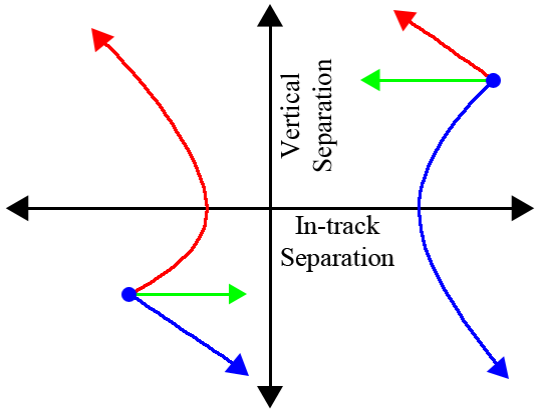

Figure 4.9: Example maneuvers conducted with different initial conditions.

Figure 4.9 shows example maneuvers conducted with different initial conditions. If the chaser minimizes its cross-sectional area while the target maximizes its cross-sectional area, the chaser moves upward relative to the target, as shown in red. When the chaser is below the x-axis (in a lower orbit than the target), it moves forward, but the

closer it gets to the x-axis, the slower this motion is. When the coordinated attitude maneuver is reversed, that is, with the chaser maximizing and the target minimizing drag, the chaser moves toward a lower orbit than the target, as shown in blue. Conceptually, if the chaser and target match the amount of drag they experience, they will maintain the same vertical separation, as shown in green.

The state rendezvous procedure can be broken up into three legs that follow one of two paths, either a 'forward' or a 'reverse' path.

4.3.1 Braking/Reversing Procedure

The 'braking' procedure consists of three sections. The first section entails bringing the chaser craft above the target craft. That is, the first leg of the state rendezvous is to minimize the cross-sectional area of the chaser, maximize the cross-sectional area of the target, and then wait for the chaser to 'rise' into an orbit that is higher than the target.

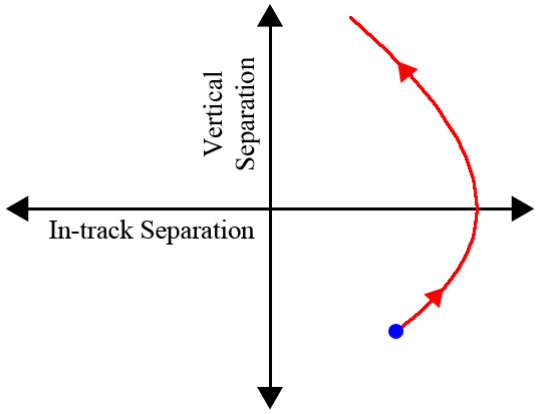

Figure 4.10: The first leg of a trajectory to place the chaser in proximity of the target.

A switching curve will be developed below, but it suffices to say that the first leg is terminated when the craft reaches a certain vertical position above the x-axis. Once

this position is reached, both craft attempt to match the area-to-mass ratios. To minimize drag and maximize mission lifetime, one of the craft should be utilizing the absolute minimum theoretical area for this maneuver, which results in the least loss in altitude over the execution time of the maneuver, prolonging the total mission duration. This maneuver has the effect of maintaining the altitude of the chaser relative to the target and precessing the position of the chaser over time.

The 'holding' leg allows for discrepancies in the long-range model. Variations in the atmosphere, operational limitations on the cross-sectional area, or other factors could accelerate or decelerate the motion of the two craft relative to one another. To allow for this type of error, the craft are given a buffer window that may be shortened or lengthened to account for fluctuations in the real path taken compared with the theoretical path. In the models below, a buffer window of three days was chosen. The longer the maneuver is, the larger are the errors that accumulate along the theoretical path, so using a holding window during the maneuver is desirable to give mission planners the opportunity to make corrections mid-maneuver.

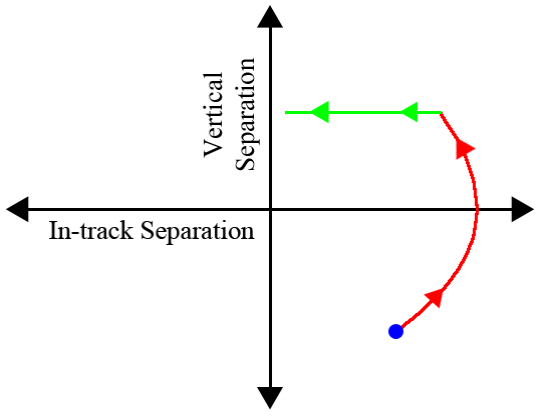

Figure 4.11: Following the ‘braking’ procedure, a ‘hold’ procedure is executed where the chaser and target match their drag, shown in green.

The third step entails developing a final curve that tracks in towards the target. In the example, the target minimizes the cross-sectional area, the chaser maximizes its area, and the chaser appears to drop down on the target from above. The chaser and target craft will need to start this maneuver when the chaser is still ahead of the target on the x-axis.

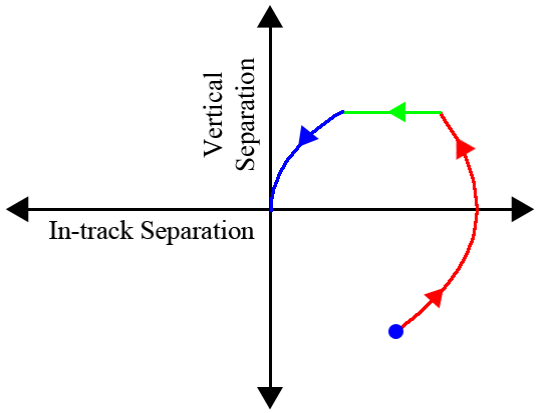

Figure 4.12: Above, in blue, is shown the final leg of the reverse maneuver to 'return' the chaser to the origin.

4.3.2 Accelerating/Forward Procedure

As mentioned previously, it is possible to reach the target through multiple paths. One path as described above entails doubling back to reach the target in the most direct fashion. However, it is also possible to wait for the chaser to drift around the Earth relative to the target and only initiate a maneuver when the two craft are in close proximity.

The first leg of the forward procedure is comparable to the first leg of the reverse procedure, except that it does not cross the x-axis. Rather the craft conduct attitude maneuvers such that the chaser moves away from the x-axis until it hits the first switching curve.

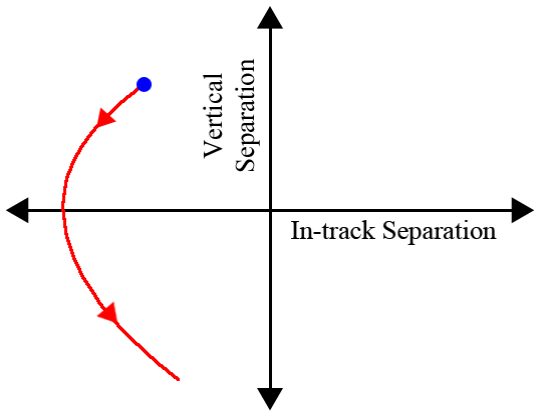

Figure 4.13: The first leg of a forward maneuver entails maximizing the area of the chaser and minimizing the area of the target, producing the 'braking' trajectory shown in red.

Upon hitting the switching curve, as will be discussed in the following sections, the craft attempt to match their area-to-mass ratios.

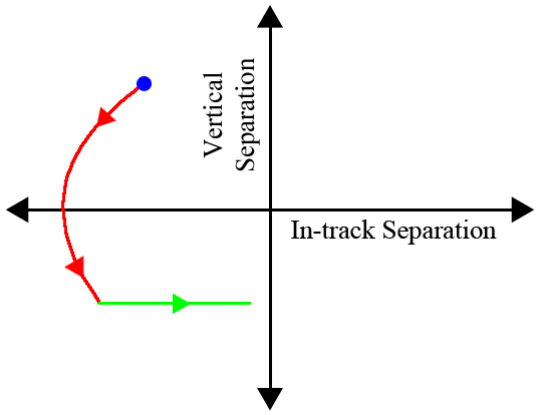

Figure 4.14: The craft attempt to match their drag in the 'hold' procedure, producing the trajectory shown in green.

Finally, the chaser hits the second switching curve and follows a trajectory toward the target.

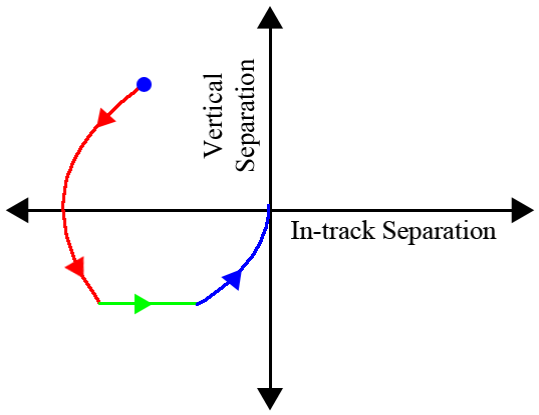

Figure 4.15: The final 'return' leg of the maneuver is generated by minimizing the area of the chaser and maximizing the area of the target, producing the trajectory in blue.

4.3.3 Procedure Overview

The procedure in Sections 4.3.1 and 4.3.2 details two paths that the craft can take to align themselves in the state space. These paths can be conceptually traced out using the following state transition diagram.

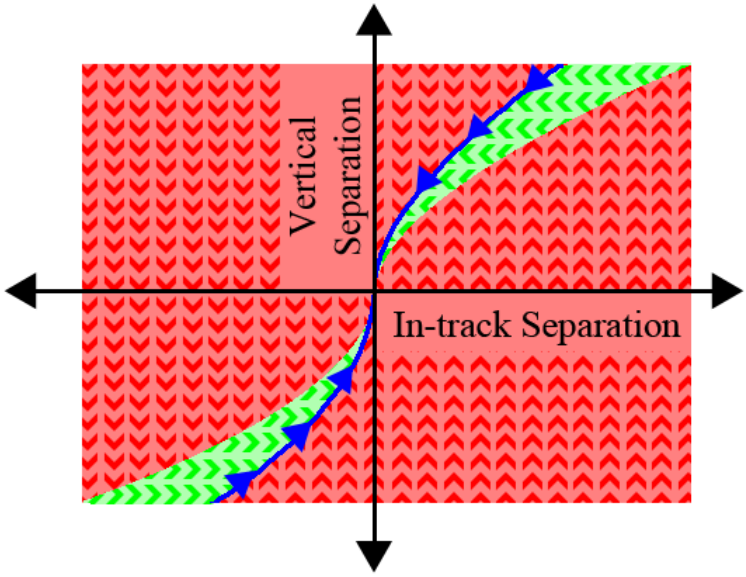

Figure 4.16: Conceptual state transition diagram.

Figure 4.16 depicts a conceptual state diagram for generating a proximity operation maneuver. Wherever the chaser is initially in relation to the target, a maneuver can be found by following the maneuver dictated by the region it lies within. For example, if the chaser is initially above and behind the target (upper left quadrant), the first maneuver is to maximize the chaser area, minimize the target area, and wait for the chaser to enter the green region, at which time the two craft equate their drag until the chaser reaches the blue line. The craft reverse their attitude configuration from the red region and are drawn together. Over time, the state diagram will change. As the altitude of the craft decreases, the green and blue curves will become steeper as drag becomes greater.

If circular-orbit and static atmosphere approximations are made, the following equation can be used to relate the orbital decay rates to the properties of each craft (Tapley, Schutz and Born 2010):

$$\frac{da}{dt} = -\left(\frac{C_d A}{m}\right)\frac{\rho a^2}{\mu}V^3 \tag{4.2}$$

Here, a refers to the semi-major axis of the craft being inspected, C_d is the chosen drag coefficient, A is the area of the craft facing into the direction of motion, m is the mass of the vehicle, ρ is the density of the air at the current altitude, μ is the standard gravitational coefficient for Earth, and finally V is the speed of the craft.

Additionally, using the semi-major axes from each craft at any moment in time, the rate of motion along the x-axis can be derived:

$$\frac{\mathrm{d}\theta}{\mathrm{dt}} = \frac{\mathrm{V_c}}{\mathrm{a_c}} - \frac{\mathrm{V_t}}{\mathrm{a_t}} \tag{4.3}$$

In this equation, θ is the angular separation between the chaser and the target about the earth, between 0 and 2π. The subscripts c and t refer to the chaser and target, respectively.

An ODE45 propagator is seeded with the initial state of the chaser relative to the target, and then the propagator is used to integrate these two equations of motion synchronously over a span of several days until the ending conditions are met.

The equation of motion for orbital decay relies on atmospheric density estimates. These values are computed from an exponential curve fit to the Naval Research Lab Mass Spectrometer and Incoherent Scatter Radar through the Exosphere, release year 2000 (NRLMSISE 2000) as discussed in Section 3.2.3 (U.S. Naval Research Laboratory 2012).

4.3.4 Procedure Execution

The procedure for computing the reverse path is as follows:

1. Compute the trajectory the chaser would follow to perfectly align with the target. If the current position of the chaser is initially to the right of the magenta line shown in Figure 4.17, the area of the chaser is maximized, the area of the target is minimized, the chaser is placed at the origin, and the two crafts' relative positions are integrated backward for up to one month (an arbitrarily chosen threshold). This line forms an estimate of the trajectory the chaser will follow during the final leg of the proximity maneuver.

   It would be more precise to repeatedly estimate the position for the chaser to meet the target after a specific quantity of time. These paths are shown as the blue lines in Figure 4.17; their tips form the threshold line shown in red. The red line represents all positions where the chaser could initially be placed in order to reach

the target by performing the correct attitude maneuver. However, it is computationally easier to place the chaser at the origin (with the target), min/max or max/min the areas of the chaser and target, and then propagate the relative position of the chaser backwards in time. This method is faster since it only requires one integration rather than several, but it does have the effect of producing a discrepancy against the actual path that would be taken by the chaser. Propagating backward has the effect of starting the target and chaser at a higher initial altitude where the atmosphere is less dense and has a lesser drag effect. Thus, the vertical acceleration of the chaser relative to the target is lower (as seen in the magenta line) than it would be by propagating the position of the chaser forward in time, as seen with the red line in Figure 4.17.

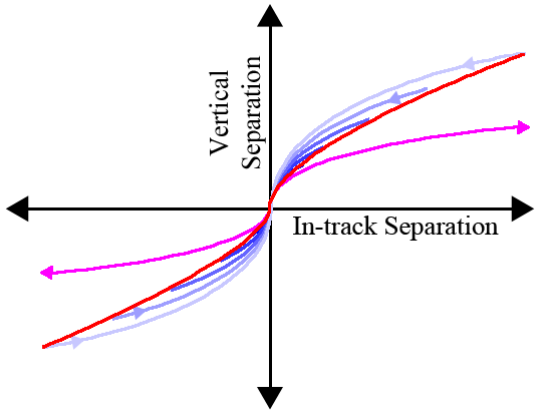

Figure 4.17: Two methods for computing the trajectory to align the chaser with the target.

Shown in red in Figure 4.17 is a line representing initial starting conditions that, when propagated forward, would align the chaser with the target. This red line would require several trajectories be computed, shown in blue, to generate the

line. To reduce computational overhead, the magenta line is created and used by propagating the desired state backwards in time (as indicated by arrows pointing away from the origin).

2. Using the magenta curve created in Step 1, a second line is generated. This new line, shown in black in the following figures, satisfies two conditions: 1) is at a minimum 150 km away from the origin and 2) if the chaser is placed on the line, it will take a minimum of 3 days to reach the magenta line. Three days was chosen for the dwell period to give ample opportunity for a ground pass to exchange mission data while also minimizing the total duration of the maneuver. The ordinary differential equation used to calculate the chaser trajectories in this section can be used to find the rate of change of motion of the chaser along the x-axis direction. Multiplying this rate of motion along the x-axis by a period of three days produces a displacement along the x-axis. This separation, shown as black arrows in Figure 4.18, is a function of vertical separation between the chaser and the target. By subtracting this displacement from the magenta line, a new black line is formed.

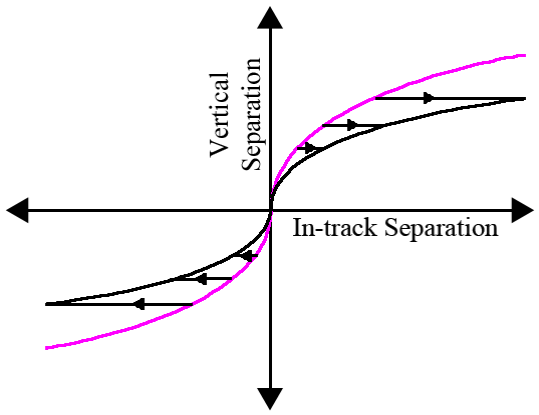

Figure 4.18: The black transition line is formed by calculating an x-axis displacement at each relative altitude and subtracting this value from the magenta transition line.

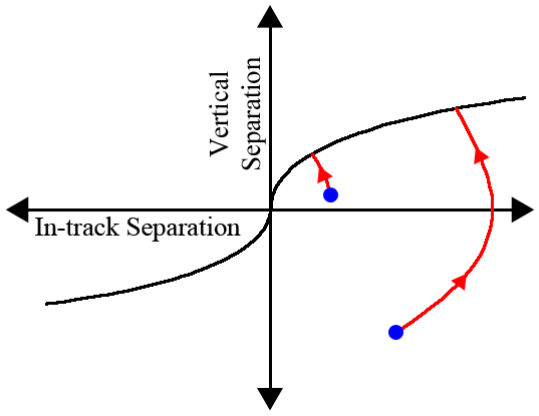

Figure 4.19: Illustration of the first leg of the trajectory from two example initial placements of the chaser.

As seen in Figure 4.19, if the chaser is initially to the right of the black line, the cross-sectional area of the chaser is minimized and the area of the target is maximized. Over time the chaser drifts above the target until it intersects the black line, at which time the first leg of the maneuver is complete. Two example scenarios are shown where a blue dot represents the chaser's initial relative position.

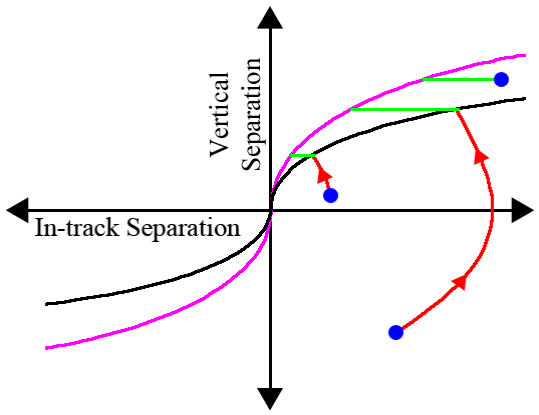

Figure 4.20: Visualization of the 'hold' maneuver imitated from three different initial conditions.

Conceptually, the remaining steps aim to maintain the altitude of the chaser (green line) for a short period, roughly three days, and then conduct a maneuver to bring the chaser into close proximity to the target (following the magenta line to the origin).

3. Set the area-to-mass ratios equal between the chaser and the target. Ideally, this action equates the drag force experienced by both craft. However, the further the two craft are separated vertically, the greater the difference in atmospheric density that each craft experiences. To produce a perfectly horizontal line would require differences in atmospheric density to be included in the computation of the area facing the wind. A perfectly horizontal line is not explicitly needed for this operation and the maneuver only serves as a safety region to reassess the relative position of the chaser before proceeding with the following maneuvers (to account for variations in atmospheric density from theory over long periods). For operational simplicity, a generic matching of the area-to-mass ratios was used, which produces slightly inclined lines.

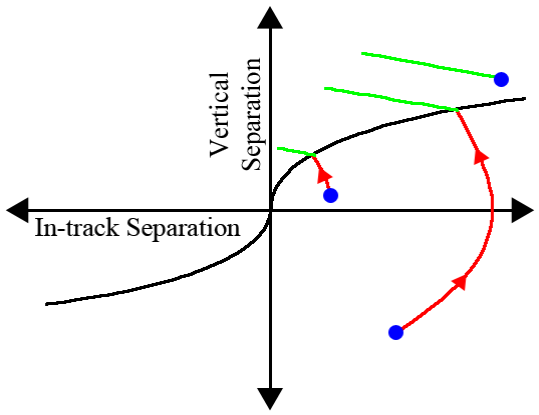

Figure 4.21: Illustration of the 'hold' maneuver used in three different trajectories.

As shown in Figure 4.21, upon reaching the black transition line, the area-to-mass ratios of the chaser and target are matched. This produces slightly inclined trajectories, shown in green, due to the difference in atmospheric density at different altitudes. If the initial position of the chaser is above the x-axis and to the left of the black line, but still close to the black line, it may be still be possible to complete the maneuver by starting with a green line as shown with the top right blue dot.

4. Propagate the relative position of the chaser forward for one month in five-minute intervals. Five-minute intervals were chosen as a reasonable trade-off between run-time and maneuver precision. One month was chosen as the maximum duration one leg would be allowed to take to complete.
5. Form a performance statistic as the final position of the chaser on the x-axis. The goal will be to reach the origin as closely as possible.
6. Use a binary search algorithm to choose a point on the green line that, when propagated until it intersects the x-axis, places the chaser as close to the origin as possible. This final leg of the maneuver is formed by reversing the areas of the

chaser and target. That is, maximize the area of the chaser and minimize the area of the chaser to form the blue lines shown in Figure 4.22.

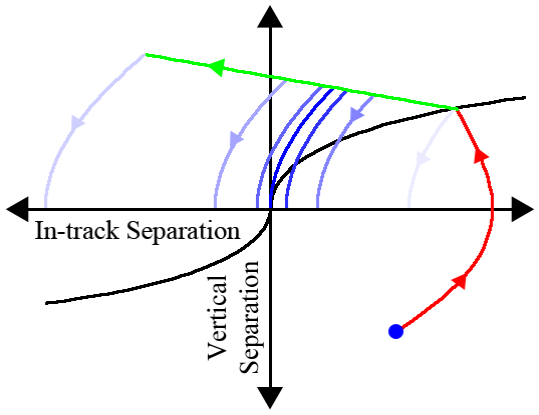

Figure 4.22: Visualization of the binary search algorithm.

A binary search algorithm is run on the points on the green line. Trajectories, shown in blue, are computed from the initial point on the green line by maximizing the area of the chaser and minimizing the area of the target. Successive iterations of the binary search are shown with darker blue lines until one ends at the minimum distance from the origin.

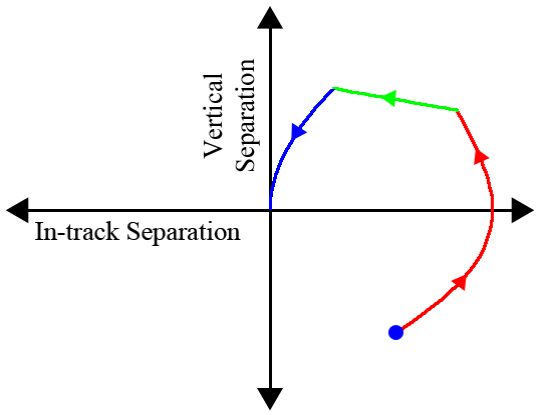

Figure 4.23: Depiction of the complete reverse maneuver.

Since the reference frame repeats every revolution about the Earth, there are effectively multiple ways to reach the same target. It may be more time-efficient to initially move the chaser forward rather than backward. The procedure for the forward maneuver is extremely similar except that the transition curves are propagated with craft attitudes that are reversed:

1. Compute the trajectory the chaser follows in approaching the target at the origin. This line is computed by moving the chaser to the origin, minimizing the area of the chaser, maximizing the area of the target and propagating backward. This line is shown as the magenta line below the x-axis in Figure 4.18.
2. Calculate the second line as described in the reverse procedure. The only difference is that this line will now lie on the opposite side of the x-axis from before. This line is shown as the black line below the x-axis in Figure 4.18.
3. If the chaser is initially to the left of the black line, maximize the area of the chaser, minimize the area of the target and propagate the initial state of the craft forward until the chaser intersects the black line generated in Step 2.
4. Match the area-to-mass ratios of the two craft.

5. Propagate the relative position of the chaser forward for one month using five-minute intervals
6. Minimize the area of the chaser, maximize the area of the target, and use a binary search algorithm to determine an optimal path from the green line to the origin.

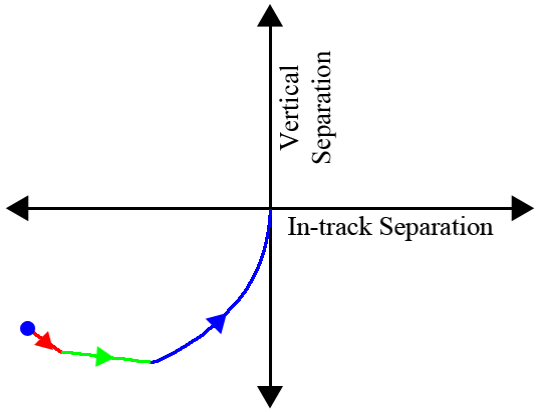

Figure 4.24: Depiction of the complete forward maneuver.

As seen in Figure 4.24, the forward maneuver is comprised of the same forms of curves as the reverse maneuver, but in opposite directions. Differences in area-to-mass ratios that each craft can achieve alter the exact curvature of the paths from those produced by the reverse maneuver.

The outputs of these two processes are time stamps when specific attitude maneuvers should be conducted by each craft. Of the two trajectories calculated, the one that is predicted to take the shortest amount of time is chosen.

While the craft execute the maneuver, the theoretical trajectory may be updated with current atmospheric density estimates derived from past flight dynamics, combined with predictive models provided by NRLMSISE 2000. Since the craft will be holding a constant cross-sectional area towards the direction of motion to conduct each leg of the

maneuver, the procedure described in Section 4.2 can be used to partially update the atmospheric model. The atmospheric density model can be scaled to match the drop in altitude observed vs. theory.

4.3.5 Simulations

Several simulations were run for the LONESTAR Mission 2 configuration to characterize the expected performance of long-duration attitude maneuvers. Two series of plots were generated for each simulation: a reverse maneuver set and a forward maneuver set. Points on the plot represent the initial placement of the chaser relative to the target and how long it is predicted to take to complete a proximity operation maneuver. At each initial chaser placement, the maneuver that took the shortest duration was chosen as the maneuver duration in the final plot.

If a maneuver could not be executed because it resulted in a final altitude below 200 km (chosen as an arbitrary cutoff), or if any leg of a maneuver took longer than a month to complete, the maneuver was marked with the deepest shade of red in the following heat plots.

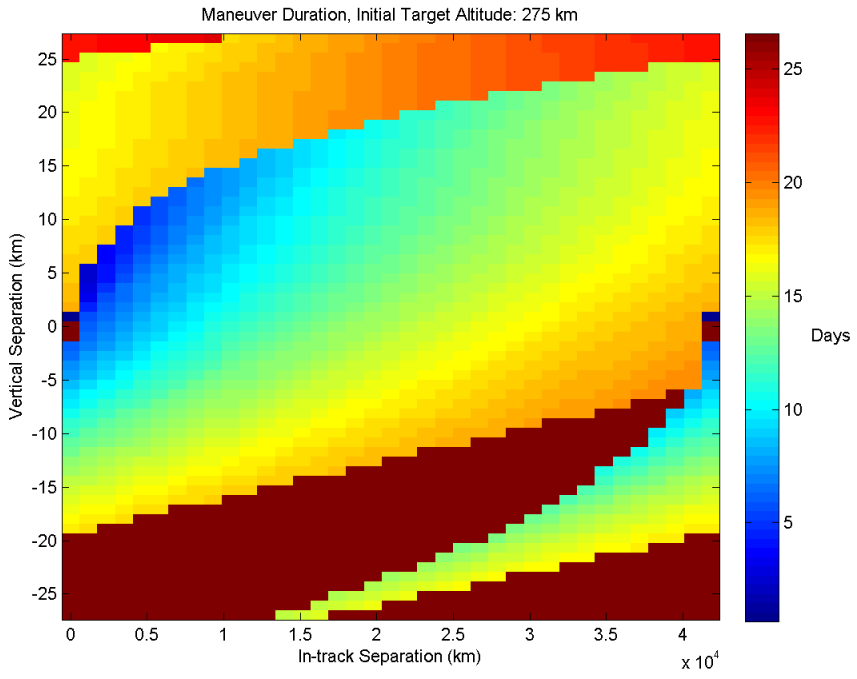

Figure 4.25: Mission duration for reverse maneuvers initiated when the target is at 275 km altitude.

In Figure 4.25, note that the large red sections low in the diagram are created when the craft attempts to execute a maneuver that places the final altitude below 200 km. Also notice that it is quickest to conduct a maneuver when the chaser is immediately above and in front of the target (shown in dark blue).

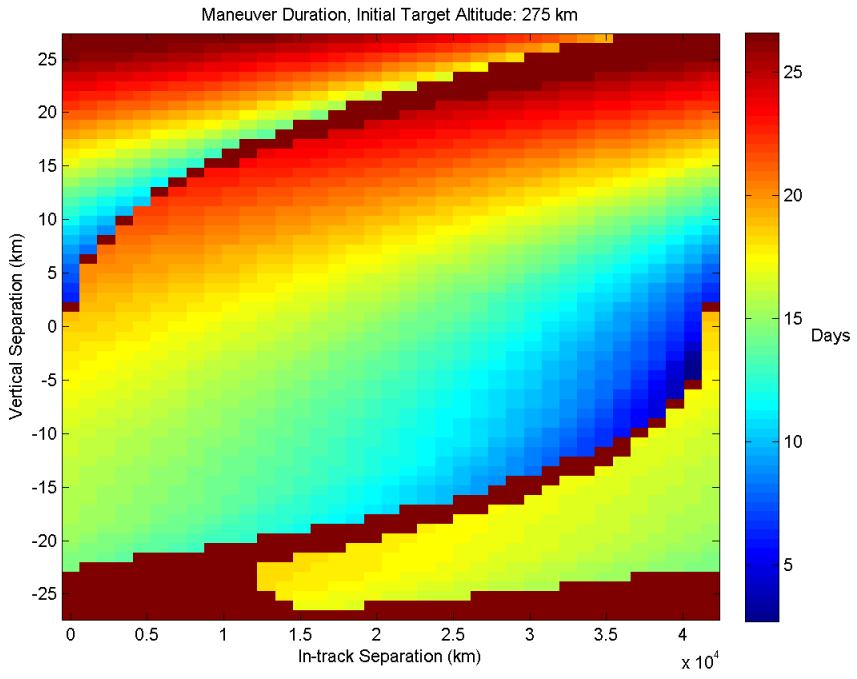

Figure 4.26: Mission duration for forward maneuvers initiated when the target is at 275 km.

Note in Figure 4.26 that it is quickest to perform a maneuver when the chaser is below and behind the target (shown in blue).

The above plot is comprised of an upper, middle and lower section. Each section is separated by a region of deep red that expands further away from the origin. These deep red curves, which contrast with the otherwise smooth transitions in the heat plot, are caused by several factors, as described below.

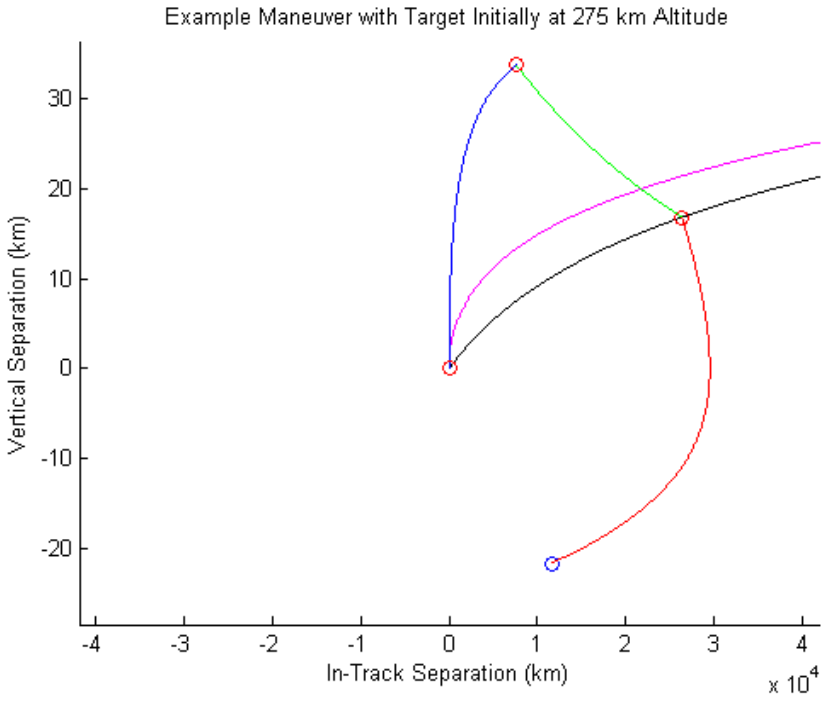

Figure 4.27: An example trajectory with the target initially at 275 km.

Figure 4.27 shows the mission path with the target initially at 275 km. The target is initially below and ahead of the chaser, marked with a blue circle. The red circles represent changes in the coordinated attitude maneuvers conducted by the crafts.

At lower altitudes, the assumption that matching area-to-mass ratios will minimize vertical separation rate of the craft fails. Rather than holding level, the green line curves upwards due predominantly to the difference in atmospheric density to which each craft is subjected. Additionally, while the transition point on the black line was chosen to produce a straight line that was horizontal for three days, the actual path requires approximately five days to traverse. Finally, while a full maneuver is shown in the diagram, the maneuver ends with a final altitude below 200 km, making it an unviable path.

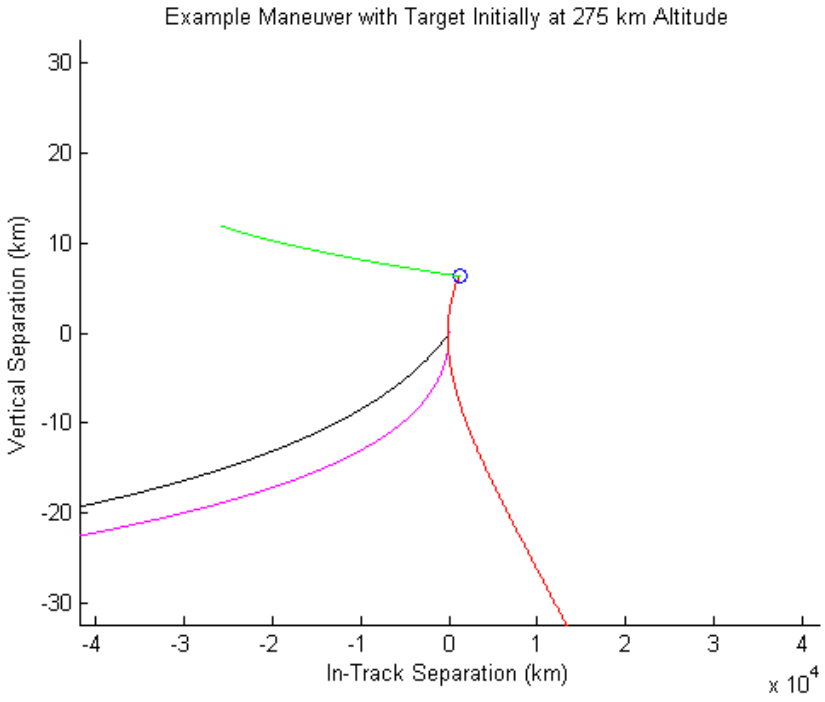

Figure 4.28: The algorithm does not detect a viable ending condition on the first leg of the trajectory.

Figure 4.28 is a diagram of an attempted trajectory that did not produce a complete maneuver. The first leg does not pass through the black line that would normally trigger a transition to the 'hold' state where the craft match their area-to-mass ratios.

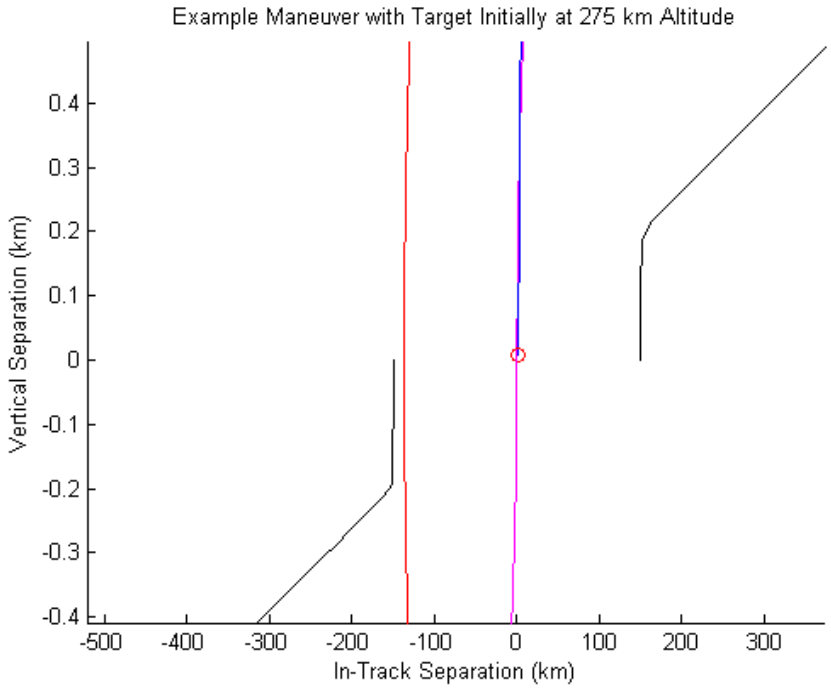

Figure 4.29: Detail about the origin of Figure 4.28.

Figure 4.29 is a diagram showing an expanded view of the previous diagram and including both black transition lines (for use in forward and reverse maneuver calculation). In some rare cases, the chaser can be placed in a position such that the first leg of the maneuver (shown in red) serves as a solution to placing the chaser within 150 km horizontally of the target, thus providing a valid solution. These cases were not detected in this simulation, resulting in some potentially short maneuvers not being included. These cases often manifest as deep red pixels (marking impossible maneuvers) surrounded by blue (indicating short total maneuver time) curving off in an 'S' shape in the following heat plots.

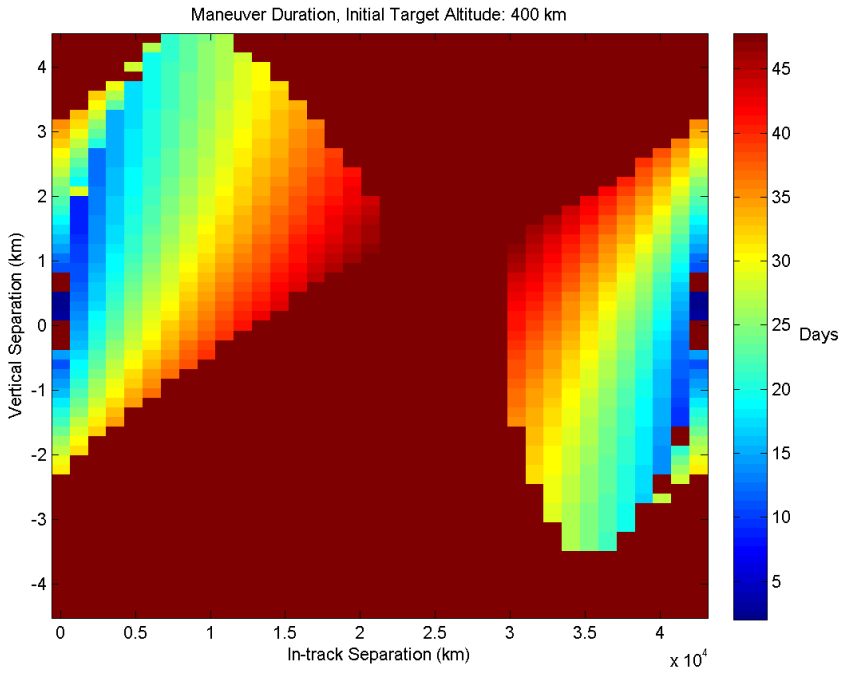

Figure 4.30: Mission duration for maneuvers initiated when the target is at 400 km.

When the target is initially placed in a 400 km orbit, the diagram in Figure 4.30 depicts how long it would take for the chaser craft to reach a close proximity. Note that there are large regions where it would take longer than a month to align the craft. The deep red indicates that a viable maneuver could not be found with the given starting conditions and lasting less than a month; this condition may be reached multiple ways. The deep red in this figure is predominantly caused by the one-month maneuver limitation. It is possible to align the craft before reentry, but such a maneuver would take in excess of a month to execute. There are a few deep red pixels surrounded by blue which are caused by the algorithm not detecting the ending condition for the first leg of the trajectory as discussed above.

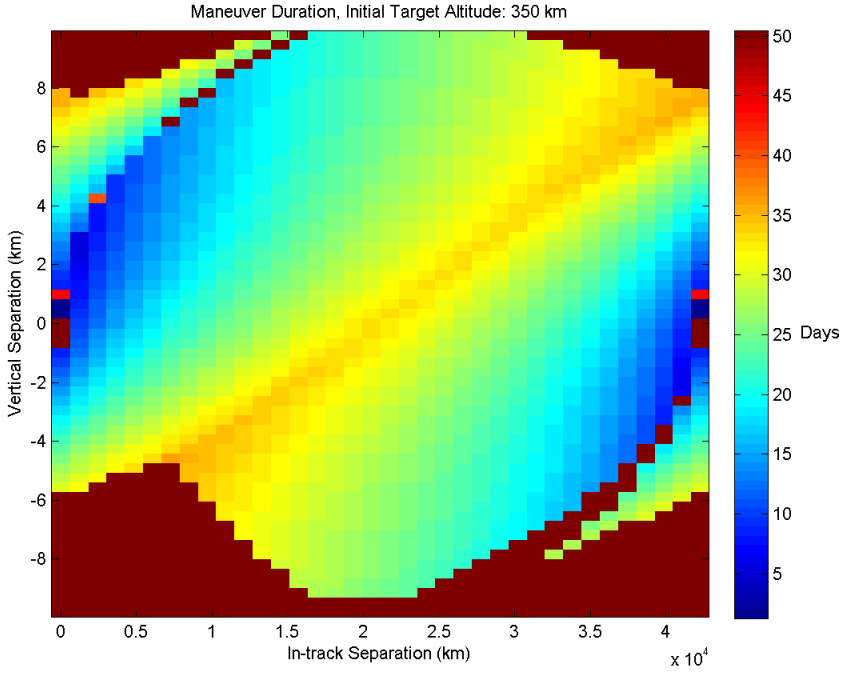

Figure 4.31: Mission duration for maneuvers initiated when the target is at 350 km.

As seen in Figure 4.31, by starting the target at 350 km, it is possible for the chaser to reach the desired state from a wider breadth of initial conditions. At lower altitudes, the effect of drag is greater, allowing for increased controllability and faster relative motion.

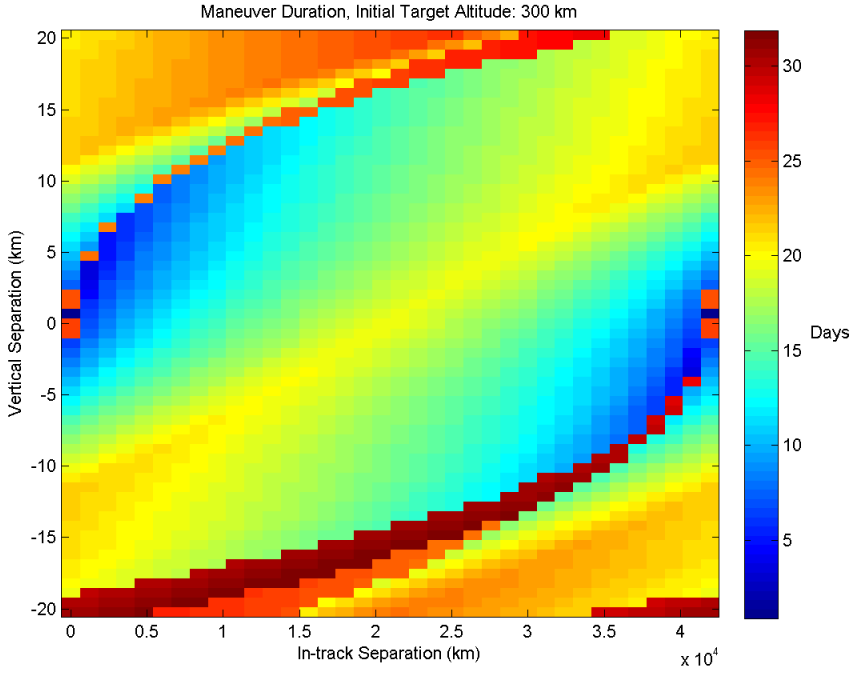

Figure 4.32: Mission duration for maneuvers initiated when the target is at 300 km.

With the target starting at a lower initial altitude of 300 km, Figure 4.32 shows that it is possible for the chaser to complete the maneuver in a shorter period (note that the time scale has decreased in this figure). The lower 'S' shaped deep red and orange arc that splits the main regions is caused by the forward maneuver being detected as the only viable path, whereas the reverse maneuver could be potentially be used to reach the desired state in a shorter time frame if the ending condition was tested during the first leg of the maneuver.

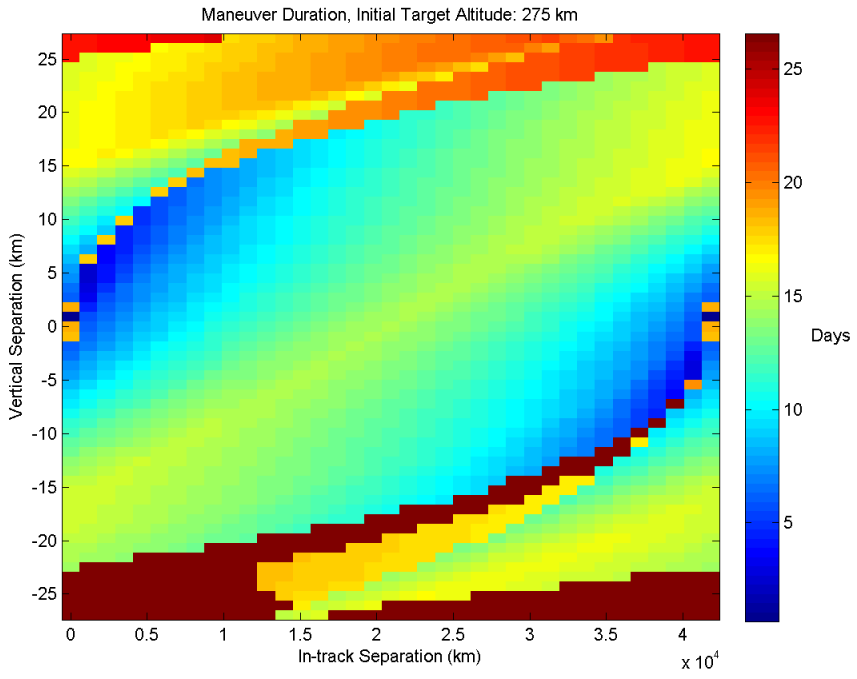

Figure 4.33: Mission duration for maneuvers initiated when the target is at 275 km.

Finally, Figure 4.33 shows that starting the target at an even lower initial altitude of 275 km produces maneuvers that are solved even faster, despite allowing for a greater variation in initial altitude separations. Some paths, like those in the lower right of the figure, are not feasible and are shaded deep red.

4.4 Operational Recommendations

The algorithm developed in this chapter can be used to align two spacecraft in co-planar LEO orbits using attitude maneuvers alone. If no target is physically present, a simulated target can be generated for testing purposes. The algorithm can be executed with the current satellite's position along with a desired in-track and altitude adjustment to demonstrate the validity of the maneuver. However, propagating a virtual target over

the span of days or months may not be accurate and the results from a single-satellite test will be more uncertain.

The major limiting factor in the duration of the attitude maneuvers is the maximum range of attitudes each craft can achieve. For future mission planners, it would be beneficial to know how far from ideal the attitude of each craft is from the attitude commanded. While it may be desirable to minimize or maximize the area facing into the direction of motion, other criteria such as star-tracker, antenna, and solar panel pointing requirements may override the long-duration attitude maneuver requirements. A log of the actual attitude maintained over time should be kept during the execution of the mission. In the future, a 'degradation factor' can be calculated between the commanded attitude and the actual mission profile attitude, allowing the administration of future missions to make more informed decisions about the capabilities of attitude maneuvers. While theoretical attitudes can be calculated, it will be more realistic to use average attitudes calculated from a real mission.

Chapter 5: Conclusion

The analysis presented here encompasses ejection, thruster and attitude maneuvers between two craft in LEO. With these tools, LONESTAR Mission 2 will be capable of demonstrating coordinated attitude maneuvers and flight testing the thruster aboard Bevo-2. The work presented here enables future missions to conduct long-duration attitude maneuvers with the objective of accomplishing a proximity operation such as establishing radio contact with another vehicle. The algorithms for conducting thruster operations are a vital step in aligning the orbit planes of craft prior to rendezvous, as is the final goal for the LONESTAR program.

Chapter 2 dealt with the separation of the Bevo-2 craft from AGS4 to maximize the time within communication range. The predominant factor that drives separation of the craft is a difference in drag effects. The primary procedure to keep the craft within transmitting range of each other is to equate the drag effects between the two craft, which is nearly equivalent to matching their area-to-mass ratios. The specifics of Mission 2 entail ejecting Bevo-2 from AGS4 at a velocity of less than 1 meter/sec. Due to the procedures conducted immediately following deployment, such as the release of the whip antennas for ground communication, Bevo-2 will likely begin tumbling at a very slow rate. Since the cross-sectional area of Bevo-2 cannot be predicted for long time spans until attitude control is established, the craft is assumed to have a single average area. From this assumption, the AGS4 craft must maximize its area facing into the direction of motion to match the area-to-mass ratio and subsequently the drag of the two craft.

If left uncorrected, the effect of drag accumulates over time, resulting in a varying rate of orbital decay between the craft. The difference in orbital altitudes is synonymous with a difference in orbital period, which is the primary factor in separating the craft over

time. Therefore, orbital maneuvers should aim to minimize the velocity between the craft in the direction of motion (positive or negative). In other words, the launch of Bevo-2 must be made in a direction perpendicular to the direction of motion of AGS4. This theoretically produces no motion along the direction of travel. If the drag effect is controlled by matching the area-to-mass ratios, then the time spent in communication range is maximized. The relative motion as a result of this ejection maneuver is oscillatory in nature since it is cause by minute differences in orbit eccentricity, inclination and RAAN. The relative oscillatory motion between the craft resulting from separation lies well within the communication range. The velocity component of the ejection maneuver in the direction of motion and the effects of drag are the predominant drivers of separation and the eventual loss of contact between the craft.

Chapter 3 described a procedure that can be modified for multiple applications. The procedure involves filtering GPS coordinates to estimate the initial state of a spacecraft. The filtering algorithm was used to determine the separation velocity of the two spacecraft relative to one another after deployment. Additionally, this algorithm was used to measure the velocity imparted by firing a thruster. Finally, the original algorithm and the propagator were altered to estimate the timing and magnitude of corrective thruster maneuvers to negate the out-of-plane motion between the orbits of the craft. The orbital angular momentum vectors were found, a node on the chaser's orbit was determined, and a burn conducted to align the craft in the same orbital plane.

Chapter 4 defined a process to utilize spacecraft attitude as a control for reaching a desired position relative to a target craft. By alternating which craft is minimizing or maximizing cross-sectional area, Bevo-2 can be moved vertically relative to AGS4. The vertical orientation of the two craft dictates how they separate in the in-track direction.

By judiciously planning min/max and max/min procedures, the craft can be aligned both in the in-track direction and vertically, thus concluding a proximity operation.

The procedures detailed here are applicable to missions outside the scope of the LONESTAR program. The algorithm developed in Chapter 4 may be directly applied to craft with different attitude and mass characteristics under the condition that the area-to-mass ratios of the craft are not entirely dissimilar. The two craft must be capable of alternating which experiences greater drag force in order to complete the maneuvers dictated by the algorithm. Similarly, any craft equipped with a thruster and GPS unit may conduct scheduled thruster maneuvers using the orbit determination algorithm developed in Chapter 3 without restrictions on vehicle design or mass.

The maneuvers outlined in this document form a fundamental basis to achieve the objectives of LONESTAR Mission 2. This paper focused on the Bevo-2 craft and some simple maneuvers it can perform to accomplish rough proximity operations. These maneuvers extend prior work such as that done by Lum (Lum 2011) to complete proximity operations required for rendezvous in low earth orbit. With these procedures, spacecraft can begin with a far broader set of initial configurations and still reach close proximity.

BIBLIOGRAPHY

U.S. Naval Research Laboratory. *NRLMSISE-00: A New Empirical Model of the Atmosphere.* February 1, 2012. http://www.nrl.navy.mil/research/nrl-review/2003/atmospheric-science/picone/ (accessed August 24, 2013).

Analytical Graphics, Inc. *Getting Started with the STK Software Suite* . 2003.

Arestie, Steven, Glenn Lightsey, and Brian Hudson. "Development of a Modular, Cold Gas Propulsion System for Small Satellite Applications." *JoSSOnline* (Deepak Publishing), 2012: 12.

Johl, Shaina. *Mission Concept of Operations.* Internal Document, Austin: UT-Austin, 2013.

Kaula, William. *Theory of Satellite Geodesy.* Dover, 2000.

Kjellberg, H. *Design of a CubeSat Guidance, Navigation, and Control Module.* 2012.

Kjellberg, Henri. *Bevo-1 Lessons Learned.* Slide Show, Austin: UT-Austin, 2011.

Lee, Simon. "CubeSat Design Specification Rev. 12." *CubeSat.* September 1, 2009. http://www.cubesat.org/images/developers/cds_rev12.pdf (accessed August 22, 2013).

Lum, Annie Megan. *Examining Differential Drag Control in a Full System Simulation.* Master's Thesis, Austin: UT-Austin, 2011.

Misra, Pratap, and Per Enge. *Global Positioning System: Signals, Measurements, and Performance.* 2010.

Tapley, Byron, Bob Schutz, and George Born. *Statistical Orbit Determination.* Elsevier Academic Press, 2010.

Tribble, Alan. *The Space Environment, Implications for Spacecraft Design.* 2003.